MODELING OF THE DISPENSING-BASED TISSUE SCAFFOLD FABRICATION PROCESSES

A Thesis Submitted to the College of

Graduate Studies and Research

in Partial Fulfillment of the Requirements

for the Degree of Doctor of Philosophy

in the Department of Mechanical Engineering

University of Saskatchewan

Saskatoon

By

Minggan Li

PERMISSION TO USE

In presenting this thesis in partial fulfilment of the requirements for a Postgraduate degree from the University of Saskatchewan, I agree that the Libraries of this University may make it freely available for inspection. I further agree that permission for copying of this thesis in any manner, in whole or in part, for scholarly purposes may be granted by the professor or professors who supervised my thesis work or, in their absence, by the Head of the Department or the Dean of the College in which my thesis work was done. It is understood that any copying or publication or use of this thesis or parts thereof for financial gain shall not be allowed without my written permission. It is also understood that due recognition shall be given to me and to the University of Saskatchewan in any scholarly use which may be made of any material in my thesis.

Requests for permission to copy or to make other use of material in this thesis in whole or part should be addressed to:

Head of the Department of Mechanical Engineering

University of Saskatchewan

Saskatoon, Saskatchewan S7N 5A9

ABSTRACT

Tissue engineering is an emerging area with an aim to create artificial tissues or organs by employing methods of biology, engineering and material science. In tissue engineering, scaffolds are three-dimensional (3D) structure made from biomaterials with highly interconnected pore networks or microstructure, and are used to provide the mechanical and biological cues to guide cell differentiation in order to form desired three-dimensional tissues or functional organs. Hence, tissue scaffold plays a critical role in tissue engineering. However, fabrication of such scaffolds has proven to be a challenge task. One important barrier is the inability to fabricate scaffolds with designed pore size and porosity to mimic the microstructure of native tissue. Another issue is the prediction of process-induced cell damage in the cell-involved scaffold fabrication processes. By addressing these key issues involved in the scaffold fabrication, this research work is aimed at developing methods and models to represent the dispensing-based solid free form scaffold fabrication process with and without the presence of living cells.

The microstructure of scaffolds, featured by the pore size and porosity, has shown to significantly affect the biological and mechanical properties of formed tissues. As such, during fabrication process the ability to predict and determine scaffold pore size and porosity is of great importance. In the first part of this research, the flow behaviours of the scaffold materials were investigated and a model of the flow rate of material dispensed during the scaffold fabrication was developed. On this basis, the pore size and porosity of the scaffolds fabricated were represented by developing a mathematical model. Scaffold fabrication experiments using colloidal gels with different hydroxylapatite volume fractions were carried out and the results obtained agreed with those from model simulations, indicating the effectiveness of the models

developed. The availability of these models makes it possible to control the scaffold fabrication process rigorously, instead of relying upon a trial and error process as previously reported.

In the scaffold fabrication process with the presence of living cells, cells are continuously subjected to mechanical forces. If the forces exceed certain level and/or the forces are applied beyond certain time periods, cell damage may result. In the second part of this research, a method to quantify the cell damage in the bio-dispensing process is developed. This method consists of two steps: one step is to establish cell damage models or laws to relate cell damage to the hydrostatic pressure / shear stress that is applied on cells; and the second step is to represent the process-induced forces that cells experience during the bio-dispensing process and then apply the established cell damage law to model the percent cell damage in the process. Based on the developed method, the cell damage percents in the scaffold fabrication processes that employ two types of dispensing needles, i.e., tapered and cylindrical needles, respectively, were investigated and compared. Also, the difference in cell damage under the high and low shear stress conditions was investigated, and a method was developed to establish the cell damage law directly from the bio-dispensing process. To validate the aforementioned methods and models, experiments of fabricating scaffolds incorporating Schwann cells or 3T3 fibroblasts were carried out and the percent cell damage were measured and compared with the simulation results. The validated models allow one to determine of the influence of process parameters, such as the air pressure applied to the process and the needle geometry, on cell damage and then optimize these values to preserve cell viability and/or achieve the desired cell distribution within the scaffolds**.**

ACKNOWLEDGEMENTS

I am heartily thankful to my supervisor, Prof. Daniel Chen, whose encouragement, guidance and support through my study program enabled me continuously reach my research goals. His expertise and enthusiasm inspired me to explore every challenge in my research. I will be always grateful.

I also would like to extend my appreciation to the members of my Advisory Committee: Prof. Greg Schoenau, Prof. Chris Zhang and Prof. Robert Gander for their examination and advices in my research program.

Several other professors and technician also enriched my research. I would like to thank Prof. David Schreyer and Mrs. Ruilin Zhai in the Department of Anatomy and Cell Biology. They provided me with a lot of valuable advice and technical support in my experiments at City Hospital. Also, my thanks goes to Mr. Doug Bitner in our department for his technical assistance for my experiments.

Special thanks are due to my friends for their help and support during my research. They are Christopher James Little, Ning Zhu, Nahshon Bawolin, Yijing Guang, Ning Cao, Xin Yan, Mindan Wang, Peng Zhai and Jinyang Peng.

I gratefully acknowledge the financial support from the Department of Mechanical Engineering (through the Scholarship), Natural Science and Engineering Research Council (NSERC) and Saskatchewan Health Research Foundation (SHRF). I also acknowledge the copy right permission from the publisher of American Society of Mechanical Engineering (ASME), Institute of Physics (IOP) and Marry Ann Liebert to include the published papers in my thesis.

Finally, I wish to thank my devoted wife, Xiaoyu Tian, for her continuous support and valuable advices for my research.

CONTENTS

CHAPTER 1

INTRODUCTION AND OBJECTIVES

1.1 Introduction

Tissue engineering is an emerging field that combines engineering principles and the biological sciences toward the repair and replacement of damaged or diseased tissues or organs in the human body. The general strategy of tissue engineering is to incorporate autologous cells into a three-dimensional (3D) biomaterial scaffold that is designed to promote cell function and form new tissue. In these processes, engineered 3D scaffolds provide a biological environment and mechanical support to guide cell differentiation and assembly into 3D tissues. Thus, tissue scaffolds play a vital role in tissue engineering and their fabrication is of fundamental importance.

Various techniques have been explored for tissue scaffold fabrication. Among them, the dispensing-based method is a promising Rapid Prototyping (RP) technique that has drawn a great deal of attention, as it can overcome the shortcomings of conventional techniques by producing scaffolds with customized external shape and predefined internal morphology. A schematic of the method, and the scaffold produced by it is shown in Figure 1. This technique can not only achieve the designed pore size, porosity, and pore distribution of scaffolds but also build microstructures that enhance the mass transfer of oxygen and nutrients. However, since the biomaterials used in the fabrication process are paste-like gels, the strands of the scaffold, once dispensed, will deform and fuse into each other. As a result, the pore size and porosity of scaffolds obtained degrade from the designed ones. Therefore,

there is a great need to model and control the scaffold fabrication process for improved pore size and porosity control.

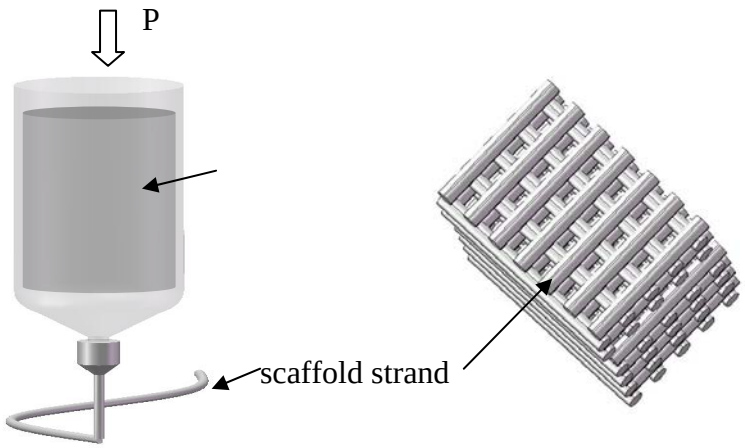

(a) (b)

Figure 1 (a) schematic of dispensing-based scaffold fabrication and (b) scaffolds fabricated.

To promote the cell attachment to the scaffold surface and tissue formation in the scaffolds, cells are often incorporated into, and extruded with the biomaterials to form cell-encapsulated tissue scaffolds. Since cells are subjected to mechanical forces during these processes, not all cells can survive the process. Investigation into the cell damage occurring in such a bio-fabrication process and development of models for the cell damage rate are of great importance to preserve the cell viability and optimally control the bio-fabrication process.

1.2 Objectives

The aim of this research work is to carry out a comprehensive study on the dispensing-based tissue scaffold fabrication process with and without the incorporation of living cells. In particular, two main objectives are set to achieve in this research.

The first objective is to develop models to represent the fabrication processes, including the flow rate of the gel dispensed and the pore size and porosity of the scaffolds fabricated.

The second objective is to develop cell damage models to predict cell damage in different bio-dispensing processes, including the processes using a cylindrical needle or a tapered needle and the processes involving high shear stresses.

1.3 Organization of the Dissertation

This dissertation comprises of seven chapters. Besides this chapter, it includes five manuscripts, followed by the conclusions drawn from this research.

Chapter 2 presents a literature review on the scaffold fabrication techniques and their advantages and disadvantages. The technical features of the dispensing-based RP method are highlighted and the issues involved in this technique are also discussed.

Chapter 3 describes the modeling of dispensing-based tissue scaffold fabrication processes. In particular, it includes an improved model of the flow rate in the dispensing process by considering the slip between the biomaterial being dispensed and the needle wall. It also presents the development of a model for the pore size and porosity of the scaffolds fabricated.

Chapter 4 deals with the cell damage in the cell-encapsulated dispensing process. Particularly, a cell damage law that relates cell damage to the force and force exposure time was established and then was applied to the bio-dispensing process employing a cylindrical needle to predict the cell damage percent in the process. Cell damage percents under different process control conditions were investigated and the models developed were validated by comparing the experimental and simulation results.

Chapter 5 presents a comparative study on the performance between the bio-dispensing process using cylindrical needles and the one using tapered needles. The flow rate and the cell damage percents are used for the performance comparison. The flow rates dispensed by means of the cylindrical and tapered needles, respectively, were modeled based on the identified non-Newtonian flow behaviours of the biomaterial; and the cell damage occurring in these two kinds of needles was represented based on the cell damage law established in Chapter 4.

Chapter 6 presents the development of a cell damage law for the cells that experience high stresses in the bio-fabrication process. Due to the fact that the time when cell damage occurs greatly differs between high and low stresses, the cell damage law established in Chapter 4 may not work well when applied to bio-dispensing processes involving high stresses. This chapter presents the development of a method to establish the cell damage law directly from the bio-dispensing process.

Chapter 7 presents the conclusions drawn from this research. This is followed by suggestions and recommendations for possible future work.

1.4 Contributions of the Primary Investigator

All papers are co-authored; however it is mutual understanding of the authors that Minggan Li, as the first author, is the primary investigator of the research work. The contributions of other authors are limited to an advisory and editorial capacity and they are acknowledged.

CHAPTER 2

REVIEW OF DISPENSING-BASED RAPID PROTOTYPING TECHNIQUES IN TISSUE SCAFFOLD FABRICATION

Published as:

- Li, M.G., Tian, X.Y., and Chen, X.B. (2009) A brief review of dispensing-based rapid prototyping techniques in tissue scaffold fabrication: role of modeling on scaffold properties prediction. Biofabrication. 1(3): 032001

2.1 Introduction and Objectives

This paper presents a brief review on the background of tissue engineering and the techniques developed for tissue scaffold fabrication. Particularly, the dispensing-based RP method was reviewed and evaluated; and the flow rate of dispensing, pore size and porosity of scaffolds fabricated and cell damage in the cell-encapsulated dispensing processes were discussed. This is a critical step in understanding the current challenges in dispensing-based RP techniques and establishing the objectives of this research work.

2.2 Justification of the Research

Dispensing-based rapid prototyping is a promising technique for tissue scaffold fabrication and has been widely used in the literature. But in despite of its various advantages, the control of fabrication process is proven to be a challenging task.

In the literature, the pore sizes and porosities of the fabricated scaffolds differed from the designed ones and this normally was neglected due to the difficulties in controlling the pore size and porosity. The determination of the actual pore size and porosity in the practice relied on trial-and-error method, which was not only costly but also time consuming. One of the objectives of this dissertation is to develop models to represent the fabrication process. By doing so, the process control can be greatly improved. Most importantly, based on the developed models, one can determine the operating conditions to achieve designed pore sizes and porosities.

Predicting cell damage in the cell involved fabrication process was also missing in the literature. Although some results were obtained from experiments and reported in the literature, the process conditions, including dispensing methods, air pressure, needle type and needle geometrical parameters, differ greatly. Thus the results obtained in one experiment may be not valid to another. To address this issue, a cell damage law, which relates cell damage to its cause, mechanical stress, is desired. By analyzing the stress distribution in the fabrication process and applying this cell damage law to it, one can predict cell damage percent in different fabrication processes with various process conditions. Based upon these issues, the second objective of this dissertation is set to develop mechanical stress induced cell damage law and apply it to different bio-dispensing fabrication processes to predict cell damage percents in them.

Biofabrication **1** (2009) 032001 (10pp) doi:10.1088/1758-5082/1/3/032001

TOPICAL REVIEW

A brief review of dispensing-based rapid prototyping techniques in tissue scaffold fabrication: role of modeling on scaffold properties prediction

M G Li[1], X Y Tian[2] and X B Chen[1]

[1] Department of Mechanical Engineering, University of Saskatchewan, Saskatoon, Saskatchewan S7N 5A9, Canada
[2] Division of Biomedical Engineering, University of Saskatchewan, Saskatoon, Saskatchewan S7N 5A9, Canada

E-mail: mil715@mail.usask.ca

Received 23 May 2009
Accepted for publication 31 July 2009
Published 21 August 2009
Online at stacks.iop.org/BF/1/032001

Abstract
Artificial scaffolds play vital roles in tissue engineering as they provide a supportive environment for cell attachment, proliferation and differentiation during tissue formation. Fabrication of tissue scaffolds is thus of fundamental importance for tissue engineering. Of the variety of scaffold fabrication techniques available, rapid prototyping (RP) methods have attracted a great deal of attention in recent years. This method can improve conventional scaffold fabrication by controlling scaffold microstructure, incorporating cells into scaffolds and regulating cell distribution. All of these contribute towards the ultimate goal of tissue engineering: functional tissues or organs. Dispensing is typically used in different RP techniques to implement the layer-by-layer fabrication process. This article reviews RP methods in tissue scaffold fabrication, with emphasis on dispensing-based techniques, and analyzes the effects of different process factors on fabrication performance, including flow rate, pore size and porosity, and mechanical cell damage that can occur in the bio-manufacturing process.

(Some figures in this article are in colour only in the electronic version)

1. Introduction

Tissue engineering has advanced to meet the tremendous need for the repair or replacement of damaged tissues and organs, by applying the principles of biology and engineering to develop artificial tissue substitutes [1–4]. Scaffolds are used to mimic the extracellular matrix by providing nutrients, oxygen and growth factors, encouraging cell proliferation and supporting the tissue in its 3D structure [5]. Tissue scaffolds play a vital role in tissue engineering, and advancing techniques for their fabrication are of fundamental importance.

A variety of scaffold fabrication techniques have been explored and can be classified into two categories—conventional techniques and rapid prototyping (RP) methods—based on the channeling micro-architectures they create [6]. Conventional techniques include solvent casting and particulate leaching [7], solution casting [8], freeze drying [9–11], phase separation [12], gas forming [13], melt molding [14], fiber bonding [15] and electrospinning [16, 17]. These techniques are summarized and analyzed in other reviews [6, 18, 19]. Conventional scaffold fabrication techniques

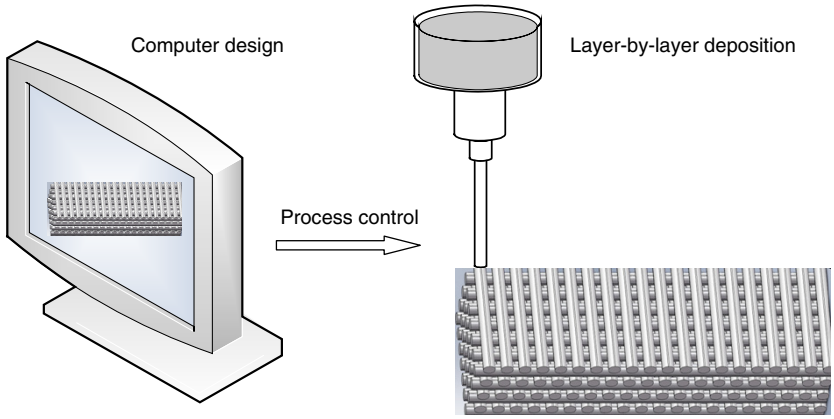

Figure 1. Schematic of RP fabrication of tissue scaffolds.

lack precise control over pore size, pore interconnectivity, porosity and spatial distribution of pores within the scaffold. These techniques are also incapable of incorporating cells and proteins in the fabrication process because they are normally implemented under harsh conditions such as high temperature or in the presence of organic solvents.

To overcome these disadvantages, RP techniques have been introduced for the fabrication of tissue scaffolds. Customized three-dimensional (3D) scaffold models can be designed using computer-aided design (CAD) technology; the models are then used to drive an RP machine to deposit biomaterial/cells in a layer-by-layer fashion (figure 1). As RP techniques are able to fabricate scaffolds with designed microstructure and allow for the incorporation of living cells and protein/growth factors in the fabrication process, they are currently widely employed in tissue engineering.

Although a range of techniques exist, dispensing processes are often employed in RP techniques to deposit minute amounts of material at designated positions to form the required 3D structure. To accurately deposit a designated volume of material at each position, the flow rate and speed of the dispensing head must be carefully controlled or the material will stack or break. In direct writing techniques, dispensed materials are piled up directly layer-by-layer to form 3D scaffolds. Upon deposition, the dispensed strands may deform to some extent due to the viscoelasticity of the polymer material, causing deviations in the scaffold pore size and porosity. Thus, understanding both the mechanical properties of the scaffold material and the effect of process parameters on pore size and porosity are important. In recent years, cells have been incorporated into scaffold construction materials and dispensed to form scaffold-based cell-seeded implants that mimic the microstructure of native tissues. During the dispensing process, cells are subjected to continuous mechanical force, which may cause cell damage and a failure to achieve the desired cell number and cell distribution in the scaffold.

This article reviews RP techniques in tissue engineering, with special focus on dispensing-based techniques, and analyzes both the effects of different process factors on fabrication performance, including flow rate, pore size and porosity, and mechanical cell damage in the fabrication process.

2. Dispensing-based rapid prototyping techniques in tissue engineering

To address the limitations of conventional scaffold fabrication techniques, RP principles have been employed to fabricate complex scaffolds with customized external shape and reproducible internal microstructure. These techniques can enable the fabrication of vascular networks in the scaffolds, thereby facilitating the transfer of nutrients to the scaffolds and improving the survival of larger tissue constructs after implantation. To date, various RP techniques have been successfully applied in tissue engineering (table 1) and have been well reviewed elsewhere [6, 18, 20–26]. In these techniques, a number of mechanical means have been used to deliver scaffold materials. Roller extruders have been used to deliver semi-molten polymer fiber [27]. Because the polymer fiber is not in a liquid phase, this method does not require a nozzle at the material exit to regulate fiber shape. Two rollers drive the fiber forward, and thus material clogging may be avoided. Vacuum pump [28] and pipette [29] methods have been used to transfer massive material where the accuracy of volume control is not necessarily required. A jetting method [30] was inspired by printer technologies, and most equipment used in tissue engineering applications to date has been adapted from commercial printers. This method utilizes thermal bubble or piezoelectric ceramics to drive small amounts of fluid material out of a needle, forming small fluid droplets. This method has been successfully used to create 3D scaffolds and print living cells [31]. Powder rolling has been utilized to supply solid particles by resurfacing the work layer [32]. Overall, dispensing is the most widely used method in tissue scaffold fabrication for material delivery due to its ability to adapt to different material states from thin liquid to thick paste. Unlike vacuum pump, pipette or powder rolling techniques, which are easy to control, or roller extrusion or jetting, which are normally adapted from commercial machines, dispensing devices in tissue engineering are usually developed in-house by researchers.

Table 1. RP techniques for tissue engineering.

Technology	Mechanism of 3D formation	Material delivery	Material state	References
Non-dispensing-based approaches				
Fused deposition modeling	Cool to solidify	Roller extruder	Semi-molten	[27, 33, 34]
Micromolding	Solvent evaporation	Vacuum pump	Liquid	[28]
Stereolithography	Crosslink	Pipette	Liquid	[29, 35]
Ink-jetting	Crosslink	Jetting	Liquid	[30, 31, 36]
Selective laser sintering	Material fuse	Powder rolling	Solid	[32]
Dispensing-based approaches				
Precision extrusion manufacturing	Cool to solidify	TP[a]	Semi-molten	[37]
Microsyringe deposition	Solvent evaporation	TP	Liquid	[28, 38]
3D plotting	Moisture cure	TP	Liquid	[39]
Robotic dispensing	Crosslink	TP	Liquid or paste	[40]
3D-printing™	Crosslink, high yield stress	TP	Liquid, paste	[41–44]
Cell assembly	Crosslink	TP	Liquid	[45–49]
Photopatterning	Crosslink	TP	Liquid	[50]
Direct writing	Crosslink	TP & PD	Liquid	[51]
Bioassembly	Crosslink	TP or PD	Liquid	[52–54]
Multi-nozzle deposition manufacturing	Lower temp. frozen	TP & RS	Liquid	[55]
Precision extrusion	Cool to solidify	RS	Semi-molten	[56, 57]
Low-temperature deposition manufacturing	Lower temp. frozen	RS	Slurry	[58]
Robocasting	High yield stress	PD	Colloid	[59]
3D fiber deposition	Cool to solidify	PD	Semi-molten	[33]

[a] Abbreviations for dispensing approaches: TP, time pressure; PD, positive displacement; RS, rotary screw.

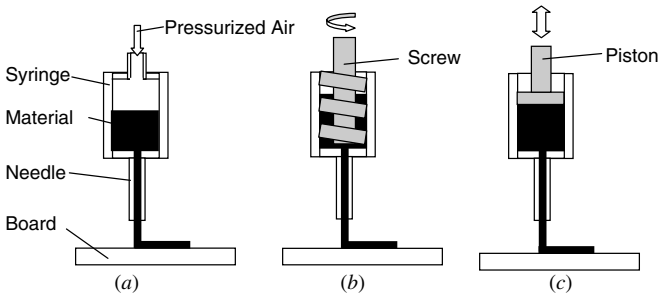

Figure 2. Schematic of fluid dispensing approaches, (*a*) time pressure, (*b*) rotary screw, and (*c*) positive displacement.

Three kinds of dispensing approaches are generally employed: time pressure, positive displacement and rotary screw (figure 2). Time-pressure dispensing utilizes pressurized air to drive fluid out of the needle. The amount of fluid dispensed is controlled by regulating the magnitude and duration of pressurized air. Rotary-screw dispensing utilizes the rotation of a motor-driven screw to move fluid down a syringe and then out of a needle. A large pressure can be produced in the fluid at the syringe bottom due to the spiral screw configuration. In positive-displacement dispensing, fluid in the syringe is driven by the linear movement of a piston to force fluid out of the needle.

Time-pressure approaches are flexible for adapting to multiple application situations and are simple to operate systems with easy maintenance. Due to these benefits, the time-pressure approach is a popular dispensing method in tissue engineering and has been used to dispense different states of material including pure liquids [28], pastes [43] and semi-molten polymers [37] (table 1). The main disadvantage of this method is that fluid viscosity and air compressibility in the syringe significantly affect the amount of fluid dispensed [60]. Furthermore, due to the limitation of supplied air pressure, the dispensing nozzle may become blocked by the particles in paste materials if the nozzle diameter to particle size ratio is too small [61]. Compared to the time-pressure approach, rotary-screw methods provide a major improvement in control over small volume fluid dispensing. In this approach, minute amounts of fluid can be dispensed by accurate control of the screw rotation. However, the complex configuration of the mechanism reduces its popularity for scaffold fabrication applications. Positive displacement provides a distinct advantage in that the volume of fluid dispensed is only dependent on the mechanical movement of the piston. However, while this advantage is present under conditions of continuous piston movement, the advantage is lost when dispensing very small amounts of material due to the effects of fluid compressibility as well as the inertia of both the piston and the mechanism used to drive the piston [62].

Dispensing approaches are selected depending upon the desired application. Time pressure is a simple approach that can theoretically dispense different kinds of material from liquid to paste. However, due to limitations with the supplied air pressure, extruding material with a very fine nozzle is difficult; rotary-screw or positive-displacement methods are better options for very thick material applications.

3. Flow rate control for dispensing-based scaffold fabrication

In dispensing-based scaffold fabrication processes, the speed of the dispensing head must be carefully selected to produce continuous strands without material stacking or strand breakage. Assuming that the diameter of the strands formed is equal to the internal diameter of the needle by ignoring material swelling, the speed (V) of the dispensing head can be determined by [63]

$$V = \frac{4Q}{\pi D^2} \tag{1}$$

where Q is the volumetric flow rate and D is the diameter of the strands. The appropriate dispensing head speed is dependent on or determined by the flow rate in the dispensing process.

Many parameters in the dispensing process affect the flow rate. Operational parameters, such as air pressure applied for time pressure, screw angular speed for rotary screw and piston linear speed for positive displacement, directly contribute to the driving force. The viscous resistance produced by the scaffold construction materials impedes the fluid flow. In tissue engineering, the scaffold materials employed are normally polymers, which possess non-Newtonian fluid behavior, and the resistance force produced by these fluids cannot be simply obtained from a linear relationship. Instead, the resistance depends upon their non-Newtonian flow behavior, which is usually expressed by the generalized power-law equation [63]:

$$\tau = \tau_0 + K\dot{\gamma}^n \tag{2}$$

where τ is the shear stress, τ_0 the yield stress at which the fluid yields and starts to flow, $\dot{\gamma}$ is the shear rate, and K and n are the consistency index and flow behavior index, respectively, which are constants for a given fluid.

The geometries of different dispensing setups, such as the needle diameter and length, act as the boundaries of the fluid flow and thus affect the flow rate. Generally, the flow rate (Q) in the dispensing process is a function of operational parameters (O_p), flow behaviors (F_b) and geometry parameters (G_p), i.e.

$$Q = f(O_p,\ F_b,\ G_p). \tag{3}$$

Numerous efforts to find the flow rate function, f, have been reported in the literature for different dispensing approaches. For time-pressure dispensing approaches, the flow rates in most reported studies were determined by trial and error [40, 42, 56]. An improvement to this approach came with the application of the Hagen–Poiseuille law to the development of models of the flow rate in the scaffold fabrication process [38, 64], under the assumption of a fully developed laminar Newtonian flow in the needle. According to these models, the flow rate can be related to operational parameters, fluid viscosity and geometry parameters as follows:

$$Q = \frac{\pi d^4 \Delta P}{128\eta L} \tag{4}$$

where d and L are the nozzle diameter and length, respectively, η is the viscosity of the material and ΔP is the pressure drop applied in the dispensing needle.

The limitation of this model is the assumption of Newtonian flow in the dispensing nozzle, as most scaffold materials are high-molecular-weight polymers that behave in a non-Newtonian fashion. Non-Newtonian fluid behaviors of polymer solutions and colloid gels were investigated in [65, 66]. In these studies, the non-Newtonian fluid behaviors of the material were examined and expressed in the form of equation (1), and then flow rate models to reflect the non-Newtonian properties of the material were developed. For non-Newtonian polymer solutions, the flow rate is governed by [65]

$$Q = \left(\frac{n}{3n+1}\right)\pi\gamma_0^{\frac{n-1}{n}}\left(\frac{\Delta P}{2\eta_0}\right)^{1/n} R^{\frac{3n+1}{n}} \tag{5}$$

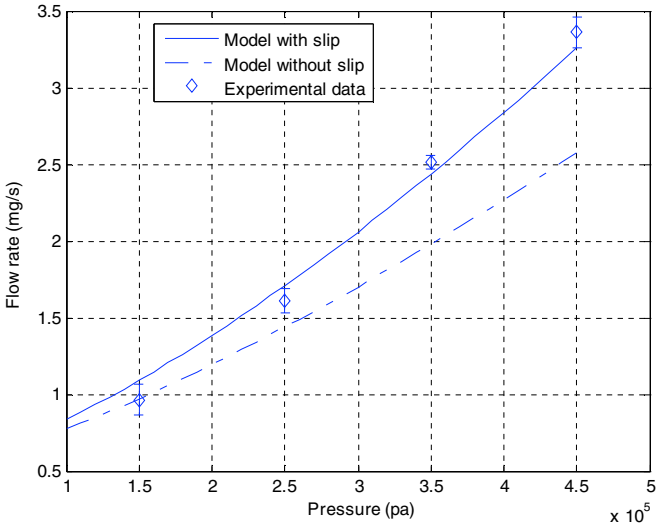

Figure 3. Flow rate model with and without consideration of wall slip. The discrepancy between these two models suggests that wall slip significantly affects the flow rate [68]. The material used in this study is a mixture of 45% of hydroxylapatite in 3% of chitosan solution.

where η_0 is the limited viscosity at low shear rates and the constant γ_0 is the corresponding shear rate.

In scaffold fabrication processes, nozzle diameters are normally very small. As a result, the effect of the surface tension of the material being dispensed becomes significant and affects the dispensing process. By taking into account the surface tension, the pressure difference between the inside and the outside of the material is given by

$$P_s = \frac{2\sigma}{D} \tag{6}$$

where σ is the surface tension of the material and D is the diameter of the dispensing nozzle. For example, the surface tension of water is 0.071 N m^{-1} at room temperature, and the pressure difference across the water interface at the nozzle exit comes out to be 2840 Pa if water is dispensed by means of a nozzle with a diameter of 0.1 mm. Recognizing this significance, such an effect was considered in the model development of the flow rate, as reported in [67].

In some direct writing RP techniques, colloidal gels, which are mixtures of fine particles and high-molecular-weight polymers, are dispensed to fabricate scaffolds. To describe the flow of colloidal gel in the dispensing needle, the slip between the shear flow and the needle wall should be considered due to the interactions of the solid fine particles and high-molecular-weight polymer solution [68]. This wall slip significantly influences the flow rate during dispensing, and a model to include this effect was developed to better predict the flow rate for scaffold fabrication [63] (figure 3). Furthermore, fluid flow behaviors change with temperature; this effect must be taken into account as it can greatly affect the flow rate [69] or strand width and height [70] during dispensing.

A flow rate model has also been developed for the rotary-screw approach [71]. In addition to the angular speed of the screw, increasing air pressure in the material reservoir can also

increase the flow rate. In positive-displacement dispensing processes, the steady-state flow is solely dependent upon the speed of the moving piston. However, for dispensing very small amounts of fluid material, the fluid compressibility and the inertia of the driving mechanism can cause a dynamic or variable flow rate [62].

In summary, these models provide technical means to predict the flow rate of the material dispensed, thereby avoiding the trial and error processes for scaffold fabrication. Depending on applications, the assumptions made are critical for modeling the flow rate in the dispensing-based scaffold fabrication. Given that most of scaffold materials used in RP tissue engineering are high-molecular-weight polymers, the non-Newtonian behaviors of the material must be recognized to develop accurate flow rate models. If solid particles are involved in the dispensing process, the influence of wall slip must also need to be considered.

4. Pore size and porosity modeling in paste direct writing fabrication

Paste direct writing fabrication is a promising technique for tissue scaffold fabrication because it does not involve a high-temperature process [55, 72] or need organic solvents and local radiation [61, 73]. These conditions meet the requirements for the manipulation of living cells and biomolecules (e.g. growth factors) for fabricating 3D tissue constructs [22]. Due to the viscoelasticity of the pastes, the strands of the scaffold once dispensed will deform and fuse together. As a result, the actual pore size and porosity of the scaffolds decrease from those designed. For example, pore sizes in the vertical direction can decrease up to 50% compared to design values [72]. This discrepancy is often neglected in the literature due to the difficulty in predicting the actual pore size. However, pore size and porosity can significantly influence the mechanical properties of the scaffolds, which may greatly degrade the scaffold performance as applied in tissue engineering [18].

4.1. Influence of pore size and porosity on scaffold mechanical properties

Mechanical properties of a tissue scaffold are typically characterized by the stress–strain relationship under a mechanical load on the scaffold. The requirement for tissue scaffolds is that they should not only support cell growth and tissue formation *in vitro*, but also maintain the load from peripheral tissues after implantation *in vivo*, without showing symptoms of fatigue and failure. To design tissue scaffolds with desired mechanical properties for a specific application, mathematical models are often used to estimate the mechanical properties based on the microstructure of scaffolds, including pore size and porosity [21, 74].

A finite element method (FEM) has been widely employed to predict the mechanical properties [74–76]. In this method, the periodical unit cell (or representative volume element) is meshed and analyzed, and one surface of the unit cell is held stationary while the opposite surface experiences mechanical forces. Based on the information of known stresses through the applied forces, the surface area, and unit cell deformation as well, the effective stiffness $[C]^{\text{eff}}$ of the unit cell can be obtained [74]:

$$[C]^{\text{eff}} = \frac{1}{|V_{\text{RVE}}|} \int_{V_{\text{RVE}}} [C][M]\, \mathrm{d}V_{\text{RVE}} \tag{7}$$

where V_{RVE} is the volume of representative volume element, $[C]$ is the material stiffness and $[M]$ is the local structure matrix. Pore size changes lead to the variation of the local structure matrix, and thus the mechanical property of the scaffolds, as seen from the above equation. For a given volume of a unit cell, the increase in porosity means the decrease in the amount of material, thereby reducing the stiffness of the scaffold. In the aforementioned studies, the mechanical properties of the scaffold materials are assumed to be linear elastic. However, this is not true since most of the scaffold materials are high-molecular-weight polymers, which often posses nonlinear mechanical properties. For improvement, the nonlinear constitutive material models were used in [77] to better predict the mechanical properties of cell-seeded alginate scaffolds.

The above models can be used to well represent the mechanical properties of tissue scaffolds upon the fabrication of the scaffolds. However, with scaffold degradation as well as cell growth on the scaffold, the mechanical properties vary with time, exhibiting their time dependence, and the model developed for the initial stage of scaffolds may no longer be valid after a certain time period. To address this problem, methods based on the concept of model updating seem to be promising. Model updating is a method to improve the accuracy of a model by updating model parameters that are considered to be less accurately known. In the method reported in [78, 79], model updating was adopted and used to update the parameters of the model for the mechanical properties in order to account for the influence of cell growth and scaffold degradation. In particular, this method involves (1) developing a finite element model for the effective mechanical properties of the scaffold by employing numerical techniques; (2) parameterizing the finite element model by selecting parameters associated with the scaffold microstructure and material properties, both varying with cell growth and scaffold degradation; and (3) identifying the selected parameters as functions of time based on measurements from compressive tests on the scaffolds. Thus, the finite element model developed with the so-identified time-variable parameters allows for the prediction of the mechanical properties of tissue scaffolds. The ability to predict the time-dependent mechanical properties of tissue scaffold would represent a major advance in tissue engineering, as it would allow one to design/determine the scaffold microstructure with the mechanical properties appropriate for a given application.

4.2. Modeling of pore size and porosity of scaffolds

The pore size and porosity of a scaffold affect not only its mechanical properties but also its biological properties. For

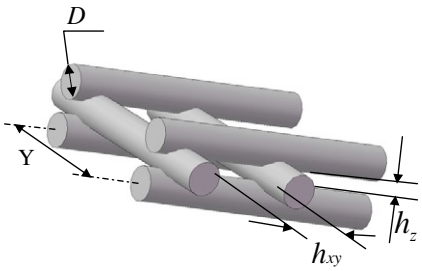

Figure 4. Schematic of the internal structure of tissue scaffolds made from RP techniques. h_z is the vertical pore size and h_{xy} is the horizontal pore size.

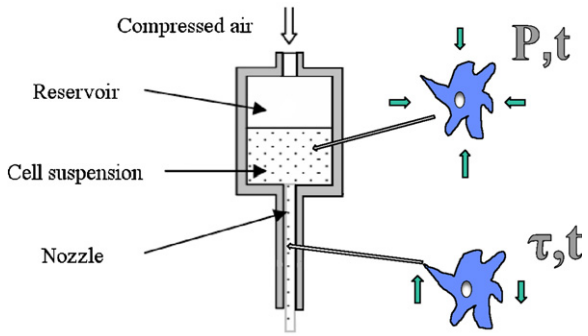

Figure 5. Schematic representation of stresses on cells in dispensing-based bio-manufacturing processes.

example, rates of both tissue growth and extracellular matrices deposition increase with the porosity [80], and cells may not grow in scaffolds or matrices where the pore sizes are too small [81] as the pore size can affect cell formation and cell attachment [15]. Moreover, porosity down to a certain range may lead to poor scaffold mechanical properties [74]. Thus, fabricating a scaffold with desired pore size and porosity is of extreme importance in tissue engineering but remains a challenge.

In most published studies, the fabricated pore size has been assumed to be equal to the designed pore size. While this may be reasonable in the horizontal direction, the pore size in the vertical direction will be significantly reduced due to fusion of two contacting strands (figure 4). To better predict the pore size in the vertical direction, a mathematical model has recently been developed in which the vertical pore size was derived from the depth that two strands fused into each other based on the mechanical properties of the scaffold material [63].

Li *et al* [63] reported that the elasticity limit stress of the paste was found to play an important role in the deformation of the dispensed strands, and the depth of two strands fused together was derived to calculate the vertical pore size. The authors also suggest that the material should be sufficiently stiff to support the strands in the gaps and avoid collapse of the scaffold structure.

Several porosity models use designed geometry based on a unit cell of the scaffold [64, 65]. As the strands fuse together once dispensed, resulting in compression of the void space in the scaffold, and the resulting porosity is smaller than the model prediction. This was taken into consideration in the porosity model developed in [63] to predict the vertical pore size. As both the void volume and the apparent volume of the scaffolds were derived from the squeezed vertical pore size, this model can more accurately represent the actual porosity of fabricated scaffolds.

In paste direct writing fabrication, the mechanical properties of the dispensed material greatly affect pore size and porosity: the stiffer the paste, the more likely the scaffold keeps its 3D structure. Elasticity limit stress is a good measure of the stiffness of paste-like materials used in scaffold fabrication; pore size and porosity can also be predicted based on this physical property.

5. Mechanical cell damage in dispensing-based bio-manufacturing processes

5.1. Cell damage in current applications

In recent years, cell-seeded implants have been developed based on the scaffolds that both mimic the microstructure of native tissues and incorporate biomolecules. Different mechanical manipulation techniques have been employed in their construction, including bio-dispensing cell deposition [39, 52, 82], inkjet-based cell printing [30, 83–85] and photo- and electro-patterning [86, 87]. Among them, dispensing-based bio-manufacturing is a promising technique due to its capacity for fast and efficient material processing. In dispensing-based bio-manufacturing processes, cells are encapsulated in a biocompatible material and then extruded and delivered to designated targets in a controllable manner.

During dispensing-based bio-manufacturing, cells are subjected to the pressure (P) in the reservoir and the shear stress (τ) in the nozzle (figure 5). Within a physiological range, these forces elicit both acute and chronic adaptive responses. If the stresses exceed certain thresholds and/or the stresses are applied beyond a certain time period, the cell membrane may succumb to the force, resulting in cell damage [88]. In dispensing-based bio-manufacturing, the pressures and the shear stresses are functions of process parameters: the pressure applied in the syringe, the needle length and the needle diameter. It is reported in the study [89] that pressures lower than 5 MPa do not affect cell viability. Thus, the cell damage during dispensing is mainly attributed to the shear stresses in the nozzle. Cell damage increases with applied pressure; larger needle diameters reduce cell damage [90]. Thus, cell damage varies in different applications and is a function of process and geometrical parameters [90]. Figure 6, for example, shows the results adapted from the experimental study, reported in [84], on the cell damage by applying different air pressures and using different sizes of the nozzle diameter. The variations of cell damage were also observed in other studies. Cell damage has been reported during the various dispensing processes at 40% for fibroblasts [53], 2% for hepatocytes [47], 15.7–31.4% of the control value in HepG2 cells [82] and 6% for chondrocytes [52]. Although the cell damage during the fabrication can be measured and investigated experimentally, a systematic method or model to relate cell damage to the bio-dispensing

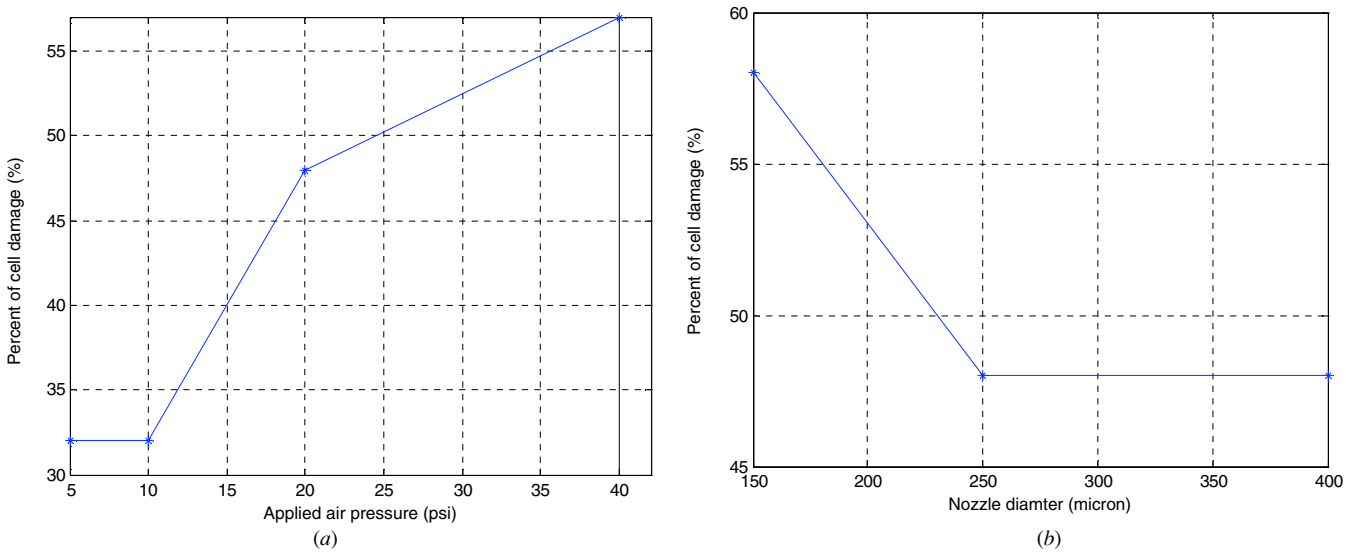

Figure 6. Cell damage as a function of (*a*) air pressure and (*b*) nozzle diameter (adapted from [84]).

process parameters has not yet been developed. Such a model is essential for reproducible control over the distribution of cells within the cell-seeded scaffolds.

5.2. Cell damage prediction strategy

To develop a model to predict cell damage during the dispensing process, a relationship is needed to correlate the cell damage with mechanical force and exposure time. This can be obtained through experiments applying different stress levels with varying time courses and recording cell damage at each condition. A power-law function can be used to describe the cell damage (I) under different shear conditions and can be expressed as [91]

$$I(\%) = Ct^a\tau^b \tag{8}$$

where τ is the shear stress applied to the cells for exposure time t, and C, a and b are constants that can be obtained through regression.

Establishing such a relationship between the cell damage and the mechanical, referred as the cell damage law in the literature, is crucial for cell damage prediction as the shear stresses in the radial direction in the dispensing nozzle are not uniform and their exposure times vary due to the nonlinear fluid velocity distribution in the nozzle. Through stress and velocity derivation, the shear stress and time for cells to travel through the nozzle can be obtained. The stresses and exposure time can then be applied to the cell damage law to predict the cell damage in the dispensing process.

Further development and application of this cell damage law are very important for the prediction of cell damage that occurs during different bio-dispensing processes. It will not only increase our understanding of mechanical force-induced cell damage but also allow for the estimation of cell damage under complex stress conditions. Most importantly, its incorporation into a cell damage model for the bio-dispensing process will help minimize cell damage in the process and control cell distribution in scaffolds.

6. Conclusions and future perspectives

RP techniques are very promising for tissue engineering applications as they allow for the fabrication of tissue scaffolds with defined external shape and internal architecture as well as construction of cell-seeded implants with desired cell and nutrient distributions. Dispensing is widely used in different RP techniques to deliver minute volumes of material with precise placement. Three RP dispensing approaches are routinely used for scaffold construction in tissue engineering; the limitations of each method determine which is appropriate for a given application. Development of a simple and robust dispensing d[7] ce that could handle a large range in viscosity of construction materials without complex maintenance would extend the possible applications of dispensing in tissue engineering.

Flow rate models for different dispensing approaches have been developed and successfully applied in tissue scaffold fabrication processes. To improve the reported flow rate models, the influence of temperature on the flow behavior of scaffold construction materials should be investigated to inform applications under different temperatures. In addition, the particle-like phase formed when cells are incorporated into scaffold fabrication may change the fluid flow in the nozzle and affect the flow rate model.

Methods to predict pore size and porosity are not fully developed due to the complex fabrication process and the microstructure of scaffolds. Development of online control of flow rate and pore size/porosity in the future will advance scaffold fabrication applications. The ability to predict cell damage during dispensing-based bio-manufacturing would allow for the optimization of process parameters to minimize cell damage and precisely control cell distribution in tissue constructs.

Acknowledgments

The financial support from the Saskatchewan Health Research Foundation (SHRF) and the Natural Science and Engineering Research Council (NSERC) of Canada to the present study is acknowledged.

References

[1] Fuchs J R, Nasseri B A and Vacanti J P 2001 Tissue engineering: a 21st century solution to surgical reconstruction *Ann. Thorac. Surg.* **72** 577–91
[2] Langer R and Vacanti J P 1993 Tissue engineering *Science* **260** 920–6
[3] Niklason L E and Langer R 2001 Prospects for organ and tissue replacement *JAMA* **285** 573–6
[4] Stock U A and Vacanti J P 2001 Tissue engineering: current state and prospects *Ann. Rev. Med.* **52** 443–51
[5] Whitaker M J, Quirk R A, Howdle S M and Shakesheff K M 2001 Growth factor release from tissue engineering scaffolds *J. Pharm. Pharmacol.* **53** 1427–37
[6] Sachlos E and Czernuszka J T 2003 Making tissue engineering scaffolds work. Review: the application of solid freeform fabrication technology to the production of tissue engineering scaffolds *Eur. Cell. Mater.* **5** 29–40
[7] Mikos A G, Thorsen A J, Czerwonka L A, Bao Y, Langer R, Winslow D N and Vacanti J P 1994 Preparation and characterization of poly(L-lactic acid) foams *Polymer* **35** 1068–77
[8] Schmitz J P and Hollinger J O 1988 A preliminary study of the osteogenic potential of a biodegradable alloplastic-osteoinductive alloimplant *Clin. Orthop. Relat. Res.* **237** 245–55
[9] Whang K, Thomas C H, Healy K E and Nuber G 1995 A novel method to fabricate bioabsorbable scaffolds *Polymer* **36** 837–42
[10] Hsu Y Y, Gresser J D, Trantolo D J, Lyons C M, Gangadharam P R and Wise D L 1997 Effect of polymer foam morphology and density on kinetics of *in vitro* controlled release of isoniazid from compressed foam matrices *J. Biomed. Mater. Res.* **35** 107–16
[11] Schoof H, Apel J, Heschel I and Rau G 2001 Control of pore structure and size in freeze-dried collagen sponges *J. Biomed. Mater. Res.* **58** 352–7
[12] Lo H P and Leong K W 1995 Fabrication of controlled release biodegradable foams by phase separation *Tissue Eng.* **1** 15–28
[13] Mooney D J, Baldwin D F, Suh N P, Vacanti J P and Langer R 1996 Novel approach to fabricate porous sponges of poly(D, L-lactic-co-glycolic acid) without the use of organic solvents *Biomaterials* **17** 1417–22
[14] Thompson R C, Yaszemski M J, Powers J M and Mikos A G 1995 Fabrication of biodegradable polymer scaffolds to engineering trabecular bone *J. Biomater. Sci-Polym.* E **7** 23–38
[15] Cima L G, Vacanti J P, Vacanti C, Inger D, Mooney D J and Langer L 1991 Tissue engineering by cell transplantation using degradable polymer substrates *J. Biomech. Eng.* **113** 143–51
[16] Li W J, Laurencin C T, Caterson E J, Tuan R S and Ko F K 2002 Electrospun nanofibrous structure: a novel scaffold for tissue engineering *J. Biomed. Mater. Res.* **60** 613–21
[17] Ma Z, Kotaki M, Inai R and Ramakrishna S 2005 Potential of nanofiber matrix as tissue-engineering scaffolds *Tissue Eng.* **11** 101–9
[18] Hutmacher D W 2000 Scaffolds in tissue engineering bone and cartilage *Biomaterials* **21** 2529–43
[19] Lu L and Mikos A G 1996 The importance of new processing techniques in tissue engineering *MRS Bull.* **21** 28–32
[20] Fedorovich N E, Alblas J, de Wijn J R, Hennink W E, Verbout A J and Dhert W J 2007 Hydrogels as extracellular matrices for skeletal tissue engineering: state-of-the-art and novel application in organ printing *Tissue Eng.* **13** 1905–25
[21] Hollister S J 2005 Porous scaffold design for tissue engineering *Nature Mater.* **4** 518–24
[22] Hutmacher D W, Sittinger M and Risbud M V 2004 Scaffold-based tissue engineering: rationale for computer-aided design and solid free-form fabrication systems *Trends Biotechnol.* **22** 354–62
[23] Wang X, Yan Y and Zhang R 2007 Rapid prototyping as a tool for manufacturing bioartificial livers *Trends Biotechnol.* **25** 505–13
[24] Yeong W Y, Chua C K, Leong K F and Chandrasekaran M 2004 Rapid prototyping in tissue engineering: challenges and potential *Trends Biotechnol.* **22** 643–52
[25] Lee J, Cuddihy M J and Kotov N A 2008 Three-dimensional cell culture matrices: state of the art *Tissue Eng.* B **14** 61–86
[26] Peltola S M, Melchels F P, Grijpma D W and Kellomaki M 2008 A review of rapid prototyping techniques for tissue engineering purposes *Ann. Med.* **40** 268–80
[27] Zein I, Hutmacher D W, Tan K C and Teoh S H 2002 Fused deposition modeling of novel scaffold architectures for tissue engineering applications *Biomaterials* **23** 1169–85
[28] Vozzi G, Flaim C, Ahluwalia A and Bhatia S 2003 Fabrication of PLGA scaffolds using soft lithography and microsyringe deposition *Biomaterials* **24** 2533–40
[29] Dhariwala B, Hunt E and Boland T 2004 Rapid prototyping of tissue-engineering constructs, using photopolymerizable hydrogels and stereolithography *Tissue Eng.* **10** 1316–22
[30] Varghese D, Deshpande M, Xu T, Kesari P, Ohri S and Boland T 2005 Advances in tissue engineering: cell printing *J. Thorac. Cardiovasc. Surg.* **129** 470–2
[31] Boland T, Tao X, Damon B J, Manley B, Kesari P, Jalota S and Bhaduri S 2007 Drop-on-demand printing of cells and materials for designer tissue constructs *Mater. Sci. Eng.* C **27** 372–6
[32] Tan K H, Chua C K, Leong K F, Cheah C M, Cheang P, Abu Bakar M S and Cha S W 2003 Scaffold development using selective laser sintering of polyetheretherketone-hydroxyapatite biocomposite blends *Biomaterials* **24** 3115–23
[33] Endres M, Hutmacher D W, Salgado A J, Kaps C, Ringe J, Reis R L, Sittinger M, Brandwood A and Schantz J T 2003 Osteogenic induction of human bone marrow-derived mesenchymal progenitor cells in novel synthetic polymer-hydrogel matrices *Tissue Eng.* **9** 689–702
[34] Bose S, Darsell J, Kintner M, Hosick H and Bandyopadhyay A 2003 Pore size and pore volume effects on alumina and TCP ceramic scaffolds *Mater. Sci. Eng.* C **23** 479–86
[35] Arcaute K, Mann B K and Wicker R B 2006 Stereolithography of three-dimensional bioactive poly(ethylene glycol) constructs with encapsulated cells *Ann. Biomed. Eng.* **34** 1429–41
[36] Radulescu D, Dhar S, Young C M, Taylor D W, Trost H J, Hayes D J and Evans G R 2007 Tissue engineering scaffolds for nerve regeneration manufactured by ink-jet technology *Mater. Sci. Eng.* C **27** 534–9
[37] Xiong Z, Yan Y N, Zhang R J and Sun L 2001 Fabrication of porous poly(L-lactic acid) scaffolds for bone tissue engineering via precise extrusion *Scr. Mater.* **45** 773–9
[38] Vozzi G, Previti A, De Rossi D and Ahluwalia A 2002 Microsyringe-based deposition of two-dimensional and three-dimensional polymer scaffolds with a well-defined geometry for application to tissue engineering *Tissue Eng.* **8** 1089–98

[39] Landers R and Mulhaupt R 2000 Desktop manufacturing of complex objects, prototypes and biomedical scaffolds by means of computer-assisted design combined with computer-guided 3D plotting of polymers and reactive oligomers *Macromol. Mater. Eng.* **282** 17–21

[40] Ang T H, Sultana F S A, Hutmacher D W, Wong Y S, Fuh J Y H, Mo X M, Loh H T, Burdet E and Teoh S H 2002 Fabrication of 3D chitosan-hydroxyapatite scaffolds using a robotic dispensing system *Mater. Sci. Eng.* C **20** 35–42

[41] Landers R, Pfister A, Hubner U, John H, Schmelzeisen R and Mulhaupt R 2002 Fabrication of soft tissue engineering scaffolds by means of rapid prototyping techniques *J. Mater. Sci.* **37** 3107–16

[42] Landers R, Hubner U, Schmelzeisen R and Mulhaupt R 2002 Rapid prototyping of scaffolds derived from thermoreversible hydrogels and tailored for applications in tissue engineering *Biomaterials* **23** 4437–47

[43] Lam C X F, Mo X F, Teoh S H and Hutmacher D W 2002 Scaffold development using 3D printing with a starch-based polymer *Mater. Sci. Eng.* C **20** 49–56

[44] Weinand C, Pomerantseva I, Neville C M, Gupta R, Weinberg E, Madisch I, Shapiro F, Abukawa H, Troulis M J and Vacanti J P 2006 Hydrogel-beta-TCP scaffolds and stem cells for tissue engineering bone *Bone* **38** 555–63

[45] Yan Y N, Wang X H, Pan Y Q, Liu H X, Cheng J, Xiong Z, Lin F, Wu R D, Zhang R J and Lu Q P 2005 Fabrication of viable tissue-engineered constructs with 3D cell-assembly technique *Biomaterials* **26** 5864–71

[46] Yan Y N, Wang X H, Xiong Z, Liu H X, Liu F, Lin F, Wu R D, Zhang R J and Lu Q P 2005 Direct construction of a three-dimensional structure with cells and hydrogel *J. Bioact. Compat. Polym.* **20** 259–69

[47] Wang X H *et al* 2006 Generation of three-dimensional hepatocyte/gelatin structures with rapid prototyping system *Tissue Eng.* **12** 83–90

[48] Liu H X, Yan Y N, Wang X H, Cheng J, Lin F, Xiong Z and Wu R D 2006 Construct hepatic analog by cell-matrix controlled assembly technology *Chin. Sci. Bull.* **51** 1830–35

[49] Xu W, Wang X H, Yan Y N, Zheng W, Xiong Z, Lin F, Wu R D and Zhang R J 2007 Rapid prototyping three-dimensional cell/gelatin/fibrinogen constructs for medical regeneration *J. Bioact. Compat. Polym.* **22** 363–77

[50] Liu V A and Bhatia S N 2002 Three-dimensional photopatterning of hydrogels containing living cells *Biomed. Microdev.* **4** 257–66

[51] Geng L, Feng W, Hutmacher D W, Wong Y, S,Loh H T and Fuh J Y H 2005 Direct writing of chitosan scaffolds using a robotic system *Rapid Proto. J.* **11** 90–97

[52] Cohen D L, Malone E, Lipson H and Bonassar L J 2006 Direct freeform fabrication of seeded hydrogels in arbitrary geometries *Tissue Eng.* **12** 1325–35

[53] Smith C M, Stone A L, Parkhill R L, Stewart R L, Simpkins M W, Kachurin A M, Warren W L and Williams S K 2004 Three-dimensional bioassembly tool for generating viable tissue-engineered constructs *Tissue Eng.* **10** 1566–76

[54] Smith C M, Warren W L, Hoying J B and Williams S K 2005 Utilizing a three-dimensional bioassembly tool to fabricate spatially organized multicellular vascular constructs *FASEB J.* **19** A160

[55] Yan Y N, Xiong Z, Hu Y Y, Wang S G, Zhang R J and Zhang C 2003 Layered manufacturing of tissue engineering scaffolds via multi-nozzle deposition *Mater. Lett.* **57** 2623–6

[56] Wang F, Shor L, Darling A, Khalil S, Sun W, Guceri S and Lau A 2004 Precision extruding deposition and characterization of cellular poly-epsilon-caprolactone tissue scaffolds *Rapid Proto. J.* **10** 42–9

[57] Shor L, Gueceri S, Gandhi M, Wen X and Sun W 2008 Solid freeform fabrication of polycaprolactone/hydroxyapatite tissue scaffolds *Trans. ASME, J. Manuf. Sci. Eng.* **130** 021018

[58] Xiong Z, Yan Y N, Wang S G, Zhang R J and Zhang C 2002 Fabrication of porous scaffolds for bone tissue engineering via low-temperature deposition *Scr. Mater.* **46** 771–6

[59] Therriault D, White S R and Lewis J A 2003 Chaotic mixing in three-dimensional microvascular networks fabricated by direct-write assembly *Nature Mater.* **2** 265–71

[60] Chen X B, Schoenau G and Zhang W J 2002 On the flow rate dynamics in time-pressure dispensing processes *Trans. ASME, J. Dyn. Syst. Meas. Control* **124** 693–8

[61] Xie B J, Parkhill R L, Warren W L and Smay J E 2006 Direct writing of three-dimensional polymer scaffolds using colloidal gels *Adv. Funct. Mater.* **16** 1685–93

[62] Chen X B and Kai J 2004 Modeling of positive-displacement fluid dispensing processes *IEEE Trans. Electron. Packag. Manuf.* **27** 157–63

[63] Li M G, Tian X Y and Chen X B 2009 Modeling of flow rate, pore size, and porosity for dispensing-based tissue scaffolds fabrication *Trans. ASME, J. Manuf. Sci. Eng.* **131** 034501

[64] Woodfield T B F, Malda J, de Wijn J, Peters F, Riesle J and van Blitterswijk C A 2004 Design of porous scaffolds for cartilage tissue engineering using a three-dimensional fiber-deposition technique *Biomaterials* **25** 4149–61

[65] Khalil S and Sun W 2007 Biopolymer deposition for freeform fabrication of hydrogel tissue constructs *Mater. Sci. Eng.* C **27** 469–78

[66] Smay J E, Cesarano J and Lewis J A 2002 Colloidal inks for directed assembly of 3-D periodic structures *Langmuir* **18** 5429–37

[67] Chen X B, Li M G and Ke H 2008 Modeling of the flow rate in the dispensing-based process for fabricating tissue scaffolds *Trans. ASME, J. Manuf. Sci. Eng.* **130** 021003

[68] Barnes H A 1995 A review of the slip (wall depletion) of polymer-solutions, emulsions and particle suspensions in viscometers—its cause, character, and cure *J. Non-Newton. Fluid Mech.* **56** 221–51

[69] Chen X B and Ke H 2006 Effects of fluid properties on dispensing processes for electronics packaging *IEEE Trans. Electron. Packag. Manuf.* **29** 75–82

[70] Kim J Y, Yoon J J, Park E K, Kim D S, Kim S Y and Cho D W 2009 Cell adhesion and proliferation evaluation of SFF-based biodegradable scaffolds fabricated using a multi-head deposition system *Biofabrication* **1** 1–7

[71] Chen X B 2007 Modeling of rotary screw fluid dispensing processes *J. Electron. Packag.* **129** 172–8

[72] Xu M J, Gratson G M, Duoss E B, Shepherd R F and Lewis J A 2006 Biomimetic silicification of 3D polyamine-rich scaffolds assembled by direct ink writing *Soft Matter* **2** 205–9

[73] Li Q and Lewis J A 2003 Nanoparticle inks for directed assembly of three-dimensional periodic structures *Adv. Mater.* **15** 1639–43

[74] Hollister S J, Maddox R D and Taboas J M 2002 Optimal design and fabrication of scaffolds to mimic tissue properties and satisfy biological constraints *Biomaterials* **23** 4095–103

[75] Fang Z, Starly B and Sun W 2005 Computer-aided characterization for effective mechanical properties of porous tissue scaffolds *Comput.-Aided Des.* **37** 65–72

[76] Estelles J M, Krakovsky I, Hernandez J C R, Piotrowska A M and Pradas M M 2007 Mechanical properties of porous crosslinked poly(ethyl-acrylate) for tissue engineering *J. Mater. Sci.* **42** 8629–35

[77] Nair K, Yan K C and Sun W 2008 A computational modeling approach for the characterization of mechanical properties of 3D alginate tissue scaffolds *J. Appl. Biomater. Biomech.* **6** 35–46

[78] Bawolin N K, Chen X B and Zhang W J 2007 A method for modeling time-dependant mechanical properties of tissue scaffolds *Proc. ICAM (Heilongjiang, China)*

[79] Bawolin N K, Li M G, Chen X B and Zhang W J 2008 Modeling of time-dependent elastic properties of tissue scaffolds *Proc. TERMIS-NA 2008 Annual Conf. & Exposition (CA, USA)*

[80] Mikos A G, Sarakinos G, Lyman M D, Ingber D E, Vacanti J P and Langer R 1993 Prevascularization of porous biodegradable polymers *Biotech. Bioeng.* **42** 716–23

[81] Sampath T K and Reddi A H 1984 Importance of geometry of the extracellular-matrix in endochondral bone differentiation *J. Cell Biol.* **98** 2192–7

[82] Khalil S, Nam J and Sun W 2005 Multi-nozzle deposition for construction of 3D biopolymer tissue scaffolds *Rapid Proto. J.* **11** 9–17

[83] Boland T, Mironov V, Gutowska V, Roth E A and Markwald R R 2003 Cell and organ printing 2: fusion of cell aggregates in three-dimensional gels *Anat Rec. A Discov. Mol. Cell. Evol. Biol.* A **272** 497–502

[84] Xu T, Jin J, Gregory C, Hickman J J and Boland T 2005 Inkjet printing of viable mammalian cells *Biomaterials* **26** 93–9

[85] Mironov V, Boland T, Trusk T, Forgacs G and Markwald R R 2003 Organ printing: computer-aided jet-based 3D tissue engineering *Trends Biotech.* **21** 157–61

[86] Albrecht D R, Tsang V L, Sah R L and Bhatia S N 2005 Photo- and electropatterning of hydrogel-encapsulated living cell arrays *Lab. Chip* **5** 111–8

[87] Albrecht D R, Underhill G H, Wassermann T B, Sah R L and Bhatia S N 2006 Probing the role of multicellular organization in three-dimensional microenvironments *Nature Meth.* **3** 369–75

[88] Barbee K A 2005 Mechanical cell injury *Ann. N. Y. Acad. Sci.* **1066** 67–84

[89] Parkkinen J J, Lammi M J, Inkinen R, Jortikka M, Tammi M, Virtanen I and Helminen H J 1995 Influence of short-term hydrostatic-pressure on organization of stress fibers in cultured chondrocytes *J. Orthop. Res.* **13** 495–502

[90] Chang R and Sun W 2008 Effects of dispensing pressure and nozzle diameter on cell survival from solid freeform fabrication-based direct cell writing *Tissue Eng.* A **14** 41–8

[91] Grigioni M, Daniele C, Morbiducci U, D'Avenio G, Di Benedetto G and Barbaro V 2004 The power-law mathematical model for blood damage prediction: analytical developments and physical inconsistencies *Artif. Org.* **28** 467–75

CHAPTER 3

MODELING OF FLOW RATE, PORE SIZE AND POROSITY FOR THE DISPENSING-BASED TISSUE SCAFFOLDS FABRICATION

Published as:

- Li, M.G., Tian, X.Y., and Chen, X.B. (2009) Modeling of flow rate, pore size and porosity for the dispensing-based tissue scaffolds fabrication. ASME Journal of Manufacturing Science and Engineering, 131: 034501

3.1 Introduction and Objectives

Porous solid scaffolds provide mechanical support and chemical cue for cell proliferation and tissue regeneration and have been widely used in tissue engineering. In this chapter, dispensing-based rapid prototyping technique was used to fabricate such scaffolds using the mixture of polymer solution and fine particles.

Since the biomaterial used is a mixture of fine particles and high molecular weight polymers, wall slip between the biomaterial and the needle wall exists, which is unfortunately ignored in the models reported in the literature. One of the objectives of this paper is to develop an improved model by considering the wall slip; and the other one is to develop models to represent the pore size and porosity of the scaffolds fabricated.

3.2 Methods

For the flow rate model improvement, the rheological behaviour of the biomaterials were characterized by using a cone-and-plate rheometer, and these behaviours were then applied to a wall slip model to represent the slip speed. The total flow rate is the summation of the flow rate due to slip and the flow rate due to shear. To develop models for the pore size and porosity, the yield stresses and elasticity limit stresses of the biomaterials were characterized by using the same rheometer and then the pore size at the contact field was expressed based on the material's obtained mechanical properties and the geometry of the contact field. The porosity model was then developed based on the pore size model.

3.3 Results

The results show that the flow rate model with the consideration of wall slip is more accurate than the ones reported in the literature. Also, the effectiveness of the pore size and porosity models was demonstrated by experiments.

3.4 Contributions

The contribution of this paper rests on the improvement of the flow rate model and the development of models to predict the pore size and porosity of scaffolds fabricated from dispensing-based RP techniques. With these models, it becomes possible to rationally determine the process parameters in order to achieve scaffolds with predefined microstructures, instead of using a trial and error process.

Modeling of Flow Rate, Pore Size, and Porosity for the Dispensing-Based Tissue Scaffolds Fabrication

M. G. Li
e-mail: mil715@mail.usask.ca

X. Y. Tian

X. B. Chen

Department of Mechanical Engineering,
University of Saskatchewan,
Saskatoon, SK, S7N 5A9, Canada

Dispensing technique is one of the promising solid freeform (SFF) methods to fabricate scaffolds with controllable pore sizes and porosities. In this paper, a model to represent the dispensing-based SFF fabrication process is developed. Specifically, the mechanical properties of the scaffold material and its influence on the fabrication process are examined; the flow rate of the scaffold material dispensed and the pore size and porosity of the scaffold fabricated in the process are represented. In order to generate scaffold strands without either tensile or compressive stress, the optimal moving speed of the dispensing head is determined from the flow rate of the scaffold material dispensed. Experiments were also carried out to illustrate the effectiveness of the model developed. [DOI: 10.1115/1.3123331]

Keywords: tissue scaffolds, SFF technique, flow rate, pore size

1 Introduction

Tissue engineering is an emerging and exciting area with one goal of creating artificial tissues and organs to repair or replace the damaged tissues or organs in the human body. In tissue engineering, porous engineered scaffolds provide the physical and chemical cues to guide cell differentiation and assembly into three-dimensional (3D) tissues [1]. Solid freeform (SFF) technique has recently drawn much attention in scaffold fabrication as it can overcome the shortages of conventional techniques [2] by producing scaffolds with customized external shape and predefined internal morphology. This technique can not only control pore size, porosity and pore distribution of scaffolds but also build structures to increase the mass transfer of oxygen and nutrients.

Currently, a variety of SFF techniques have been employed in scaffold fabrication. Among them, dispensing-based SFF technique (or direct writing technique) is a promising one because it does not involve a high temperature process [3] nor does it need organic solvents and local radiation [4,5]. In our previous work [6], we have demonstrated the effectiveness of the dispensing-based SFF process by fabricating scaffolds with well-controlled internal structures. The schematic of a typical scaffold created by employing this technique is shown in Fig. 1. To generate continuous and uniform strands, the moving speed of the needle should be chosen carefully so as to not produce either tensile or compressive stress in the strands. Since moving speed is dependent on the flow rate, the representation of the flow rate in the fabrication process is of great importance. In the literature, several models for the flow rate in tissue scaffolds fabrication process were developed [6,7] under the assumption that there is no slip between the material being dispensed and the needle wall. However, with the addition of particles to the solution, the slip becomes having a significant influence on the flow rate. As a result, such an influence must be taken into account.

It is also noted that, since colloidal gel is a pastelike material, the strands of the scaffold, once dispensed, will deform and fuse into each other. As a result, the actual pore size and porosity of scaffolds degrade from those designed [8]. Unfortunately, this is often neglected in literature due to the difficulty in estimating the actual pore size. However, research in tissue engineering shows that scaffold pore size and porosity can have a significant influence on both its biological [9] and mechanical [10] properties. Hence fabricating a scaffold with the desired pore size and porosity are of great importance in tissue engineering.

In this paper, the development of a model for the flow rate in the scaffold fabrication is presented by taking into account the influence of the slip between the material and the needle wall. Also, a model to predict the pore size and porosity based on the mechanical properties of the scaffold material is developed. Experiments were carried out to verify the effectiveness of these models.

2 Mechanical Properties of Scaffold Materials

The scaffold material in a form of colloidal gel is a mixture of fine particles and high molecular weight polymers. The colloidal gel possesses both solid and fluid properties, i.e., flowing like a fluid under the action of stress and remaining at rest like a solid if the stress is small. The flow behavior of a colloid can be described by the Hershel–Bulkley model as follows:

$$\tau = \tau_y + K\dot{\gamma}^n \tag{1}$$

where τ is the shear stress, $\dot{\gamma}$ represents the shear rate, τ_y is the yield stress, n is the behavior index (dimensionless), and K is the consistency index with a unit of Pa s^n. If the applied stress is less than τ_y, there is no flow occurring and the colloid acts like a solid.

In the solid regime, the colloid can be represented by the Kelvin–Voigt model in simple shear given by

$$\tau = G\gamma + \eta\dot{\gamma} \tag{2}$$

where G is the shear modulus and η represents the viscosity. The solution to Eq. (2) is given by $\gamma=(\tau/G)[1-\exp(-Gt/\eta)]$, which is a nonlinear function of time, indicating that the process of creep is time-dependent. For a very slight motion, the solution can be linearized, yielding that the corresponding force is proportional to the displacement. This linear relationship is illustrated in Fig. 2 in a range from zero to the elasticity limit (τ_e). Also shown in the figure is the yield stress, by which the material yields and starts to flow.

3 Modeling of Dispensing-Based Scaffold Fabrication Process

3.1 Flow Rate of the Scaffold Material Dispensed. The schematic of a typical dispenser used in the scaffold fabrication process is shown in Fig. 3. It employs pressurized air to drive the colloidal gel stored in the syringe out of the needle. P is the pressure applied to the syringe; P_e is the pressure in the colloidal gel at the exit of the needle; and D and L are the internal diameter and the length of the needle, respectively. Given that the diameter of the syringe is much larger than that of the needle, the friction loss of the fluid flow in the syringe can be ignored. Thus, the pressure drop applied to the material in the needle is $\Delta P=P-P_e$.

For the colloidal gel flow in the circular needle, the slip between the flow and the needle wall occurs due to the interactions of the solid particles and high molecular weight polymer solution [11]. By taking into account the slip, the flow rate of the colloidal gel in the needle Q is [11]

Contributed by the Manufacturing Engineering Division of ASME for publication in the JOURNAL OF MANUFACTURING SCIENCE AND ENGINEERING. Manuscript received July 13, 2008; final manuscript received February 24, 2009; published online April 30, 2009. Review conducted by Wei Li.

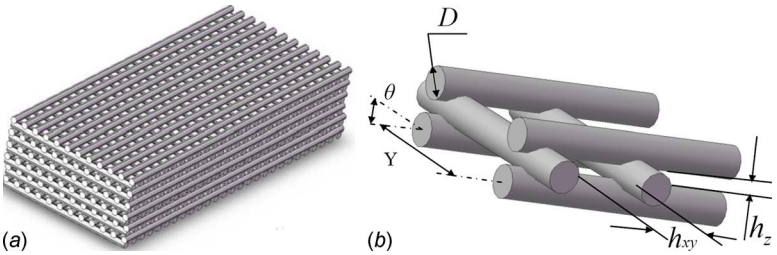

Fig. 1 Schematic of scaffolds made by SFF technique: (*a*) overview and (*b*) internal structure

$$Q = Q_{\text{shear}} + Q_{\text{slip}} \tag{3}$$

where Q_{shear} is the flow rate of the shear flow and Q_{slip} is the flow rate due to the slip. For the gel whose flow behavior is described by Eq. (1), the shear flow rate is given by [12]

$$Q_{\text{shear}} = \pi R^3 \left(\frac{\tau_w}{K_1}\right)^{s_1} \left[\frac{A^{s_1+3}}{s_1+3} + 2\left(\frac{\tau_y}{\tau_w}\right)\frac{A^{s_1+2}}{s_1+2} + \left(\frac{\tau_y}{\tau_w}\right)^2 \frac{A^{s_1+1}}{s_1+1}\right] \tag{4}$$

where R is the internal radius of the needle, $\tau_w = (\Delta P/L)(R/2)$ is the shear stress at the needle wall, $A = (\tau_w - \tau_y)/\tau_w$, and $s_1 = 1/n_1$. K_1 and n_1 are the consistency index and behavior index of the colloidal gel, respectively. The flow rate due to the slip is [13]

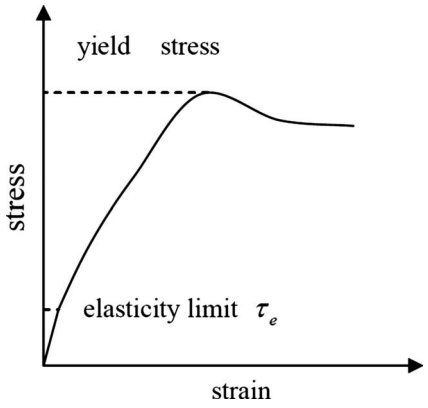

Fig. 2 Typical curve of strain versus stress

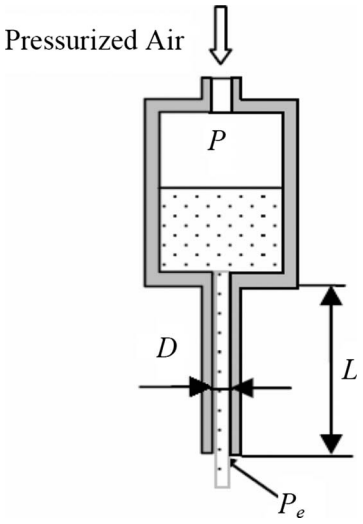

Fig. 3 Schematic of dispenser

$$Q_{\text{slip}} = U_s \pi R^2 \tag{5}$$

where U_s is the slip velocity and is determined by

$$U_s = \frac{R}{K_2^{s_2}(1+s_2)}\left[1 - \left(1 - \frac{\delta}{R}\right)^{1+s_2}\right]\tau_w^{s_2} \tag{6}$$

where $s_2 = 1/n_2$, n_2 is the behavior index of the polymer solution, K_2 is the consistency index of the solution, and δ is the thickness of the slip layer. In this paper, the thickness is taken a value of 0.06 times the mean particle size, based on the suggestions given in Ref. [12]. The mean particle size in our experiments is 30 μm and then the thickness of the slip layer is 1.8 μm. Thus, the needle moving speed of the dispensing head V can be obtained as follows:

$$V = \frac{4Q}{\pi D^2} \tag{7}$$

3.2 Pore Size and Porosity of the Scaffold. Prior to the scaffold fabrication, the internal geometry of the scaffold microstructure needs to be designed and specified, such as those shown in Fig. 1(*b*), where Y is the distance between two adjacent horizontal strand centers, D is the diameter of the strand, and θ is the angle between two layers. Also shown in Fig. 1(*b*) are the distances between the two adjacent horizontal (h_{xy}) and vertical (h_z) strands. It is observed that in the fabrication process the distance h_{xy} does not change significantly, but the vertical size h_z does due to the fusion of the two strands. In this paper, h_z is of interest and is to be represented.

For this purpose, it is assumed that (1) once a layer is dispensed onto a previous one, the previous layer is assumed dried; (2) the influence of the surface tension in the fresh strand is ignored, compared with the influence of the high stiffness of the material; and (3) the fresh strand acts as solid and maintain their cylindrical shape except in the contact region.

Once a fresh strand is laid onto the dried ones, the strand in the contact region yields and spreads until the shear stress becomes smaller than the yield stress. This spreading process is followed by creep due to the action of stress below the yield stress. Strands fusion at the contact area is shown in Fig. 4(*a*) and the contact surface is illustrated in Fig. 4(*b*). It is considered in this paper that

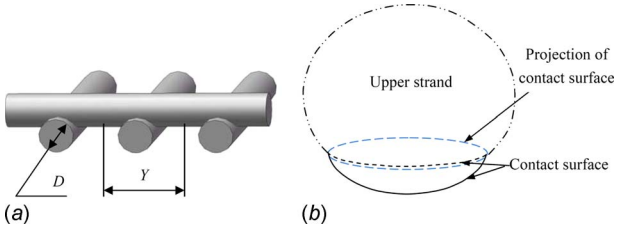

Fig. 4 (*a*) Schematic of the strands in contact and (*b*) contact surfaces

Table 1 Measured mechanical properties

Materials	Yield stress τ_y (Pa)	Flow behavior K (Pa s^n)	Flow behavior n	Elasticity limit stress τ_e (Pa)
chitosan solution	0	63.0	0.668	-
40% HA gels	683.1	102.0	0.70	11.0
45% HA gels	715.9	130.5	0.71	13.5
50% HA gels	748.6	152.3	0.73	15.4
55% HA gels	778.0	180.0	0.74	18.2
60% HA gels	812.5	215.6	0.76	20.9

the creep stops once the shear stress drops to the elastic limit. Therefore, in the final state, the shear stresses in the contact region are uniform and equal to the elastic limit stress (τ_e).

Suppose the area of the projection of the contact surface on a horizontal plane is A_p, the force balance yields

$$\sigma \cdot A_p = W \tag{8}$$

where σ is the normal stress on the surface and $W=\rho g \pi R^2 Y$ is the average weight of the strand supported by the substrand, in which ρ is the density of the material. According to mechanics of material, the maximum shear stress applied on a plane equals half of the normal stress on this plane [14]. Thus, the shear stress in the contact region is

$$\tau_e = \frac{1}{2}\sigma = \frac{1}{2}\frac{W}{A_p} \tag{9}$$

The projection of the contact area on the horizontal plane is approximately an ellipse. Based on the geometrical relationship in the contact area, the vertical space h_z in Fig. 1(b) is

$$h_z = D \cdot \sqrt{1 - \frac{\rho g Y}{2\tau_e} \cdot \sin\theta} \tag{10}$$

For generality, the dimensionless vertical size h_z^* is used in the following, defined by

$$h_z^* = \frac{h_z}{D} = \sqrt{1 - \frac{\rho g Y}{2\tau_e} \cdot \sin\theta} \tag{11}$$

In literature, the porosity of a 3D scaffold is defined as the ratio of the void volume to the apparent volume of the scaffold. Due to the fusion of strands, the porosity of the scaffold fabricated is actually dependent on h_z. Then, for a cuboidal scaffold with k layers in the z direction and a and b strands in the horizontal directions, the porosity is as follows:

$$\%\ \text{porosity} = \left(1 - \frac{abkYA_{\text{cs}}}{[(a-1)Y+D]\times[(b-1)Y+D]\times[(k-1)h_z+D]}\right) \times 100\% \tag{12}$$

where A_{cs} is the cross-sectional area of strands and h_z is determined from Eq. (10).

4 Experimental and Simulation Results

4.1 Measurement of the Mechanical Properties. 3% (w/v) chitosan solution was prepared by solving chitosan in 0.5 mol/l acetic acid, and some of the solutions obtained were added with varying volumes of hyroxylapatite (HA) particles to form colloid gels. The flow behaviors of both chitosan solutions and colloid gels were then examined on a HBDV-III rheometer (Brookfield, MA). The data of shear stress and shear rate obtained were correlated by using Eq. (1); the values of K and n were identified, which are listed in Table 1.

The yield stresses and elasticity limit stresses of the colloidal gels were also examined on the rheometer. In the measurements of yield stresses, the shear rate was set at 0.01 s^{-1}, and the yield stress was read from the built-in software; meanwhile the elasticity limit stresses were determined by using the 0.2% offset plastic strain from the strain-stress curves recorded. The measured yield stresses and elasticity limit stresses are also shown in Table 1.

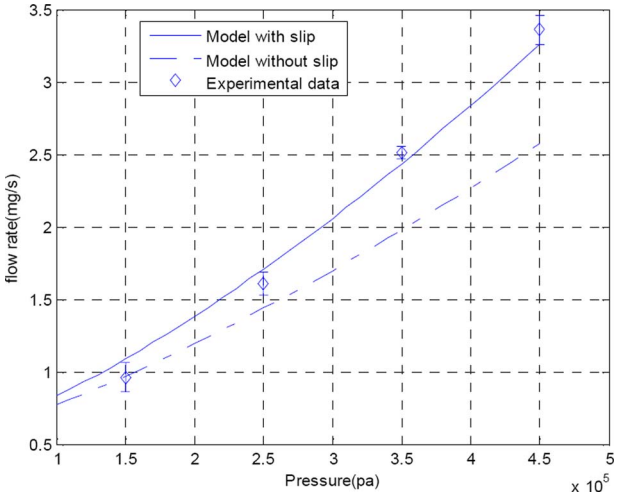

Fig. 5 Flow rate under different applied air pressures (45% HA-chitosan gel)

4.2 Verification of the Flow Rate Model. In order to verify the effectiveness of the flow rate model, two experiments of dispensing colloidal gels were carried out by using the scaffold fabrication machine adapted from a commercial fluid dispensing system (C0720M, Asymtek), in which a needle with an internal diameter of 0.61 mm and a length of 12 mm was used. In the first experiment, a 45% HA-chitosan gel was used, and the dispensing system was controlled to deliver the gel for 20 s under different pressures of 150 KPa, 250 KPa, 350 KPa, and 450 KPa, respectively. The average flow rates of three runs were measured by weighing the gels dispensed using an electronic balance with a resolution of 0.1 mg. Simulations based on Eqs. (3)–(6) with the flow behavior parameters listed in Table 1 were performed in MATLAB. Both the experimental and simulation results are shown in Fig. 5. Simulations without the consideration of slip were also carried out. The results show that slip has a significant influence on the flow rate of the material dispensed and that this influence can be well represented by means of the model developed. In the second experiment, colloidal gels with different HA volume fractions were dispensed under a pressure of 3.5 MPa for 20 s and the flow rates were measured as in the previous experiment. Simulations with and without the consideration of slip were also carried out. The comparison of the simulation results to the experimental ones is given in Fig. 6, also suggesting that the wall slipping must be taken into account in the flow rate model.

4.3 Verification of the Pore Size and Porosity Model. To verify the pore size and porosity model, the colloidal gels with different HA volume fractions were used to fabricate scaffolds with the designed structural parameters listed in Table 2. Once fabricated, the vertical sizes of the pores of the scaffold were measured by using a light microscopy; its porosity was measured by using the liquid saturation method, in which acetone was used as the liquid. The measured pore sizes and porosities are plotted in Figs. 7 and 8, respectively, against the elasticity limit stresses, which correspond to colloidal gels with different HA volume fractions. Simulations were performed for the pore size based on Eqs. (8)–(11) and for the porosity based on Eq. (12). The simulation results are shown in Figs. 7 and 8, along with the experimental results. The agreement between the model predictions and the experimental results indicates that the model developed is prom-

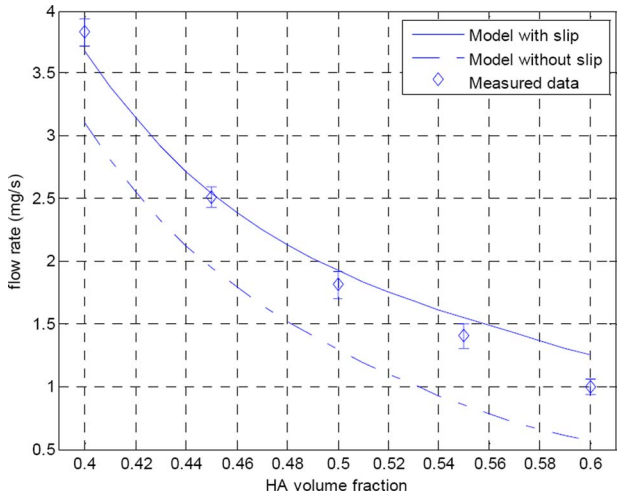

Fig. 6 Flow rate at different HA volume fractions (pressure =3.5 bars)

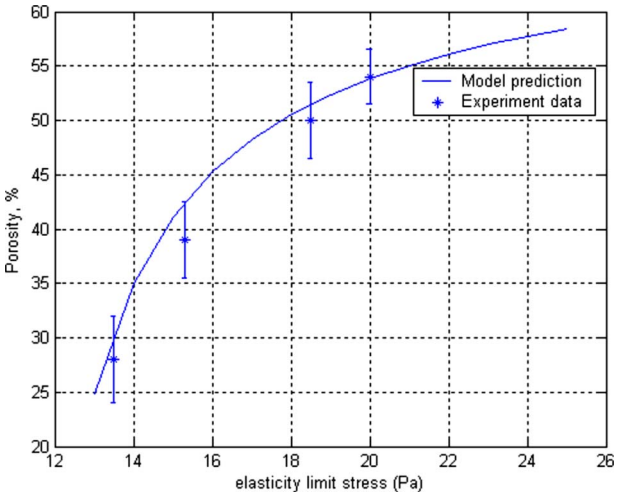

Fig. 8 Measured and predicted porosities

ising to predict the scaffold pore size and porosity. The slight difference between them may mainly have resulted from the assumption that the strands are cylindrical, which are used in the model development.

As indicated by Eq. (11), the elastic limits stress (τ_e) of the material must be high enough to form three-dimensional interconnected pores. To illustrate this concept, two scaffolds were fabricated from the materials with τ_e of about 5.0 Pa and 18.5 Pa under identical operation conditions. From the pictures taken from the scaffolds in Fig. 9, it is seen that, although there are pores in the horizontal plane, the use of the latter material can create a better interconnected pores than the former one due to the larger h_z.

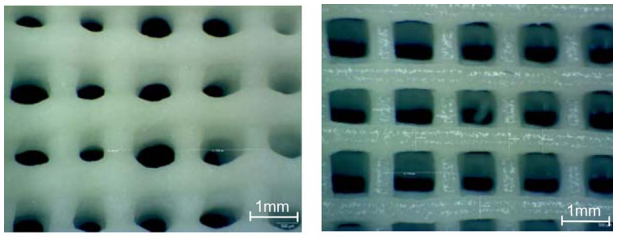

Fig. 9 Scaffolds made by using different colloids: (*a*) with lower τ_e and (*b*) with higher τ_e

5 Conclusions

In the dispensing-based SFF tissue scaffold fabrication process, a number of factors such as the material properties and process parameters can affect the process performance. These factors have a significant influence on the flow rate in the fabrication process, thereby affecting the determination of the moving speed of the needle. In this paper, the model for the flow rate is developed by taking into account the wall slip. Based on the developed model, the needle moving speed in the fabrication process is determined so as to construct scaffold strands without either tensile stress or compressive stress in the fabrication process. This paper also presents the development of a model of pore size and porosity of the scaffolds fabricated by means of the dispensing-based SFF technique. With this model, it becomes possible to rationally determine the process parameters used in the scaffold fabrication, instead of using a trial and error process as reported previously.

Table 2 Scaffold structure parameters

Strand diameter D (mm)	Span Y (mm)	Crossing angle θ (deg)	Layers
0.61	1.5	90	20

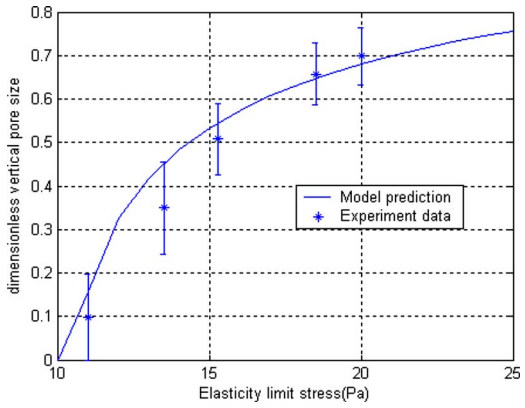

Fig. 7 Measured and predicted pore sizes

Acknowledgment

The financial supports from the Canada Foundation for Innovation (CFI) and the Saskatchewan Health Research Foundation (SHRF) are acknowledged.

References

[1] Griffith, L. G., and Naughton, G., 2002, "Tissue Engineering-Current Challenges and Expanding Opportunities," Science, **295**, pp. 1009–1014.

[2] Sachlos, E., and Czernuszka, J. T., 2003, "Making Tissue Engineering Scaffolds Work. Review on the Application of Solid Freeform Fabrication Technology to the Production of Tissue Engineering Scaffolds," Eur. Cells Mater, **5**, pp. 29–40.

[3] Yan, Y., Xionga, Z., Hu, Y., Wang, S., Zhang, R., and Zhang, C., 2003, "Layered Manufacturing of Tissue Engineering Scaffolds Via Multi-Nozzle Deposition," Mater. Lett., **57**, pp. 2623–2628.

[4] Li, Q., and Lewis, J. A., 2003, "Nanoparticle Inks for Directed Assembly of Three-Dimensional Periodic Structures," Adv. Mater., **15**, pp. 1639–1643.

[5] Xie, B., Parkhill, R. L., Warren, W. L., and Smay, J. E., 2006, "Direct Writing of Three-Dimensional Polymer Scaffolds Using Colloidal Gels," Adv. Funct. Mater., **16**, pp. 1685–1693.

[6] Chen, X. B., Li, M. G., and Ke, H., 2008, "Modeling of the Flow Rate in the Dispensing-Based Process for Fabricating Tissue Scaffolds," ASME J. Manuf. Sci. Eng., **130**(2), pp. 021003.

[7] Vozzi, G., Previti, A., Rossi, D., and Ahluwalia, A., 2002, "Microsyringe-

Based Deposition of Two-Dimensional and Three-Dimensional Polymer Scaffolds With a Well-Defined Geometry for Applications to Tissue Engineering," Tissue Eng., **8**, pp. 1089–1098.
[8] Xu, M., Gratson, G. M., Duoss, E. B., Shepherd, R. F., and Lewis, J. A., 2006, "Biomimetic Silicification of 3D Polyamine-Rich Scaffolds Assembled by Direct Ink Writing," Soft Matter, **2**, pp. 205–209.
[9] Sampath, T. K., and Reddi, A. H., 1984, "Importance of Geometry of the Extracellular Matrix in Endochondral Bone Differentiation," J. Cell Biol., **98**, pp. 2192–2197.
[10] Mikos, A.G., Sarakinos, G., Lyman, M. D., Ingber, D. E., Vacanti, J. P., and Langer, R., 1993, "Prevascularization of Porous Biodegradable Polymers," Biotechnol. Bioeng., **42**, pp. 716–723.
[11] Khan, A. U., Briscoe, B. J., and Luckhan, P. F., 2001, "Evaluation of Slip in Capillary Extrusion of Ceramic Pastes," J. Eur. Ceram. Soc., **21**, pp. 483–491.
[12] Kalyon, D. M., Yaras, P., Aral, B., and Yilmazer, U., 1993, "Rheological Behavior of a Concentrated Suspension: A Solid Rocket Fuel Stimulant," J. Rheol., **37**, pp. 35–53.
[13] Yeow, Y. L., Lee, H. L., Melvani, A. R., and Mifsud, G. C., 2003, "A New Method of Processing Capillary Viscometry Data in the Presence of Wall Slip," J. Rheol., **47**, pp. 337–348.
[14] Hibbeler, R. C., 1999, *Mechanics of Material*, 4th ed., Prentice-Hall, Englewood Cliffs, NJ.

CHAPTER 4

MODELING PROCESS-INDUCED CELL DAMAGE IN THE BIO-DISPENSING PROCESS

Published as:

- Li, M.G., Tian, X.Y., Zhu, N., Schreyer, D.J., and Chen, X.B. (2010) Modeling process-induced cell damage in the bio-dispensing process. Tissue Engineering, Part C, 16(3):533-542.

4.1 Introduction and Objectives

To better mimic the microenvironment of cells in native tissues, cells are incorporated in hydrogels to form cell-seeded hydrogel scaffolds. The advantage of these scaffolds over the solid scaffolds fabricated in the previous chapter is that their mechanical properties are highly malleable while the biological functionality is maintained by the backbone of the polymeric network. Thanks to its biomimetic properties, it has been successfully employed in different tissue engineering, such as cartilage, brain and nerve.

In the cell involved bio-dispensing processes, cells are continuously subjected to mechanical forces. If the forces exceed certain thresholds and/or the forces are applied beyond a certain time period, cells will be harmed and even damaged to the point they do not maintain their phenotype or even survive the process. The objective of this paper is to develop a model to represent the cell damage occurring in the bio-dispensing processes under different process control parameters.

4.2 Method

Development of cell damage model in the bio-dispensing processes consists of three steps: (1) establishment of a cell damage law to relate the cell damage percent under different forces and force exposure times; (2) represent the forces that cells experience and the time that cells are exposed to the forces in the bio-dispensing processes; and (3) apply the cell damage law established to the bio-dispensing processes to obtain the cell damage model.

4.3 Results

The results show that the cell damage percent in the bio-dispensing processes can be predicted by the developed model. Both the model simulation and experiments show that cell damage in the bio-dispensing processes increase with the air pressure and needle length and decrease with the needle diameter. The model simulation also indicates that the cell damage concentrated at the needle wall due to the high shear stress and long exposure time at the wall, and this is also verified by experiments.

4.4 Contributions

The contribution of this paper is the development of the cell damage model for bio-dispensing processes. The model developed in this paper can be used to determine the influence of the process parameters on the cell damage and, ultimately, to optimize the bio-dispensing process to minimize cell damage.

TEN-2009-0178-Li_1P
Type: research-article

TISSUE ENGINEERING: Part C
Volume 15, Number 00, 2009

DOI: 10.1089/ten.tec.2009.0178

Methods Article

Modeling Process-Induced Cell Damage in the Biodispensing Process

Minggan G. Li, M.Sc.,[1] Xiaoyu Y. Tian, M.Sc.,[2] Ning Zhu, M.Sc.,[2]
David J. Schreyer, Ph.D.,[3] and Daniel X.B. Chen, Ph.D., P.Eng.[1,2]

Emerging biomanufacturing processes involve incorporation of living cells into various processes and systems by employing different cell manipulation techniques. Among them, biodispensing, in which the cell suspension is extruded via a fine needle under pressurized air, is a promising technique because of its high efficiency. Cells in this process are continually subjected to mechanical forces and may be damaged if the force or manipulation time exceeds certain levels. Modeling cell injury incurred in these processes is lacking in the literature. This article presents a method to quantify the force-induced cell damage in the biodispensing process. This method consists of two steps: first is to establish cell damage laws to relate cell damage to hydrostatic pressure/shear stress; and the second is to represent the process-induced forces experienced by cells during the biodispensing process and apply the established cell damage law to represent the percentage of cell damage. Schwann cells and 3T3 fibroblasts were used to validate the model and the comparisons of experimental and simulation results show the effectiveness of the method presented in this article.

Introduction

In recent years, various biofabrication methods have been developed that employ mechanical means to incorporate cells in bioproducts.[1] Different cell manipulation techniques have been explored, including biodispensing cell deposition,[2–5] inkjet-based cell printing,[6–9] and photo- and electropatterning.[10–11] Biodispensing, in which a pneumatic or other volumetrically driven dispenser is used to deposit the material, is one promising technique because of its fast and efficient material processing capacity. As such, it has been widely applied in three-dimensional cell-seeded tissue scaffold fabrication,[12–14] microfluidic devices,[15–16] and lab-on-a-chip devices.[17–18] In these processes, cells are encapsulated in a biocompatible material and then extruded and delivered to designated targets in a controlled manner. In a pneumatic biodispensing setup, the cell suspension flows through a fine needle under pressurized air. During this process, cells are subjected to mechanical forces such as pressure and shear stress. Within a physiological range, forces elicit adaptive responses acutely and chronically.[19] If the forces exceed certain thresholds and/or the forces are applied beyond a certain time period, cells will be harmed and even damaged to the point they do not maintain their phenotype or even survive the process. Previous studies reported that the percentage of cell damage during the dispensing process is 40% for fibroblasts,[20] 2% for hepatocytes,[21] 15.7–31.4% of the control value for HepG2 cells,[3] and 6% for chondrocytes.[22] Clearly, cell damage varies with the fabrication process and depends upon cell manipulation techniques, cells types, and process parameters (such as air pressure, needle diameter, and needle length). Although the cell damage incurred during dispensing-based rapid prototyping fabrication can be measured and investigated experimentally,[23] a systematic method or model to relate cell injury to biodispensing process parameters has not yet been developed. Such a model is essential for reproducible control over the distribution of cells within the bioproducts.

As different biodispensing process parameters generate different forces and force durations on cells, cell damage models or laws that address the relationship between process-induced forces and cell damage are needed. A power law function commonly used to model the force-induced cell damage has the following general form[24–26]:

$$I\,(\%) = C t^{a} \tau^{b} \tag{1}$$

where I (%) is the percentage of cell damage, τ the stress cell experienced, and t the stress exposure time. C, a, and b are constants for a given type of cells. Equation 1 has been employed with varying degrees of success for representing force-induced cell damage.[27,28] However, the model has two disadvantages. First, the equation does not provide information regarding either the probability distribution of cell

[1]Department of Mechanical Engineering, [2]Division of Biomedical Engineering, and [3]Department of Anatomy and Cell Biology, University of Saskatchewan, Saskatoon, Canada.

damage with stress and exposure time or how the stress and exposure time are correlated. Second, this equation is not applicable for describing cell damage for large ranges of stress and/or long exposure times because, as the shear stress or exposure time becomes large or long, the right-hand side of the above equation will exceed 100%, which is obviously not true. Therefore, models that can overcome the aforementioned disadvantages are desirable.

Further, the mechanic forces that acted on cells in the biodispensing process are usually distributed in a complex manner. The shear stress generated in the cell suspension in the needle, for example, increases with the radius, specifically from zero at the needle center to a maximum value at the needle wall. In addition, given that the flow velocity of the cell suspension in the needle is a function of radius, the exposure time of the cells to the shear stress also varies in the biodispensing process. Hence, the use of maximum shear stress at the wall and the average exposure time to model the cell damage, as reported in a previous study,[29] is inappropriate. Also, it was noted that cell suspensions in the reservoir are subjected to pressures for time periods varying from seconds to hours, depending on applications.[30] All these suggest that representation of the forces on the cells during the biodispensing process is essential for the development of models for the process-induced cell damage.

In this article, we present a method to quantify the percentage of cell damage in the biodispensing process. This method consists of two steps: the first step is to monitor the response of cells to a given hydrostatic pressure and shear stress and develop experimental models or laws for cell damage; and the second step is to analyze the forces acting on the cells in the biodispensing process and then apply the developed cell damage laws to represent the percentage of cell damage in the process. Experiments using a pneumatic dispensing system were carried out to validate the developed method, in which Schwann cell and 3T3 fibroblasts were chosen for cell dispensing because of their wide applications in tissue engineering.[31,32]

Developing Cell Damage Laws

To model the percentage of cell damage in the biodispensing process, cell damage laws describing the relationship between cell damage and hydrostatic pressure/shear stress must be established. To do this, varying levels of pressure or shear stress of different durations were applied to cells, with cell damage recorded, and a relationship was derived from the experimental results. In particular, hydrostatic pressure was applied to cells in a syringe with a removable cap screwed in place of a dispensing needle. As different pressures were applied for varying durations, cell damage was observed and the percentage of cell damage was evaluated. To observe shear-induced cell damage, a rheometer with cone-and-plate geometry (RVDV-III; Brookfield, Middleboro, MA) was used to apply different shear stresses for varying durations to cells. Given that the angle between the cone and the plates is small, the shear rate, thus shear stress, throughout the suspension was considered as uniform.[33] The shear stresses and the exposure times were controlled via programming and the cell damage was monitored and recorded.

To describe the relationship between cell damage and hydrostatic pressure/shear stress, one can use the power law equation, which, however, has the limitations discussed previously. For improvement, in this article we propose the use of a bivariate normal distribution function to establish the cell damage law. The bivariate normal distribution is a generalization of the one-dimensional normal distribution to the two-dimensions and has been widely used in biostatistics.[34] Based on the normal distribution theory, the percentage of cell damage under pressure or shear stress ($CD_{pr/sh}$) is expressed as a function of stress (s) and the corresponding exposure time (t), that is,

$$CD_{pr/sh}(s,t) = \int_t \int_s f(s,t)dsdt \tag{2}$$

where $f(s, t)$ is the probability density function and is given by

$$f(s,t) = \frac{1}{2\pi\sigma_s\sigma_t\sqrt{1-\rho^2}}\exp\left[-\frac{z}{2(1-\rho^2)}\right] \tag{3}$$

where $z \equiv \left(\frac{s-\mu_s}{\sigma_s}\right)^2 - 2\rho\left(\frac{s-\mu_s}{\sigma_s}\right)\left(\frac{t-\mu_t}{\sigma_t}\right) + \left(\frac{t-\mu_t}{\sigma_t}\right)^2$; μ_s and μ_t are the mean values of stress s (pressure or shear) and exposure time t, respectively; σ_s and σ_t are the standard deviations of s and t, respectively; and ρ is the correlation coefficient between s and t. These five parameters were obtained experimentally and can be determined for both pressure and shear stress conditions.

Using the above cell damage law, the vulnerability of cells to mechanical force and duration of the applied force can be determined. The mean values and standard deviations of force and force duration for cell damage are components of the laws; the coupling effect of force and force duration on cell damage is quantitatively expressed. Further, as this cell damage law is based on probability theory, one has $\int_0^\infty \int_0^\infty f(s,t)dsdt = 1$, thereby overcoming the limitation of the power law equation when force or force duration becomes large.

Modeling Cell Damage in the Biodispensing Process

In the biodispensing process, cells are subjected to both pressure and shear stresses, resulting in cell damage concerned in this article. In this section, an analysis of the process-induced forces is performed by using the information of the flow behavior of cell suspension, and on this basis, the cell damage law established previously is applied to represent the percentage of cell damage in the biodispensing process.

Flow behavior of cell suspension

Cell suspensions are a composite of cells and high-molecular weight polymer. Because of the long molecular chain of the polymer, cell suspensions generally possess non-Newtonian flow behavior that is featured by a nonlinear relationship between the shear stress and shear rate in them, which can be expressed as

$$\tau = K\dot{\gamma}^m \tag{4}$$

where K is the consistency index with the unit of Pa s^m, m is the flow behavior index (dimensionless), and $\dot{\gamma}$ is the shear rate.

Process-induced forces in the biodispensing process

In this study, a cell-dispensing method adapted from a commercial fluid dispensing system (C0720M; Asymtek, Carlsbad, CA) was used.[35,36] The system employs pressurized air to drive the cell suspension stored in the syringe out of the needle, as schematically represented in Figure 1. In the biodispensing process, the following assumptions were made: (1) the cell suspension is incompressible, implying its density is constant during the process; (2) the fluid flow in the needle is steady and fully developed, at which the velocity profile does not change with time; (3) there is no slip between the cell suspension and the needle wall; (4) the pressure drop in the reservoir due to the fluid flow is negligible given the syringe diameter is much greater than the needle diameter; and (5) the minor losses due to entrance effects can be neglected given the fact that the flow velocity in the needle is small. Under these assumptions, the pressure drop in the needle is given as[37]

$$\Delta P = P - P_e \tag{5}$$

where P is the pressure of air applied to the syringe and P_e is the pressure at the exit or ambient air pressure.

Under assumption (4) given previously, it is known that the hydrostatic pressure experienced by the cells in the reservoir (P_r) equals the air pressure (P) applied in the syringe. Because cells are continuously subjected to the pressure until they are extruded out of the needle, cells within the syringe are exposed to this pressure for different lengths of time, depending on the cell location. For the cells that are located initially at vertical position h in the reservoir, the time period of exposure is given as

$$t_r(h) = \frac{R_r^2 h}{R_n^2 u} \tag{6}$$

where R_r and R_n are the radii of the reservoir and the needle, respectively, and u is the average flow velocity in the needle.

Based on the force balance, the shear stress distribution along the radial direction in the dispensing needle can be obtained from[38]

$$\tau_n(r) = \frac{\Delta P}{2L_n} r \tag{7}$$

where $\tau_n(r)$ is the shear stress at radial position r (Fig. 2). From equation 7, it is known that the shear stress distribution across the needle cross section is linear and, notably, the shear stress at the center of the needle is zero (Fig. 2).

For the cell suspension with the flow behavior characterized by equation 4, the flow velocity (U) in the needle is given as[38]

$$U(r) = \frac{m}{m+1}\left(\frac{-\Delta P}{KL_n}\cdot\frac{R_n}{2}\right)^{1/m} R_n\left[1-\left(\frac{r}{R_n}\right)^{(m+1)/m}\right] \tag{8}$$

From the above equation, it is known that the flow velocity distribution in the needle is not constant, but a function of radius (r) (Fig. 2). As a result, the time period of cells traveling along paths of different radius will vary, according to

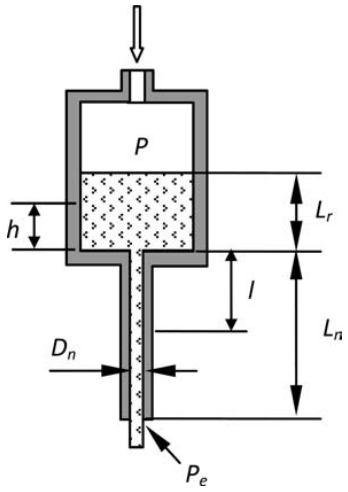

FIG. 1. Representation of process parameters during biodispensing. P is the pressure of air applied to the syringe, P_e is the pressure at the exit or ambient air pressure, D_n is the internal diameter of the needle, L_r is the suspension level in the reservoir, and L_n is the length of the needle. h represents the initial vertical position of cells in the reservoir and l represents the longitude position of cells in the needle.

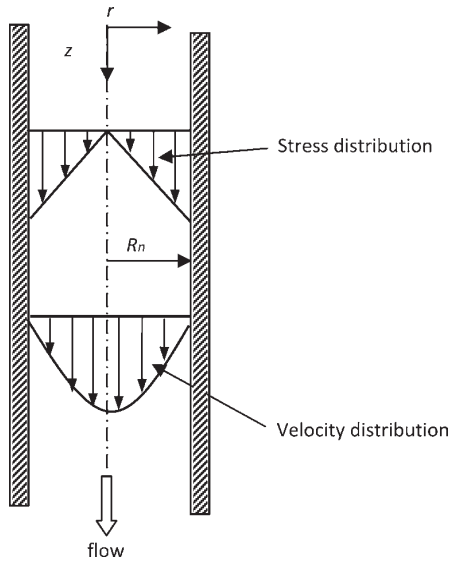

FIG. 2. Schematic representation of the shear stress and velocity distribution in the fully developed laminar flow in the cylindrical needle.

$$t_n(r) = \frac{L_n}{U(r)} \tag{9}$$

Notably, pressure is also present in the needle. Based on the force balance in the longitudinal direction, the pressure P_n at position l along the needle is given as, if ignoring the effect of the gravity of the cell suspension,

$$P_n(l) = P - \frac{l}{L_n}\Delta P \tag{10}$$

Percentage of cell damage in the biodispensing process

In the reservoir, the cell damage is caused by pressure. For the cells located initially at vertical position h (I_r), the percentage of cell damage is given as

$$I_r(h) = CD_{pr}(P_r, t_r) \tag{11}$$

where CD_{pr} is the cell damage law under hydrostatic pressure, P_r is the pressure applied on the cells in the reservoir, and t_r is the time the cells are exposed to this pressure.

In the dispensing needle, both pressure and shear stress may cause cell damage. For simplicity, the effects of pressure and shear stress on cell damage are assumed to be independent and therefore can be added to obtain the total cell damage in the needle. Suppose the cell density in the cell suspension is d, and the number of cells damaged by pressure in a volume of $2\pi r\Delta r{\cdot}\Delta l$ at longitude position l and radial position r can be expressed as $2\pi r\Delta r \cdot CD_{pr}(P_n,t_n)\Delta l \cdot d$. Thus, in a unit length at the exit of the needle, the number of damaged cells is $\int_0^{L_n}\int_0^{R_n} 2\pi r \cdot d \cdot CD_{pr}(P_n, t_n)drdl$ and the number of total cells is $d \cdot \pi R_n^2$. Hence, the cell damage caused by the pressure in the needle can be obtained with

$$I_{n,pr} = \frac{2\int_0^{L_n}\int_0^{R_n} rCD_{pr}(P_n, t_n)drdl}{R_n^2} \tag{12}$$

where CD_{pr} is the pressure-induced cell damage law.

Considering the shear stress effect at the exit of the needle, the number of damaged cells in a unit length at the exit of the needle can be expressed as $d\int_0^{R_n} 2\pi rCD_{sh}(\tau_n, t_n)dr$, where R_n is the radius of the needle, τ_n is the shear stress experienced by the cells, and t_n is the time for cells to pass through the needle. The cell damage in the needle due to shear stress (In,s) can then be obtained using the equation:

$$I_{n,sh} = \frac{2\int_0^{R_n} rCD_{sh}(\tau_n, t_n)dr}{R_n^2} \tag{13}$$

where $CD_{sh}(\tau_n,t_n)$ is the cell damage law established for shear stress. The total cell damage in the needle is therefore

$$In = In, pr + In, sh \tag{14}$$

Finally, the percentage of cell damage for the cells initially located at position h in the reservoir, once dispensed out of the needle, can be derived as follows:

$$I(h) = 1 - [1 - Ir][I - In] \tag{15}$$

Experiments and Results

Chemical formulation

Sodium alginate powder (Sigma, St. Louis, MO) was dissolved in deionized water overnight to form a 6% (w/v) solution.

Cell suspension preparation

Schwann cells (ATCC) and 3T3 fibroblasts (ATCC) were grown in Dulbecco's modified Eagle's medium (Sigma) supplemented with 5% fetal bovine serum and 1% antibiotic. The cells were then incubated at 37°C in a humidified atmosphere of 95% air and 5% CO_2. Immediately prior to use in our experiments, cell cultures were blended with sodium alginate solution to form a 50% (v/v) cell suspension and gently mixed with a pipette to ensure a uniform cell distribution. All experiments were conducted at room temperature (~23°C).

Cell viability assay

Niagara blue was used to stain cells and assess cell viability. The number of living/dead cells was counted manually under a light microscope (Leica; Microsystem, Bannockburn, IL) immediately following the dispensing process.

Statistical analysis

Statistical analysis was performed using Student's t-test, with a p-value of <0.05 considered significant.

Cell damage due to hydrostatic pressure

Two milliliters of cell suspension was delivered into the syringe using a pipette. Air pressure of 100, 200, 300, 400, and 500 kPa was then applied to the cell suspensions for 30 min. The control group was maintained at the atmospheric pressure. Each of the experiments was repeated six times ($n = 6$).

Cell damage in the control and test groups was not significantly different at any of the pressures tested (Table 1). This result suggests that cell damage in the dispensing process is independent of the initial vertical position (h) of cells in the reservoir. Further, it suggests that hydrostatic pressure in the dispensing process will not affect the viability of Schwann cells and 3T3 fibroblasts if the process lasts for less than 30 min, that is,

$$I_{pr} = 0 \tag{16}$$

The above results obtained from both Schwann cell and 3T3 cells agree with observation reported in a previous work,[39] showing that the application of less than 5 MPa hydrostatic pressure for 2 h on chondrocytes has limited damage to cell cytoskeletons or cell membranes. Therefore, the cell damage that occurs in the biodispensing process may primarily be attributed to shear stress encountered in the needle. However, it should be noted that high pressure does have a pronounced disruptive effect on cytoskeletal organization,[40] and pressures exceeding 100 MPa may lead to cell damage.[41]

Table 1. Cell Damage Under Hydrostatic Pressure ($n = 6$)

	Cell damage (% ± SD)				
	100 kPa (control)	*200 kPa*	*300 kPa*	*400 kPa*	*500 kPa*
Schwann cell	8.01 ± 3.2	8.61 ± 2.9	7.35 ± 3.8	9.01 ± 2.9	8.54 ± 2.7
3T3 fibroblast	7.85 ± 2.7	8.36 ± 2.3	8.89 ± 2.1	7.52 ± 3.5	6.52 ± 2.0

Cell damage due to shear stress

About 0.5 mL of cell suspension was carefully delivered to the rheometer by using a pipette. Cell suspensions used in each of the following experiments were also weighed to reduce the error caused by the high viscosity of the solution in the delivery process. Different shear stresses (80, 200, 400, 600, 800, 1000, and 1200 Pa) with varying durations (5, 60, 120, and 300 s) were applied to the cell suspensions. The control group was retained in tubes. Each of experiments was repeated six times ($n = 6$). The difference in cell damage between the shear stress group and the control group, denoted by *Damage_shear*, is attributed to the corresponding shear stresses and exposure times. The values were normalized from 0% to 100% as follows:

$$Normalized\_cell\_damage = \frac{Damage\_shear}{\max(Damage\_shear)} \quad (17)$$

For Schwann cell (Fig. 3a), at low shear stresses (less than 400 Pa) and short exposure time (less than 60 s) the percentage of cell damage was almost zero; with increasing shear stresses and/or exposure times, the percentage of cell damage increased in a nonlinear fashion (Fig. 3). At shear stresses above 1200 Pa and exposure times above 300 s, the cell damage plateaued at almost 100%, implying no cells can survive under these conditions. It was also observed that the percentage of cell damage increased gradually with exposure time at low shear stresses; at higher shear stresses, the percentage of cell damage increased more rapidly with time, particularly at the onset of exposure.

Similar results for 3T3 fibroblasts were also observed in Figure 3b. By comparison, the cell damage is a little higher than Schwann cells under the same conditions. For example, at the shear stress of 1200 Pa and exposure time of 5 s, the cell damage percentage is 89% for 3T3 and 78% for Schwann cells. This may indicate that 3T3 is more vulnerable than Schwann cells under shear stress.

Using the experimental data given in Figure 3, the five parameters of the bivariate normal distribution function (i.e., equation 2) were determined by means of the nonlinear least-squares regression in Matlab. More specifically, the five parameters are initially given their guessed values and then altered until the difference between the experimental data and the ones generated from the model is minimal. Table 2 lists the values of the parameters determined.

Cell damage in the biodispensing process

The flow behavior of the cell suspension was tested using an RVDV-III rheometer with a CP-52 spindle. The flow behavior parameters were identified and are given as $K = 28.7$ (Pa s^m) and $m = 0.78$ (dimensionless) for Schwann cell suspension and $K = 26.5$ (Pa s^m) and $m = 0.76$ (dimensionless) for 3T3 suspension. These values were used to calculate the cell exposure time based on equations 8 and 9.

In the experiments with dispensing cells, the pneumatic dispensing system described previously was employed, and medical-grade compressed air was used to extrude the cell suspension in the syringe out of the needle. In each of the dispensing experiments, 2 mL of cell suspension was loaded into the syringe using a pipette and then pressurized air was applied to the syringe. The cell suspension was extruded from fine needles (length, 20 mm). Control groups were maintained for each experiment and they were kept in tubes. The difference in percentage of cell damage between the

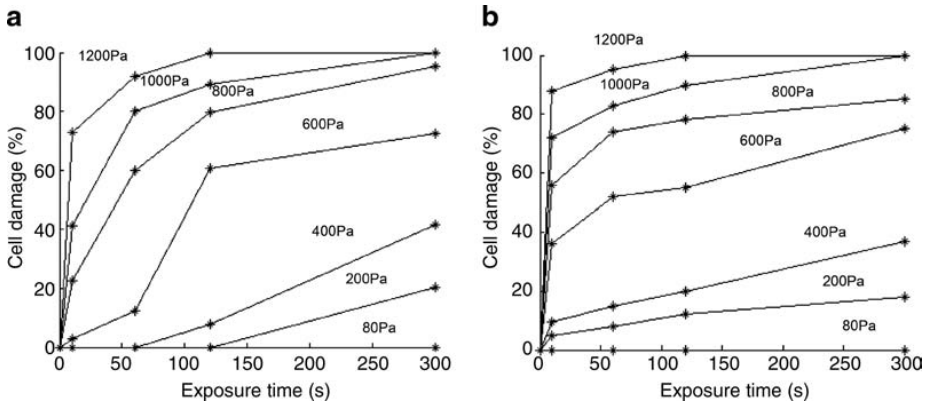

FIG. 3. Cell damage under different shear stresses and exposure times. (**a**) Schwann cell, and (**b**) 3T3 fibroblasts; mean value, $n = 6$.

Table 2. Identified Cell Damage Law Parameter Values

	μ_τ	σ_τ	μ_t	σ_t	ρ
Schwann cell	631.84	252.63	9.88	3.15	0.29
3T3 fibroblast	574.89	271.94	7.99	2.68	0.28

samples and controls was attributed to the biodispensing process. Such experiments were repeated six times ($n = 6$).

One set of experiments was aimed to investigate the influence of air pressure on cell damage in the biodispensing process. In these experiments, cell suspensions were dispensed by a needle (150 μm diameter) under pressures of 100, 200, 300, 400, and 500 kPa, respectively. As air pressure increased from 100 to 500 kPa, cell damage increased from 3% to 39% for Schwann cell (Fig. 4a) and 4% to 43% for 3T3 fibroblasts (Fig. 4b). This damage was attributed to shear stress in the needle, but not air pressure (as discussed in *Cell damage due to hydrostatic pressure* section). Because of the fact that the shear stress in the needle is dependent on the air pressure applied in the biodispensing process, higher air pressure can increase the flow rate of cell suspension dispensed in the process, meanwhile also leads to higher cell damage. The model given in equations 11–15 were used to simulate the percentage of cell damage under the identical experimental conditions and the simulation results are shown in Figure 4a and b for Schwann cell and 3T3 fibroblasts, respectively, along with the experimental results for comparison. It is seen that both simulation and experimental results are in close agreement, illustrating the promising use of the developed model.

A second set of experiments was aimed to investigate the influence of needle diameter. In these experiments, the air pressure was fixed at 500 kPa and needle diameters of 150, 250, 330, 410, and 510 μm were used, respectively. The results obtained are reported in Figure 5, showing that cell damage decreased with increasing needle diameter. Also, it is observed that, for both Schwann cell and 3T3 fibroblasts, as the needle diameter increased from 150 to 330 μm, cell damage dropped quickly, and for diameters >500 μm, the cell damage was less than 5%. However, cell damage for 3T3 is a little higher than Schwann cell under the same conditions. For example, at needle diameter of 150 μm, 43% of 3T3 fibroblasts were damaged, which is 4% higher than the cell damage of Schwann cells (39%). The simulation results from the model are shown in Figure 5a and b, illustrating that our model can also be effectively used to represent the influence of needle diameter on the percentage of cell damage.

We noted here that cell damage data were normalized (as in *Cell damage due to shear stress* section) to obtain the cell damage law and subsequent simulations. To compare the experimental and simulated results, the experimental data were also normalized using equation 17. The raw cell damage data can be obtained from reverse calculation through equation 17.

Discussion

Cell damage minimization

Both air pressure and needle diameter significantly influenced cell damage in the biodispensing process (Figs. 4 and 5). Cell damage can be minimized by use of low air pressure and a large-diameter needle. However, this may be impractical as extruding some viscous biomaterials becomes problematic at low air pressures. Moreover, both accuracy of positioning and volume control are lost with large-diameter needles, precluding some precision applications. Thus, the selection of pressure and needle diameter depends upon a given application, and the percentage of cell damage can be minimized by optimizing the process parameters.

For example, if a certain flow rate is required in an application, cell damage can be minimized by choosing the appropriate combination of needle diameter and air pressure. For instance, the optimal flow rate for the cell suspension employed in our experiments is of 0.6 mL/s, which can be achieved through different combinations of needle diameter in a range of 0.33–0.84 mm and air pressure in range of 0–500 kPa with the following flow rate equation[38]:

$$Q = \frac{\pi D_n^3}{8}\left(\frac{\tau_w}{K}\right)^{1/m}\frac{m}{3m+1} \tag{18}$$

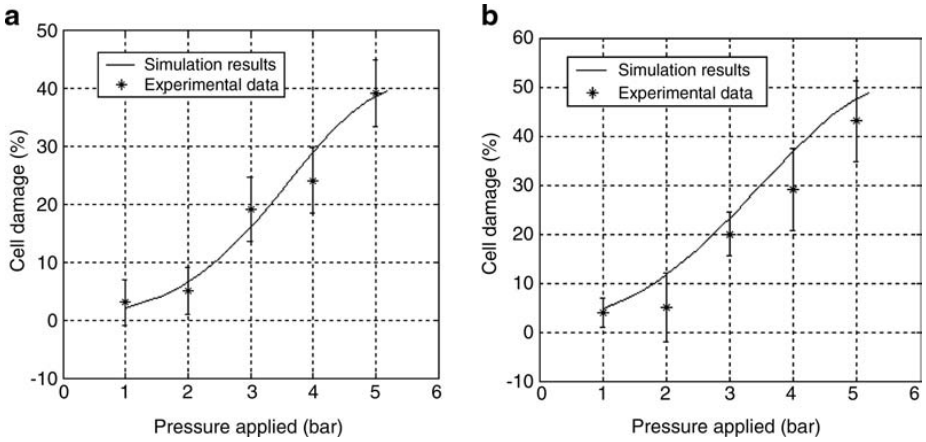

FIG. 4. Influence of air pressure on cell damage for (**a**) Schwann cell and (**b**) 3T3 fibroblasts. The needle diameters are 150 μm.

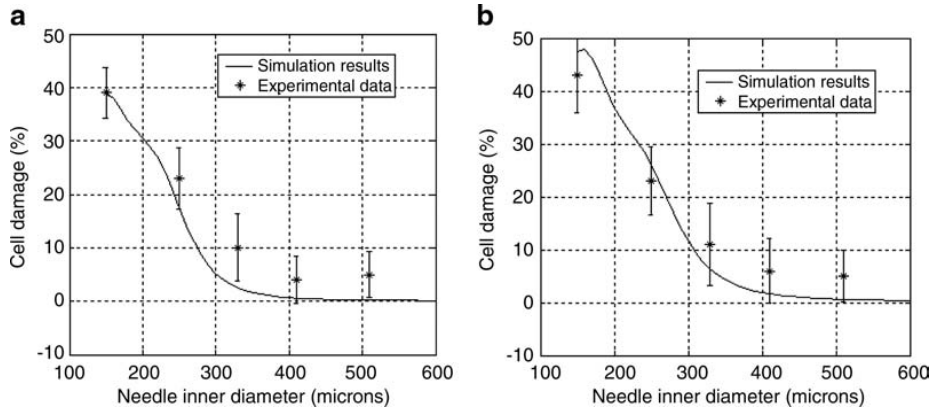

FIG. 5. Influence of needle diameter on cell damage for (**a**) Schwann cell and (**b**) 3T3 fibroblasts. The air pressures applied are 500 kPa.

We simulated the percentage of cell damage under these combinations using equations 11–15 (Fig. 6a). To maintain constant flow rate, the air pressure decreases with increasing needle diameter. The percentage of cell damage does not vary linearly with either pressure or needle diameter; cell damage peaks at $D = 410\,\mu$m and $p = 190$ kPa, and is the lowest at $D = 840\,\mu$m and $p = 20$ kPa. Experiments were also carried out to validate the simulation results. Both results are shown in Figure 6a.

Effect of needle length on cell damage

The use of shorter-length needle in the biodispensing process can decrease the resistance to the fluid flow, thereby increasing the flow rate or reducing the air pressure required. On the other hand, the use of shorter needle can linearly increase the shear stress in the needle, but decrease the time period of cell exposure to the shear stress, thereby affecting cell damage during the dispensing process in a complicated manner. This can also be seen from the developed model given in equations 11–15. To investigate the complicated effect of needle length on cell damage, both experiments and simulations from the developed model were performed, and the results are shown in Figure 6b, for the case with an air pressure of 500 kPa and a needle diameter of 840 μm. The results demonstrated that cell damage is almost zero at needle lengths of <40 mm, but increases quickly thereafter. Cell damage peaks at ~38% at a needle length of ~100 mm, thereafter decreasing a little to ~35% as the needle length approaches 120 mm. This may be caused by the lower shear stress in the needle with the increase of needle length.

Figure 6b suggests that the needle length should be carefully chosen to minimize cell damage in the biodispensing process. If higher flow rates are required for a given application, a shorter needle is favored to preserve cell viability. If a longer needle is required, for example, for the complicated *in situ* applications, the needle length should be selected to avoid the cell damage peak, as illustrated in Figure 6b.

Cell damage distribution in the radial direction of a needle

As seen from equations 7 and 9, both the shear stress and the exposure time, experienced by cells in the needle, vary in

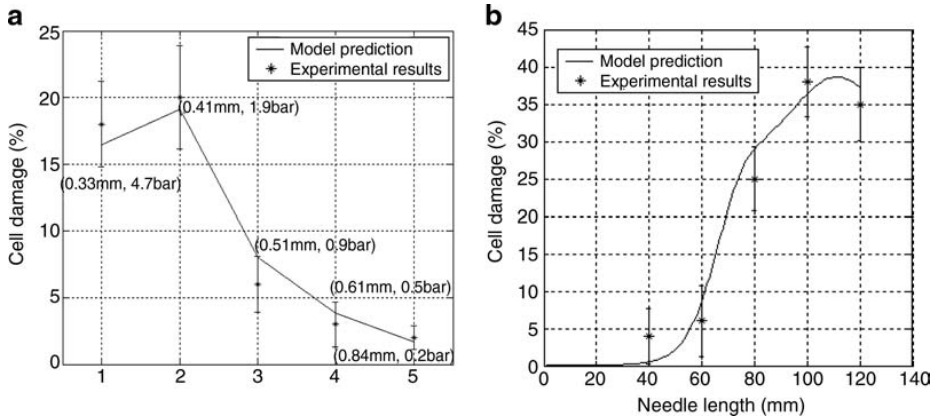

FIG. 6. Cell damages under different conditions: (**a**) Percentage of cell damage under constant flow rate; (**b**) Influence of needle length on cell damage (air pressure = 500 kPa, needle inner diameter = 840 μm).

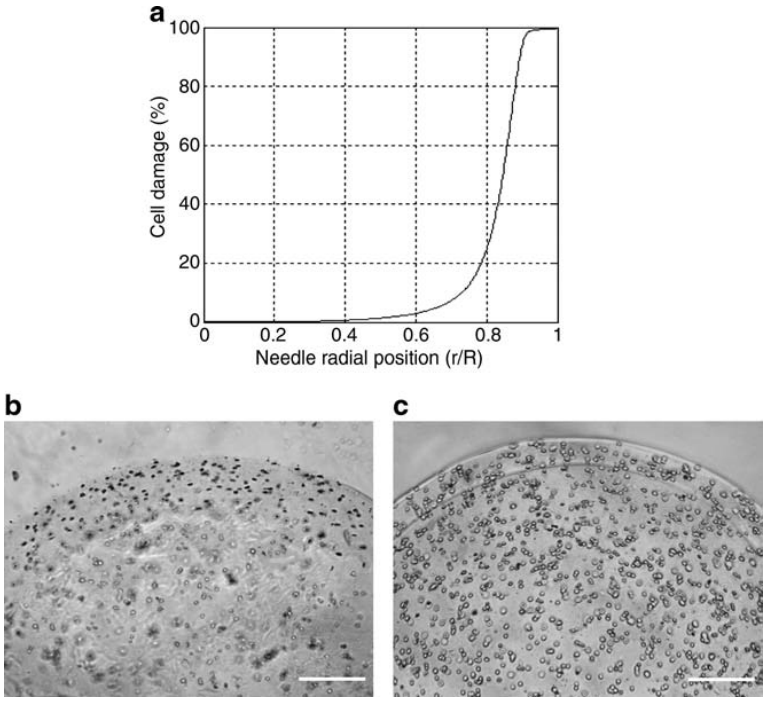

FIG. 7. Cell damage distribution in the radial direction of the needle. (**a**) Simulation results, (**b**) cell damage distribution in the cross section of the strand dispensed under a pressure of 500 kPa, and (**c**) cell damage distribution in the control group dispensed under the gravity of cell suspension. Bars = 100 μm.

the radial direction, thereby causing uneven distribution of cell damage along the direction. To investigate this distribution, the percentage of cell damage at different radii were simulated by means of the developed model and the results are shown in Figure 7a for the case where the air pressure is 500 kPa, the needle diameter is 840 μm, and the needle length is 80 mm. It is seen that damaged cells are concentrated near the needle wall where the shear stress is largest. Comparatively, most of the cells nearer to the needle center survive because of the lower shear stress presented. Therefore, it is concluded that cells near the needle wall are most vulnerable in the biodispensing process. To validate this conclusion, experiments were also carried out, in which cell suspension was dispensed into the crosslinking agent 0.5% calcium chloride solution to form a solid strand. The strand was then sliced into 50 μm and observed under a microscope. Figure 7b shows the picture of the dead/living cells distributed in the cross section of the strand, in which the dead cells are in black and the living cells are in white. Most of dead cells are located at the edge of the strands. Such an uneven distribution of cell damage along the radial direction was also previously observed and reported[21] when dispensing hepatocyte cells. In contrast, few cells are damaged and the damaged cells are evenly distributed in the cross section of the strand in the control group, which was extruded under the gravity of the cell suspension (Fig. 7c).

Conclusions

This article presents a method to model the process-induced cell damage incurred in the biodispensing process. The first step of the method is to establish the cell damage laws to relate cell damage to the hydrostatic pressure/shear stress that are applied on cells; and the second step is to represent the percentage of cell damage in the biodispensing process based on the established cell damage law as well as the analysis of the process-induced forces on the cell suspension during the dispensing process.

Using experiments, the influence of hydrostatic pressure on cell (both Schwann cell and 3T3 fibroblasts) damage was determined to be small, whereas the influence of shear stress and time period acting on cells was found to be significant. This suggests that cell damage in the biodispensing process was largely attributed to shear stresses and exposure times in the dispensing needle, while having a little connection to the air pressure present in the reservoir. To represent the influence of shear stress on cell damage, a bivariate normal distribution function was chosen for use. It has been shown that the use of bivariate normal distribution function in establishing the cell damage law is more appropriate than the use of the power law equation reported in the literature, as the limit exhibited by the power law equation is overcome when either the shear stress or the exposure time becomes really large.

Experiments with dispensing Schwann cells and 3T3 fibroblasts were carried out with varying process parameters. It is concluded that the percentage of cell damage of both Schwann cells and 3T3 fibroblasts varies, depending on the process parameters that were employed in the experiments. Particularly, the percentage of cell damage increases with the air pressure applied and decreases with the needle diameter. It is also concluded that cell damage can be affected by the needle length, but in a complicated manner. In the examined case, it is shown that the percentage of cell damage generally increases with the needle length. All of the conclusions drawn suggest that the process parameters can be optimized

to optimally preserve cell viability in the biodispensing process. Besides, the experimental results obtained also show that the cell damage is unevenly distributed along the needle radial direction. More specifically, cells located near the needle wall are more vulnerable than those near the center.

The experimental results were also compared with the simulations results obtained from the developed model to illustrate the effectiveness of the method presented in this article. It has been shown that the experimental data can be well reproduced by means of the developed model. This would represent a significant advance in tissue engineering, as the model would allow one to rigorously design/determine the biodispensing process to achieve the reproducible control over the distribution of the cell within tissue engineering constructs or devices, instead of relying upon a trial-and-error process as previously reported.

Acknowledgments

The authors acknowledge the financial support from the Canada Foundation for Innovation and the Saskatchewan Health Research Foundation.

Disclosure Statement

No competing financial interests exist for any of the authors.

References

1. Park, T.H., and Shuler, M.L. Integration of cell culture and microfabrication technology. Biotechnol Prog **19,** 243, 2003.
2. Landers, R., and Mulhaupt, R. Desktop manufacturing of complex objects, prototypes and biomedical scaffolds by means of computer-assisted design combined with computer-guided 3D plotting of polymers and reactive oligomers. Macromol Mater Eng **282,** 17, 2000.
3. Khalil, S., Nam, J., and Sun, W. Multi-nozzle deposition for construction of 3D biopolymer tissue scaffolds. Rapid Prototyping J **11,** 9, 2005.
4. Cohen, D.L., Malone, E., Lipson, H., and Bonassar, L.J. Direct freeform fabrication of seeded hydrogels in arbitrary geometries. Tissue Eng **12,** 1325, 2006.
5. Wand, X., Yan, Y., Pan, Y., Xiong, Z., Liu, H., Cheng, J., Liu, F., Lin, F., Wu, R., Zhang, R., and Lu, Q. Generation of three-dimensional hepatocyte/gelatin structures with rapid prototyping system. Tissue Eng **12,** 83, 2006.
6. Xu, T., Jin, J., Gregory, C., Hickman, J.J., and Boland, T. Inkjet printing of viable mammalian cells. Biomaterials **26,** 93, 2005.
7. Varghese, D., Deshpande, M., Xu, T., Kersri, P., Ohri, S., and Boland, T. Advances in tissue engineering: cell printing. J Thorac Cardiovasc Surg **129,** 470, 2005.
8. Mironov, V., Boland, T., Trusk, T., Forgacs, G., and Markwald, R.R. Organ printing: computer-aided jet-based 3D tissue engineering. Trends Biotechnol **21,** 157, 2003.
9. Boland, T., Mironov, V., Gutowska, A., Roth, E.A., and Markwald, R.R. Cell and organ printing 2: fusion of cell aggregates in three-dimensional gels. Anat Rec Part A **272,** 497, 2003.
10. Albrecht, D.R., Tsang, V.L., Sah, R.L., and Bhatia, S.N. Photo- and electropatterning of hydrogel-encapsulated living cell arrays. Lab Chip **5,** 111, 2005.
11. Albrecht, D.R., Underhill, G.H., Wassermann, T.B., Sah, R.L., and Bhatia, S.N. Probing the role of multicellular organization in three-dimensional microenvironments. Nat Methods **3,** 369, 2006.
12. Wang, X., Yan, Y., Pan, Y., Xiong, Z., Liu, H., Cheng, J., Liu, F., Lin, F., Wu, R., Zhang, R., and Lu, Q. Generation of three-dimensional hepatocyte/gelatin structures with rapid prototyping system. Tissue Eng **12,** 83, 2006.
13. Xu, W., Wang, X., Yan, Y., Zheng, W., Xiong, Z., Lin, F., Wu, R., and Zhang, R. Rapid prototyping three-dimensional cell/gelatin/fibrinogen constructs for medical regeneration. J Bioact Compat Polym **22,** 363, 2007.
14. Chen, J., Lin, F., Liu, H., Yan, Y., Wang, X., Zhang, R., and Xiong, Z. Rheological properties of cell-hydrogel composites extruding through small diameter tips. ASME J Manuf Sci Eng **130,** 021014, 2008.
15. Wheeler, A., Throndset, W., Whelan, R., Leach, A., Zare, R., Liao, Y., Farrell, K., Manger, I., and Daridon, A. Microfluidic device for single cell analysis. Anal Chem **75,** 3581, 2003.
16. Fu, A.Y., Chou, H.-P., Spence, C., Arnold, F.H., and Quake, S.R. An integrated microfabricated cell sorter. Anal Chem **74,** 2451, 2002.
17. Srinivasan, V., Pamula, V.K., and Fair, R.B. Droplet-based microfluidic lab-on-a-chip for glucose detection. Anal Chim Acta **507,** 145, 2004.
18. Shackman, J.G., Dahlgren, G.M., Peters, J.L., and Kennedy, R.T. Perfusion and chemical monitoring of living cells on a microfluidic chip. Lab Chip **5,** 56, 2005.
19. Barbee, K.A. Mechanical cell Injury. Ann NY Acad Sci **1066,** 67, 2005.
20. Smith, C.M., Stone, A.L., Parkhill, R.L., Stewart, R.L., Simpkins, M.W., Kachurin, A.M., Warren, W.L., and Williams, S.K. Three-dimensional bioassembly tool for generating viable tissue-engineered constructs. Tissue Eng **10,** 1566, 2004.
21. Wang, X., Yan, Y., Pan, Y., Xiong, Z., Liu, H., Cheng, J., Liu, F., Lin, F., Wu, R., Zhang, R., and Lu, Q. Generation of three-dimensional hepatocyte/gelatin structures with rapid prototyping system. Tissue Eng **12,** 83, 2006.
22. Cohen, D.L., Malone, E., Lipson, H., and Bonassar, L.J. Direct freeform fabrication of seeded hydrogels in arbitrary geometries. Tissue Eng **12,** 1325, 2006.
23. Chang, R., Nam, J., and Sun, W. Effects of dispensing pressure and nozzle diameter on cell survival from solid freeform fabrication-based direct cell writing. Tissue Eng A **1441,** 2008.
24. Blackshear, P.L., Dorman, F.D., and Steinbach, J.H. Some mechanical effects that influence haemolysis. Trans Am Soc Artif Intern Organs **11,** 112, 1965.
25. Giersiepen, M., Wurzinger, L.J., Opitz, R., and Reul, H. Estimation of shear stress related blood damage in heart valve prosthese: *in vitro* comparison of 25 aortic valves. Int J Artif Organs **13,** 300, 1990.
26. Reinhard, P., Apel, J., Klaus, S., Schugner, F., Schwindke, P., and Reul, H. Shear stress related blood damage in laminar couette flow. Artif Organs **27,** 517, 2003.
27. Grigioni, M., Daniele, C., Morbiducci, U., D'Avenio, G., Di Benedetto, G., and Barbaro, V. The power-law mathematical model for blood damage prediction: analytical developments and physical inconsistencies. Artif Organs **28,** 467, 2004.
28. Grigioni, M., Daniele, C., Morbiducci, U., D'Avenio, G., Di Benedetto, G., and Del Gaudio, C. A novel formulation for blood trauma prediction by a modified power-law mathematical model. Biomech Model Mechanobiol **4,** 249, 2005.

29. Vickroy, B., Lorenz, K., and Kelly, W. Modeling shear damage to suspended CHO cells during cross-flow filtration. Biotechnol Prog **23,** 194, 2007.
30. Nakamura, S., Arai, Y., Takahashi, K.A., Terauchi, R., Ohashi, S., Mazda, O., Imanishi, J., Inoue, A., Tonomura, H., and Kubo, T. Hydrostatic pressure induces apoptosis of chondrocytes cultured in alginate beads. J Orthop Res **24,** 733, 2006.
31. Gupta, R., Chafik, D., Bear, D., Patel, A., Jones, N.F., Kim, B., and Hung, C.T. Optimization of Schwann-cell adhesion for peripheral-nerve tissue engineering. J Reconstr Microsurg **18,** 625, 2002.
32. Wong, T., McGrath, J.A., and Navsaria, H. The role of fibroblasts in tissue engineering and regeneration. Br J Dermatol **156,** 1149, 2007.
33. Macosko, Ch.W. Rheology: Principles, Measurements, and Applications. New York: Wiley-VCH, 1994.
34. Campbell, R.C. Statistics for Biologists. Cambridge: Cambridge University Press, 1989.
35. Chen, X.B., Li, M.G., and Ke, H. Modeling of the flow rate in the dispensing-based process for fabricating tissue scaffolds. ASME J Manuf Sci Eng **130,** 021003, 2008.
36. Li, M.G., Tian, X.Y., and Chen, X.B. Modeling of flow rate, pore size and porosity for the dispensing-based tissue scaffolds fabrication. ASME J Manuf Sci Eng **131,** 034501, 2009.
37. Chen, X.B., Schonau, G., and Zhang, W.J. Modeling of time-pressure fluid dispensing processes. IEEE Trans Electron Pack **23,** 300, 2000.
38. Chhabraand, R.P., and Richardson, J.F. Non-Newtonian Flow in the Process Industries. Oxford: Butterworth-Heinemann, 1999.
39. Parkkinen, J.J., Lammi, M.J., Inkinen, R., Jortikka, M., Tammi, K., Virtanen, I., and Helminen, H.J. Influence of short-term hydrostatic pressure on organization of stress fibers in cultured chondrocytes. J Orthop Res **13,** 495, 1995.
40. Zimmerman, A.M. High Pressure Effects on Cellular Processes. New York: Academic Press, 1970.
41. Dibb, W., Morild, E., and Laerum, O.D. Effect of high hydrostatic pressure effects *in vivo*: changes in microtubule assembly, and actin organization. Cell Motil Cytoskelet **10,** 380, 1988.

Address correspondence to:
Daniel X.B. Chen, Ph.D., P.Eng.
Department of Mechanical Engineering
University of Saskatchewan
57 Campus Dr.
Saskatoon SK S7N 5A9
Canada

E-mail: xbc719@mail.usask.ca

Received: March 16, 2009
Accepted: August 27, 2009
Online Publication Date:

CHAPTER 5

EFFECT OF NEEDLE GEOMETRY ON FLOW RATE AND CELL DAMAGE IN THE DISPENSING-BASED BIOMANUFACTURING PROCESS

Submitted as:

- Li, M.G., Tian, X.Y., Zhu, N., Schreyer, D.J., and Chen, X.B. Effect of needle geometry on flow rate and cell damage in the dispensing-based biomanufacturing processes. Submitted to Tissue Engineering, part C, March, 2010.

5.1 Introduction and Objectives

In hydrogel scaffold fabrication techniques, cylindrical needles are often used as the hydrogel delivery tools, as investigated in Chapter 4. However, this kind of needle has several disadvantages such as low flow rate and high cell damage percent. Tapered needles, on the other hand, can overcome these shortcomings and facilitate the hydrogel scaffolds fabrication.

The objective of this paper is to compare the flow rates and cell damage in the bio-dispensing processes using cylindrical and tapered needles and ultimately find the better needle type for bio-dispensing processes.

5.2 Method

Flow rate models for both cylindrical and tapered needles were developed based on the non-Newtonian fluid behaviours of the biomaterials; and then simulation and experiments were carried out to compare the flow rates in the two types of needles. Cell damage in these two types of needles were also compared through models developed and experiments performed.

5.3 Results

Both the simulation and experimental results show that flow rate in the tapered needle is much larger than that in a cylindrical needle under the same process conditions and thus, the air pressure needed to produce the same flow rate is much lower in the tapered needle. The cell damage percents in the tapered needles are also lower than those in the cylindrical needles given the same flow rate.

5.4 Contributions

The contributions of this paper are the development of flow rate models and cell damage models for both cylindrical and tapered needles and the comparison of the performances of the bio-dispensing processes using cylindrical and tapered needles. These models will help to select needle types in the bio-dispensing process for better process control and cell viability maintenance.

Effect of Needle Geometry on Flow Rate and Cell Damage in the Dispensing-Based Biomanufacturing Process

Minggan. Li[1] MSc, Xiaoyu Tian[2] MSc, Ning Zhu[2] MSc,

David J. Schreyer[3] PhD, and Xiongbiao Chen[1,2]* PhD

[1]Department of Mechanical Engineering, University of Saskatchewan
[2]Division of Biomedical Engineering, University of Saskatchewan
[3]Department of Anatomy and Cell Biology, University of Saskatchewan
Saskatoon, SK, S7N 5A9, Canada

* Corresponding author

Abstract: Dispensing techniques have been widely applied in biomanufacturing processes to deliver cell suspensions and biomaterials. Under identical operating conditions, two types of dispensing needles—tapered and cylindrical—can result in different flow and cell damage rates. In this work, models of flow and cell damage rates in biodispensing systems using tapered and cylindrical needles were developed and compared. Experiments were also carried out to verify the accuracy of the developed models. Both simulations and experiments show tapered needles create much higher flow rates under identical pressure conditions than cylindrical needles. Use of a much lower pressure in a tapered needle can therefore achieve the same flow rate as that in a cylindrical needle. Consequently, at equivalent flow rates, cell damage in a tapered needle dispensing system is lower. Application of the developed models to specify the influence of process parameters, including needle geometry and air pressure, on the flow rate and cell damage rate represents a significant advance for biomanufacturing processes. The models can be used to optimize process parameters, preserve cell viability, and achieve the desired cell distribution in dispensing-based biomanufacturing.

Key words: biodispensing process, flow rate, cell damage, model development

1. Introduction

In the biomanufacturing process, living cells are mixed with biocompatible solutions and precisely delivered onto designated targets to create designed bioproducts. Among various techniques that have been explored for cell suspension delivery, biodispensing is one of the most promising. This technique employs pressurized air in a syringe to drive cell suspensions out of a fine needle (see [1] for a review of technical features). Due to its high proficiency and easy maintenance, biodispensing has been widely used in different biomanufacturing applications, such as cell-encapsulated tissue scaffolds fabrication [2-4], microfluidic devices [5, 6], and lab-on-a-chip devices [7, 8].

Two types of needles—cylindrical and tapered—are used in biodispensing techniques, and their performance may differ greatly due to their different geometries. One potential difference between these two needle types is flow rate. Tapered needles have a large diameter at their entrance and small diameter at their exit, and these features may lead to a greater flow rate than cylindrical needles under identical pressure conditions. This also implies that a lower air pressure could be used with a tapered needle dispensing system to achieve the same flow rate, which would greatly facilitate biodispensing processes, especially with high viscosity materials. Although in a cylindrical needle dispensing system where air pressure becomes the limiting factor, high flow rates can be achieved by selecting a large diameter needle, the designed features of the products may be altered; for example, the strand diameter of a tissue scaffold, which is determined by the needle size, may be altered along with its mechanical and biological properties [1, 9]. Employing tapered needles may overcome these problems. Despite the potential advantages of tapered needles, flow rates have not been quantitatively studied for biomanufacturing processes or compared to cylindrical needles. Flow rate control is one of the most important issues in biomanufacturing processes because it greatly affects the performance of the fabricated products, including pore size and porosity [9-11] as well as mechanical properties of tissue scaffolds [12]. Hence, a model to predict the flow rate for tapered

needles would be of great benefit.

Cell damage rates may also vary between systems employing tapered and cylindrical needles. During the dispensing process, cells are subjected to mechanical forces; if these forces or force duration exceed certain levels, cells are damaged to the point they may not maintain their phenotype or even survive the process [13]. In our previous study [14], we developed a mathematical model to predict cell damage in the biodispensing process using cylindrical needles. However, a tapered needle system may result in different cell damage due to its different geometry and mechanical force distribution. To optimize the biodispensing process and minimize cell damage rates in the biomanufacturing process, developing a cell damage model for a tapered needle system is essential.

Selection of needle type is very important, as it affects not only the physical performance of the techniques (e.g., flow rate of dispensing) but also influences biological properties of the bioproducts (e.g., cell damage). This work focuses on determining the effects of a tapered needle on flow rate and cell damage in the biodispensing process, and comparing results with those obtained using a cylindrical needle. The objective is to identify optimal biodispensing techniques for process control and cell damage minimization.

2. Flow rate model development

2.1 Flow behaviour of cell suspensions. Cell suspensions are a mixture of cells and biomaterial solution. Due to the high molecular weight and long molecular chains of the biomaterials, cell suspensions display non-Newtonian flow behaviour, which can be described with a power law equation, given by

$$\tau = K\dot{\gamma}^n, \tag{1}$$

where K is the consistency index with the unit of Pa·s^n, n is the flow behaviour index (dimensionless), and $\dot{\gamma}$ is the shear rate.

2.2 Flow rate models for the biodispensing processes. A typical dispensing system for use with cylindrical or tapered needles (Figure 1) employs pressurized air

to drive the cell suspension or biomaterials stored in the syringe out of the needle, where P is pressure applied to the syringe, P_e the pressure in the cell suspension at the exit of the needle, D_c and L_c are the internal diameter and the length of the cylindrical needle, respectively, D_i and D_o are the diameters at the entrance and the exit of the tapered needle, respectively, θ_0 is the half cone angle, and L_t the length of the tapered needle. For a given length L_t and diameters D_i and D_o, the half cone angle can be expressed as

$$\theta_0 = \arctan\left(\frac{D_i - D_o}{2L_t}\right). \tag{2}$$

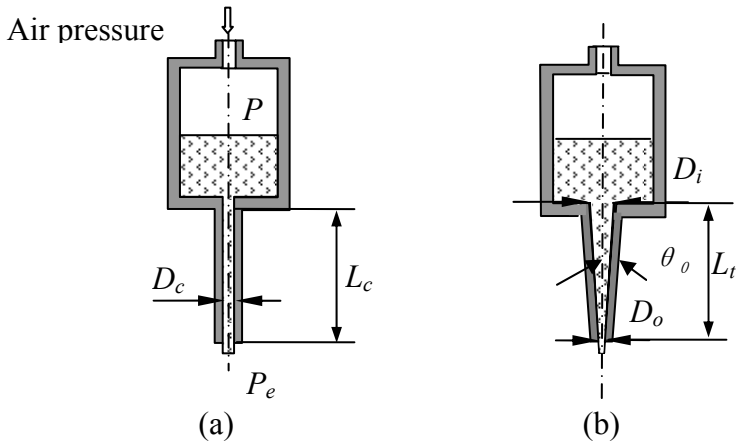

Fig. 1. Biodispensing process using a (a) cylindrical or (b) tapered needle.

In the biodispensing process, the following assumptions are made: (1) the cell suspension is incompressible, implying its density is constant during the process; (2) the fluid flow in the needle is steady and fully-developed, so the velocity profile does not change with time; (3) there is no slip between the cell suspension and the needle wall, (4) the pressure drop in the reservoir due to the fluid flow is negligible given the syringe diameter is much greater than the needle diameter; and (5) minor losses due to entrance effects can be neglected given the flow velocity in the needle is small. Under these assumptions, the pressure drop in the needle is given by [15]

$$\Delta P = P - P_e, \tag{3}$$

where P is the pressure of air applied to the syringe and P_e is the pressure at the exit or ambient air pressure.

The flow rate model in the cylindrical needle developed in our previous work has been successfully applied to biodispensing applications [9, 10]. Specifically, the flow velocity distribution along the radial direction is

$$V_c(r) = \frac{n}{n+1}\left(\frac{-\Delta P}{KL_c}\frac{D_c}{4}\right)^{1/n}\frac{D_c}{2}\left[1-\left(\frac{2r}{D_c}\right)^{(n+1)/n}\right]. \quad (4)$$

Integration of the velocity profile function of Eq. (4) along the circumferential direction yields the flow rate

$$Q_c = \frac{\pi D_c^3}{8K^m}\tau_w^m, \quad (5)$$

where m=1/n. τ_w is the wall shear stress and is related to the pressure drop by $\tau_w = D_c\Delta P / 4L_c$.

In the tapered needle (Fig. 2), for a small element of length, δl, the force balance leads to

$$\delta\Delta P\pi r_f^2 = 2\pi r_f \delta l \sec\theta_0 \delta_s \cos\theta_0. \quad (6)$$

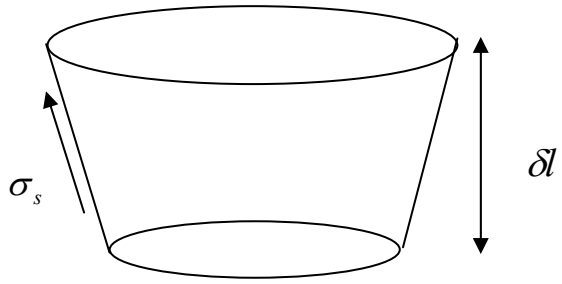

Fig. 2. Schematic of flow rate derivation in a tapered needle.

If the flow behaviour of the cell suspension is described by Eq. (1), then the flow rate model in a tapered needle is given by [16]

$$Q_t = \frac{\pi D_i^3 D_o^3}{32}\left[\frac{3n\Delta P\tan\theta_0}{2K(D_i^{3n}-D_o^{3n})}\right]^{\frac{1}{n}}. \quad (7)$$

From Eqs. (4) and (7), the flow rate for each needle type is a function of both flow behavior and needle geometry parameters.

3. Cell damage model development

3.1 Cell damage law. In the biodispensing process, cells are subjected to hydrostatic forces in the syringe and shear forces in the needle, which may cause cell damage if the forces and force duration exceed certain levels. As different biodispensing process parameters generate different forces and force durations on cells, a cell damage law that addresses the relationship between cell damage and forces and force duration is necessary. In our previous work [14], we developed a cell damage law based on a normal distribution function, in which the cell damage rate under pressure or shear force ($I_{p,s}$) is expressed as a function of force (τ) and the corresponding exposure time (t), taking the form of

$$I_{p,s}(\tau,t)=\int_t\int_\tau f(\tau,t)d\tau dt\,, \tag{8}$$

where $f(\tau,t)$ is the probability density function and given by

$$f(s,t)=\frac{1}{2\pi\sigma_s\sigma_t\sqrt{1-\rho^2}}\exp\left[-\frac{z}{2(1-\rho^2)}\right], \tag{9}$$

where $z\equiv\left(\frac{s-\mu_s}{\sigma_s}\right)^2-2\rho\left(\frac{s-\mu_s}{\sigma_s}\right)\left(\frac{t-\mu_t}{\sigma_t}\right)+\left(\frac{t-\mu_t}{\sigma_t}\right)^2$ and μ_s, μ_t are the mean values of force s (pressure or shear) and exposure time t, respectively; σ_s and σ_t are the standard deviations of the s and t, respectively; and ρ is the correlation coefficient between s and t. These five parameters are determined experimentally, and can be obtained for both pressure and shear stress conditions. Previous study shows that hydrostatic pressure under 500 kPa has no effect on cell viability and thus only shear stresses in the dispensing needle are considered as factors causing cell damage [14].

3.1 Cell damage model in a cylindrical needle biodispensing system. By applying the cell damage law to the shear force and force duration that cells experience in the dispensing needle, the cell damage in the cylindrical needle can be determined. The shear stress along the radial direction in the needle is

$$\tau_c(r)=\frac{-\Delta P}{2L_c}r\,, \tag{10}$$

and the time for cells to travel through the needle is:

$$t_c(r) = \frac{L_c}{V_c(r)} \quad , \tag{11}$$

where $V_c(r)$ is given in Eq. (4).

Then,

$$I_c = \frac{8\int_0^{\frac{D_c}{2}} rI_s(\tau_c, t_c)dr}{D_c^2} \quad , \tag{12}$$

where $I_s(\tau_c, t_c)$ is the cell damage law under shear force, and τ_c and t_c are the shear force distribution and corresponding shearing time, respectively, in the cylindrical needle. Details regarding the development of the cell damage model in the cylindrical needle dispensing system can be found in [14].

3.2 Cell damage in a tapered needle biodispensing system. Given the known relationship between cell damage and shear force, development of a cell damage model in a tapered needle dispensing system requires knowledge of the shear force distribution and shearing time. For convenience, a spherical polar coordinate is used in the tapered needle as shown in Fig. 2. For non-Newtonian fluid flow through a tapered needle, the velocity at the position (θ,r) is given by [17]

$$V_t(\theta, r) = -\frac{CQ_t(\cos^2\theta - \cos^2\theta_0)}{r^2} \quad , \tag{13}$$

where C is a constant and is defined as $C = 3/2\pi(1+2\cos\theta_0)(1-\cos\theta_0)^2$. Q_t is the flow rate in the tapered needle and can be obtained from Eq. (4). Then, on a streamline S, the arrival of cells from the entrance ($(L_t + R_1\cos\theta_0)/\cos\theta \approx R$) of the needle at position r takes a time of

$$t_t(\theta, r) = \int_r^R \frac{1}{-V_t(\theta, r)} dr \, . \tag{14}$$

The shear rate of the flow in the tapered needle at position r along θ direction can be

expressed as

$$A_t(\theta, r) = \frac{2CQ_t}{r^3}\cos\theta\sin\theta. \tag{15}$$

Thus, the shear force that cells experience at position (θ,r) in the tapered needle is

$$\tau_t(\theta, r) = KA_t^n. \tag{16}$$

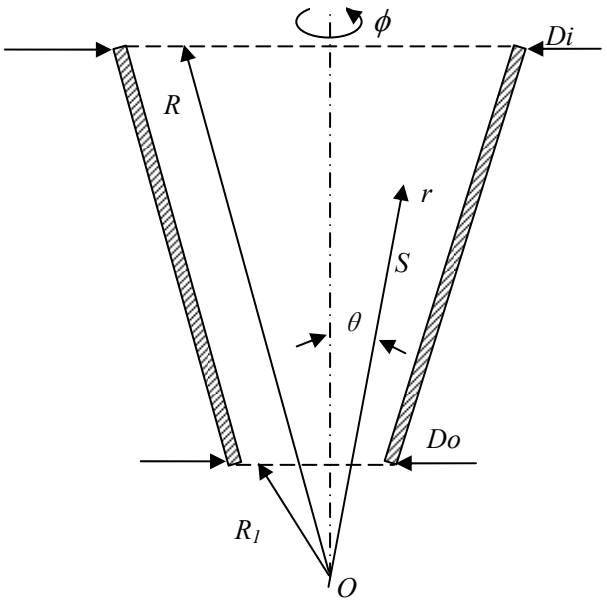

Fig. 3. Schematic of flow analysis in a tapered needle.

On a given streamline S, the cell damage rate at position (θ,r) can be obtained by integrating the cell damage density function (Eq. (8)) from the shear force at the entrance (zero) to the shear force at this position, and from the time at the entrance (zero) to the time of arriving at this position:

$$I_t(\theta, r) = \int_0^{t_t(\theta,r)} \int_0^{\tau_t(\theta,r)} f(\tau_t, t_t) d\tau dt, \tag{17}$$

Thus, the cell damage rate at the exit of the needle on this streamline can be expressed as

$$I_t(\theta) = \int_R^{R-R1} \int_R^{R-R1} f(\tau_t, t_t)\tau_t' t_t' dr dr. \tag{18}$$

Suppose cells are evenly distributed in the cell suspension at a cell density d. The total cell number in a unit length at the outside of the exit of the needle is then $\pi(\theta_0 R_1)^2 \cdot d$. The number of total dead cells in the same volume can be expressed

as $\int_0^{\theta_0} 2\pi\theta R_1^2 \cdot d \cdot I_t(\theta) d\theta$. The cell damage rate in the tapered needle dispensing system is then

$$I_t = \frac{2\int_0^{\theta_0} I_t(\theta)}{\theta_0^2}. \tag{19}$$

Because shear forces and shear times vary at different locations in both the cylindrical and tapered needles, cell damage models that include the effects of force and time are essential for predicting cell damage.

4. Experiments and Results

4.1 Chemical formulation. Sodium alginate powder (Sigma, St. Louis, MO) was dissolved in deionized water overnight to form a 7% (w/v) solution.

4.2 Cell suspension preparation. Schwann cells (derived from Schwann cell line ATCC) were grown in Dulbecco's Modified Eagle's medium (DMEM) (Sigma, St. Louis, MO) supplemented with 5% fetal bovine serum (FBS) and 1% antibiotic. The cells were then incubated at 37°C in a humidified atmosphere of 95% air and 5% CO_2. Immediately prior to use in our experiments, 5 mL of alginate solution was added respectively into 7.5, 6.7, 3.75, and 2 mL of cell culture medium to form 2, 3, 4, and 5% alginate cell suspensions. They were gently mixed with a pipette to ensure a uniform cell distribution and the final cell density was about 1×10^6/mL. All experiments were conducted at room temperature (~23°C).

4.3 Cell viability assay. Niagara blue was used to stain cells and assess cell viability. The number of living/dead cells was counted manually under a light microscope (Leica, Microsystem, Bannockburn, IL) immediately following the dispensing process.

4.4 Flow behaviour characterization of cell suspensions. Cell suspensions (0.5 mL) were carefully delivered to a cone-and-plate rheometer (HBDV-III, Brookfield, MA) and examined with a CP-52 spindle. The flow behaviour parameters *K* and *n* were then identified from the obtained flow curves (Table 1).

Table 1. Flow behaviour parameters of alginate solutions.

	Alginate Solution Concentration			
	2%	3%	4%	5%
K	2.37	3.01	6.85	10.82
n	0.67	0.65	0.60	0.54

4.5 Flow rate model verification and comparison of the effects of needle geometry on flow rate. To verify the flow rate models and compare the flow rates using the two types of needles, a biodispesing system adapted from a commercial fluid dispensing system (C0720M, Asymtek) was employed (Fig. 4). Cell suspensions were loaded into a syringe using a pipette, after which air pressure was applied to the syringe and the cell suspensions extruded through the needles. The dispensing system was controlled to deliver the cell suspension for 10 s. Data presented are the mean of flow rates from three runs, each determined by weighing the cell suspensions dispensed using an electronic balance with a resolution of 0.1 mg.

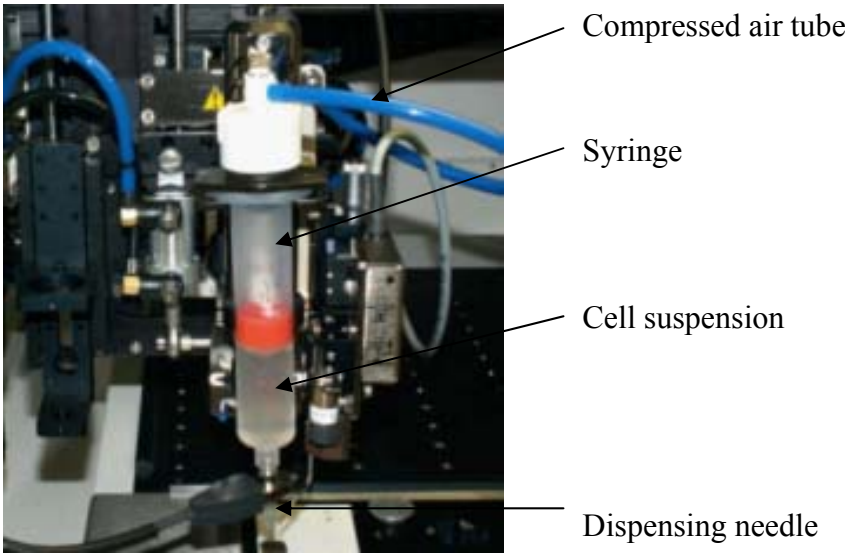

Fig. 4. Biodispensing system.

A first set of experiments investigated the effect of needle diameter on flow rate,

using cylindrical needles of 0.25, 0.33, and 0.42 mm diameter and 20 mm length. Exit diameters (D_o) of tapered needles were the same as the cylindrical needles; other geometrical parameters of the tapered needles are provided in Table 2. The air pressure was fixed at 300 kPa. Cell suspensions (5%) used in this experiment and associated flow behaviours are provided in Table 1. Experimental and simulated results, which were obtained using Matlab based on Eqs. (3)-(5) and the flow behaviour parameters, are illustrated in Fig. 5(a).

Table 2. Geometrical parameters of tapered needles (n=3)

Needle gauge	Needle parameters			
	D_i (mm)	D_o (mm)	θ_0 (grad)	L_t (mm)
25	3	0.25	0.0685	20
23	3	0.33	0.0665	20
22	3	0.41	0.0645	20

A second set of experiments compared the flow rate of each type of needle (D_o=0.25 mm for both types) at different pressures. Air pressures of 100, 200, 300, 400, and 500 kPa were applied to the dispensing system and the flow rate of each needle recorded (Fig. 5(b)); simulation results obtained using Eqs. (3)-(5) are shown for comparison.

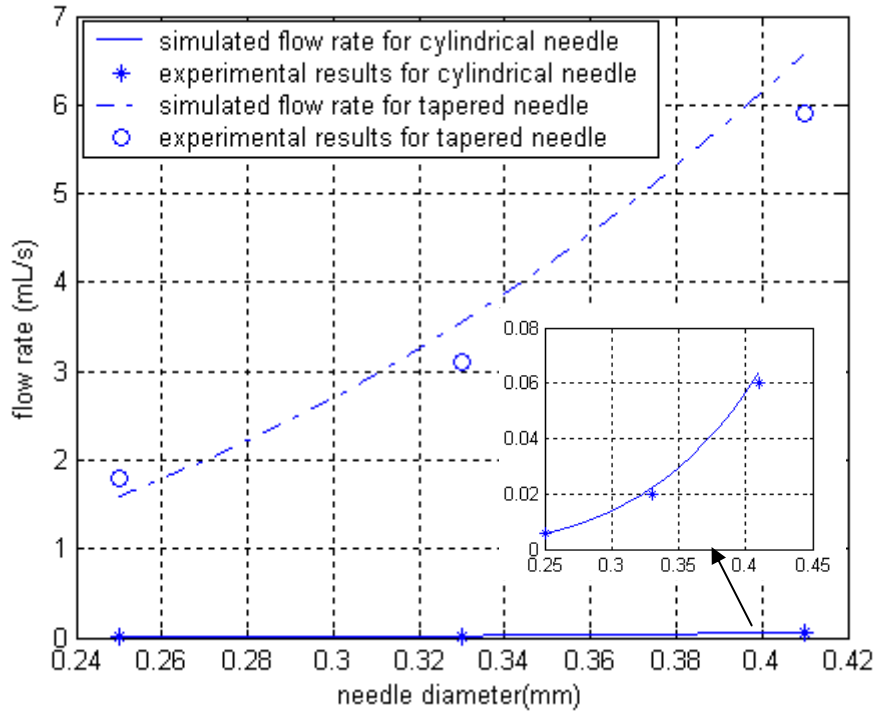

(a)

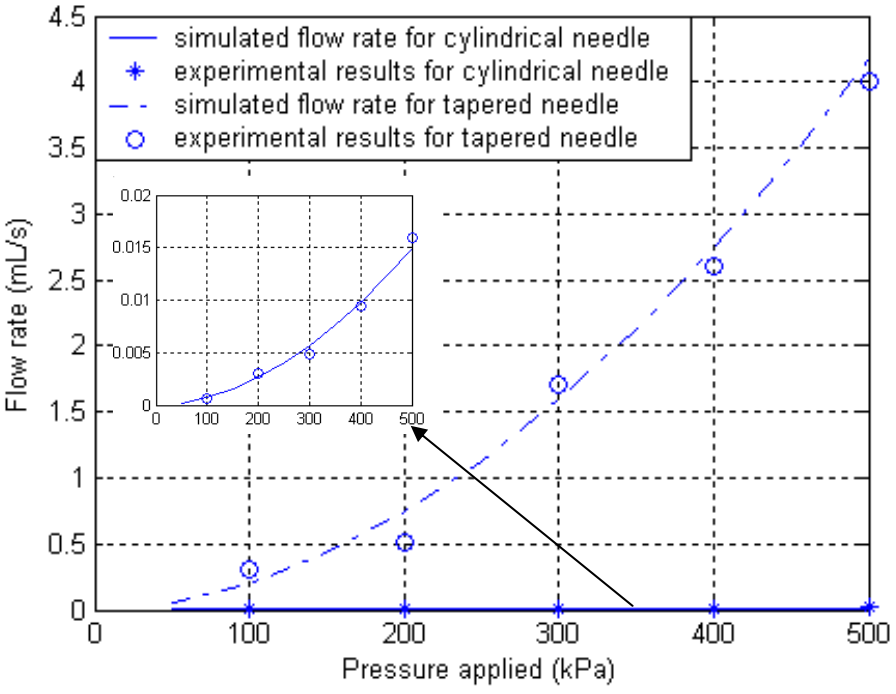

(b)

Fig. 5. Flow rate in two types of needles (a) with different diameter and (b) under different air pressure. Embedded figures are enlargements of cylindrical needle data, n=3.

Experimental results of flow rates with different needle diameters (Fig. 5(a)) and under different applied air pressures (Fig. 5(b)) agree well with the simulations, indicating the models can be used to reliably predict flow rate in biodispensing systems employing either cylindrical and tapered needles. Also clear from Fig. 5 is that the flow rate in tapered needle is much higher than in a cylindrical needle. For example, at an air pressure of 500 kPa, the flow rate in the tapered needle is almost 200-fold higher (Fig. 5(b)). This suggests tapered needles would be preferred if high flow rates are required. This is important if the biomaterial is very viscous and difficult to dispense using a cylindrical needle. It also indicates the flow rates in a cylindrical needle can be produced with lower air pressures in a tapered needle.

We also designed an experiment to investigate the air pressure required to obtain the same flow rates using the two types of needles. In this experiment, flow rates in a cylindrical needle with a diameter of 0.25 mm under pressures of 200, 300, 400, and 500 kPa were recorded. The needle was replaced with a tapered one of the same diameter (D_e), and the air pressures adjusted to produce the same flow rates as the cylindrical needle (Fig. 6). Pressures required to produce these flow rates in cylindrical and tapered needles were also obtained from the inverse calculation of Eqs. (3)-(5) and are shown for comparison as the smooth curves in Fig. 6.

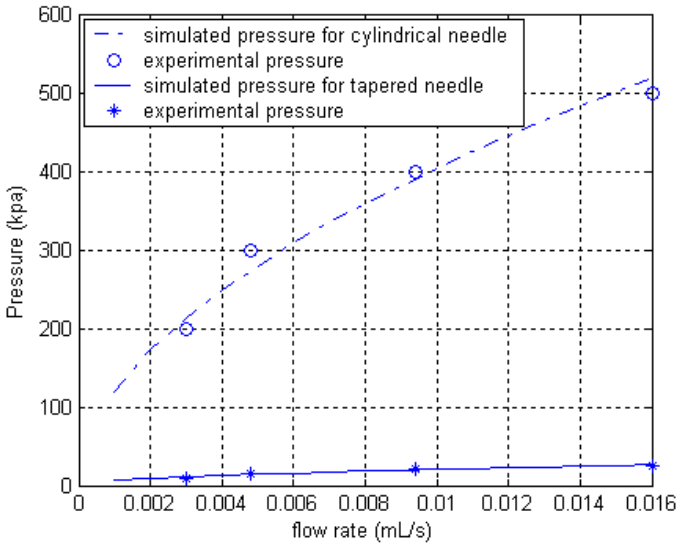

Fig. 6. Air pressures required to obtain the same flow rates in cylindrical and tapered needles, n=3.

Very low pressures, none exceeding 100 kPa, are required in the tapered needle dispensing system to achieve the same flow rates as the cylindrical needle dispensing system. This will be especially beneficial if the air pressure is limited in the application or if the biomaterials are very viscous.

4.6 Cell damage model verification and comparison of the effects of needle geometry on cell damage. The cell damage model was verified using the biodispensing system described above. In each experiment, 5 mL of cell suspension was loaded into the syringe using a pipette, after which air pressure was applied and the cell suspension extruded from the system using both cylindrical and tapered needles. Control cell suspensions were kept in tubes. The difference in percent cell damage between the test samples and controls was attributed to the biodispensing process. Each condition was repeated five times. The parameters in the cell damage law in the Eqs. (8) and (9) were determined using the method in [14] and the values for Schwann cells in this study are μ_τ=634.8 Pa, σ_τ=250.6 Pa, μ_t=10.08 s, σ_t=3.09 s, and ρ=0.29 .

One set of experiments investigated the influence of needle diameter on cell damage in the biodispensing process. Cell suspensions (5% alginate) were dispensed using cylindrical needles with diameters of 0.25, 0.33, and 0.41 mm under a constant air pressure of 500 kPa. Cell suspensions were then dispensed using tapered needles at air pressures set at values to obtain the same flow rates respectively for each needle diameter following the method described in section 4.5. Flow rates were 0.008, 0.02, and 0.06 $mL \cdot s^{-1}$ at diameters of 0.25, 0.33 and 0.41 mm, respectively. Cell damage simulations for the cylindrical and tapered needles were performed using Eqs. (10)-(12) and Eqs. (13)-(19), respectively. Experimental and simulation results are provided in Fig. 7.

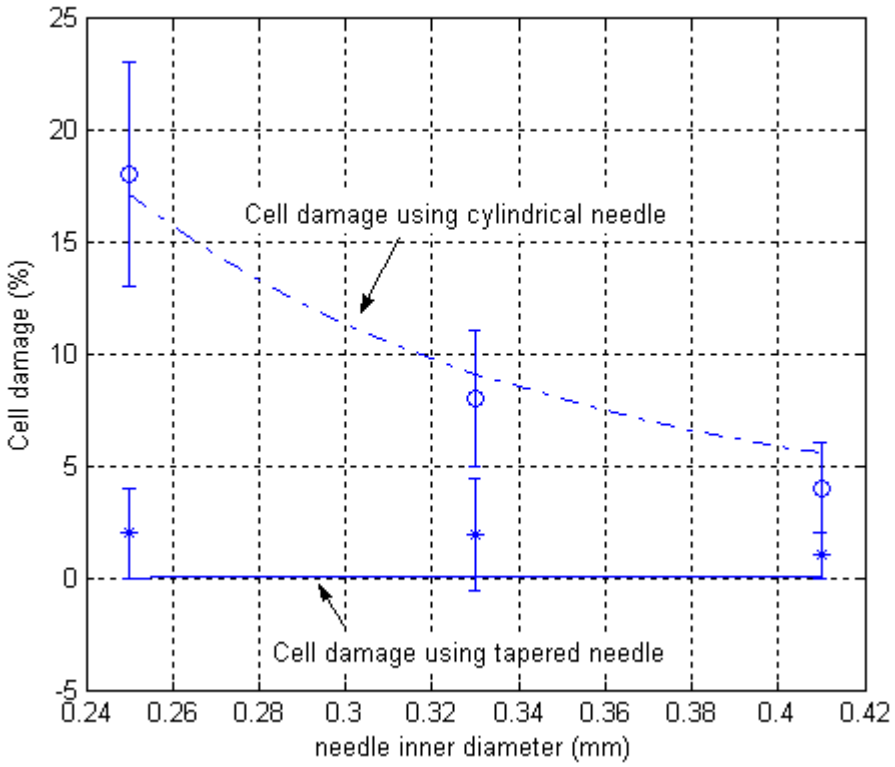

Fig. 7. Cell damage for different needle diameters at equivalent flow rates. Circles and asterisks represent the means of experimental data, n=5. Lines are simulation results.

As the needle diameter increases, cell damage resulting from both the cylindrical and tapered needles decrease. However, cell damage using the tapered needle is much lower than for the cylindrical needle, especially at small diameters. This suggests increasing the needle diameter or choosing a tapered needle will decrease cell damage in the biodispensing process. Therefore, in some precision applications, for example in microfluidic devices where the diameter of the channel is smaller than 100 μm, a tapered needle can be selected to take advantage of its ability to retain both precision and cell viability.

A second set of experiments investigated the effect of flow rate on cell damage in the two types of needles. Diameters (D_o) of 0.25 mm were selected for both types of needle. Air pressures of 200, 300, 400, and 500 kPa were applied in the cylindrical

needle dispensing process, and adjusted in the tapered needle dispensing process to achieve equivalent flow rates. Cell damage increases with increasing flow rate (Fig. 8); however, the cell damage using the tapered needle is much lower than that using cylindrical needle. At a flow rate of 0.015 mL/s, the cell damage difference is almost 15%. Simulation results based on Eqs. (10)-(12) and Eqs. (13)-(19) for cylindrical and tapered needles, respectively, are provided in the figure for comparison.

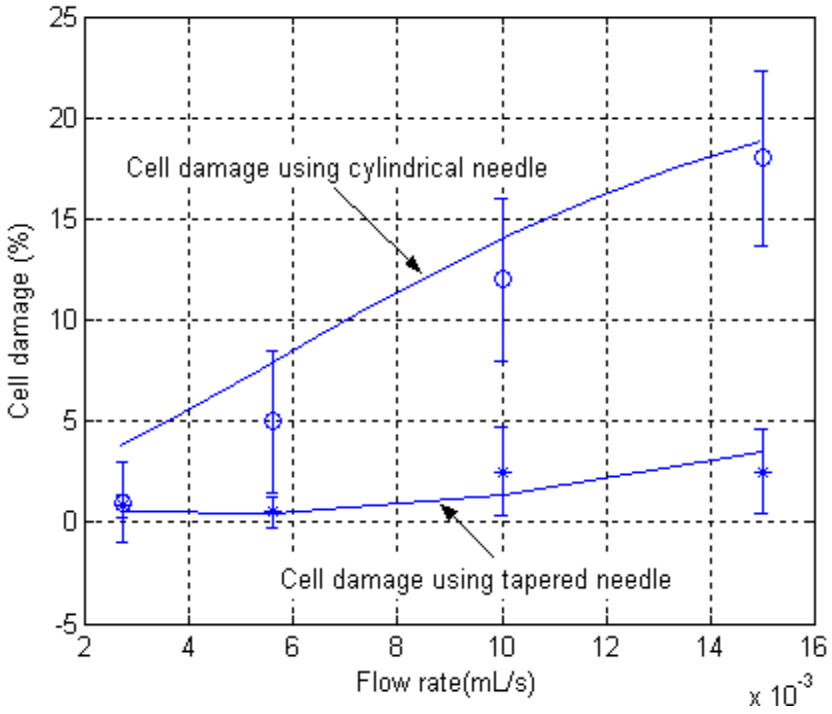

Fig. 8. Cell damage at different flow rates. Circles and asterisks are the mean of experimental data, n=5. Lines are simulation results.

A final set of experiments investigated the effect of biomaterial concentration on cell damage in the two types of needles. Cell suspensions with alginate concentrations of 2, 3, 4, and 5% were examined, using needle diameters of 0.25 mm and an air pressure of 500 kPa. Experimental results along with simulations based on flow behaviour parameters listed in Table 1 and Eqs.(10)-(12) and (13)-(19) are shown in Fig. 9. Cell damage increases with increasing alginate concentration, especially using the cylindrical needle, indicating the advantages of using a tapered needle in the

biodispensing processes.

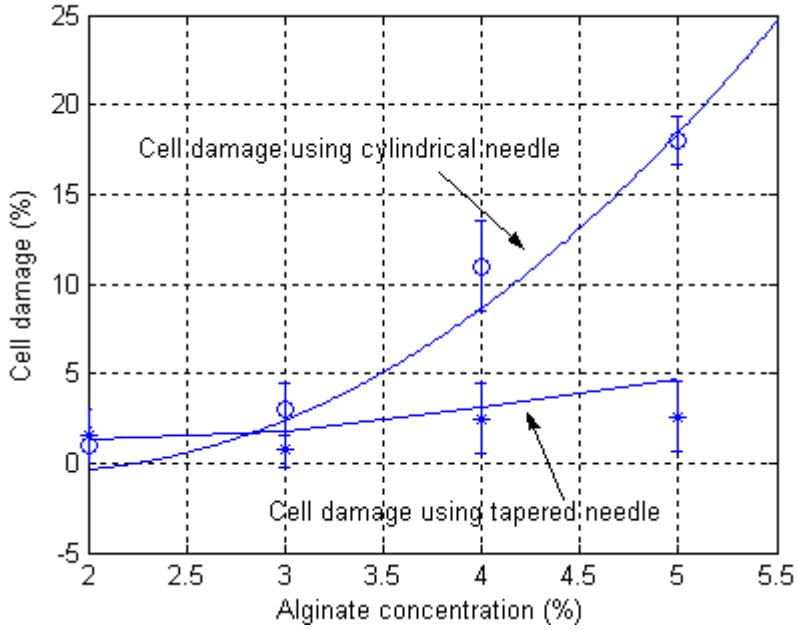

Fig. 9. Cell damage versus alginate concentration at equivalent flow rates. Circles and asterisks are the mean of experimental data, n=5. Lines are simulation results.

5. Conclusions

Two types of needles are available for biodispensing processes, with the selection having an impact on process performance. In this work, the effects of cylindrical and tapered needles on flow rate and cell damage in biodispensing applications were investigated and compared.

Flow rate models for both types of needles were presented and experiments were performed to verify the models. At a given air pressure, flow rates in tapered needles are much higher than in cylindrical needles. Thus, a much lower air pressure is required for a tapered needle system to obtain the same flow rate as a cylindrical needle system. The noted performance differences between the two types of needles will greatly facilitate needle selection in biodispensing applications to obtain desired flow rates, especially if the biomaterial has a high viscosity. The model presented will

also be helpful for flow rate control due to the good agreement between the model prediction and experimental results.

For a given flow rate, cell damage using a tapered needle is lower than using a cylindrical needle. Thus, cell damage in the biodispensing process can be minimized by choosing a tapered needle. Cell damage models were also developed based on a cell damage law, and were used to predict cell damage in different biodispensing process with close agreement with experimental results. These models will not only aid in the selection of needle types in the biodispensing process to decrease cell damage, but can also be used to optimize the biodispensing process to control cell distribution in the final bioproducts.

Acknowledgements

The authors acknowledge financial support from the Canada Foundation for Innovation (CFI), the Natural Sciences and Engineering Research Council (NSERC) of Canada, and the Saskatchewan Health Research Foundation (SHRF).

Author Disclosure Statement

No competing financial interests exist for any of the authors.

Reference

[1] M. G. Li, X. Y. Tian, and X. B. Chen, "A brief review of dispensing-based rapid prototyping techniques in tissue scaffold fabrication: role of modeling on scaffold properties prediction," *Biofabrication* **1**, 1, 2009.

[2] X. Wang, Y. Yan, Y. Pan, Z. Xiong, H. Liu, J. Cheng, F. Liu, F. Lin, R. Wu, R. Zhang, and Q. Lu, "Generation of three-dimensional hepatocyte/gelatin structures with rapid prototyping system," *Tissue Eng.* **12**, 83, 2006.

[3] J. Cheng, F. Lin, H. X. Liu, Y. N. Yan, X. H. Wang, R. Zhang, and Z. Xiong, "Rheological properties of cell-hydrogel composites extruding through small-diameter tips," *Trans. of ASME, J. Manuf. Sci. Eng.* **130**, 021014, 2008.

[4] W. Xu, X. H. Wang, Y. N. Yan, W. Zheng, Z. Xiong, F. Lin, R. D. Wu, and R. J. Zhang, "Rapid prototyping three-dimensional cell/gelatin/fibrinogen constructs for medical regeneration," *J. Bioact. Compat. Polym.* **22**, 363, 2007.

[5] A. Y. Fu, H. P. Chou, C. Spence, F. H. Arnold, and S. R. Quake, "An integrated microfabricated cell sorter," *Anal. Chem.* **74**, 2451, 2002.

[6] A. R. Wheeler, W. R. Throndset, R. J. Whelan, A. M. Leach, R. N. Zare, Y. H. Liao, K. Farrell, I. D. Manger, and A. Daridon, "Microfluidic device for single-cell analysis," *Anal. Chem.* **75**, 3581, 2003.

[7] J. G. Shackman, G. M. Dahlgren, J. L. Peters, and R. T. Kennedy, "Perfusion and chemical monitoring of living cells on a microfluidic chip," *Lab Chip* **5**, 56, 2005.

[8] V. Srinivasan, V. K. Pamula, and R. B. Fair, "Droplet-based microfluidic lab-on-a-chip for glucose detection," *Anal. Chim. Acta* **507**, 145, 2004.

[9] M. G. Li, X. Y. Tian, and X. B. Chen, "Modeling of flow rate, pore size, and porosity for dispensing-based tissue scaffolds fabrication," *Trans. of ASME, J. Manuf. Sci. Eng.* **131**, 034501, 2009.

[10] X. B. Chen, M. G. Li, and H. Ke, "Modeling of the flow rate in the dispensing-based process for fabricating tissue scaffolds," *Trans. of ASME, J. Manuf. Sci. Eng.* **130**, 021003, 2008.

[11] G. Vozzi, A. Previti, D. De Rossi, and A. Ahluwalia, "Microsyringe-based deposition of two-dimensional and three-dimensional polymer scaffolds with a well-defined geometry for application to tissue engineering," *Tissue Eng.* **8**, 1089, 2002.

[12] T. B. F. Woodfield, J. Malda, J. de Wijn, F. Peters, J. Riesle, and C. A. van Blitterswijk, "Design of porous scaffolds for cartilage tissue engineering using a three-dimensional fiber-deposition technique," *Biomaterials* **25**, 4149, 2004.

[13] K. A. Barbee, "Mechanical cell injury," *Ann N Y Acad Sci* **1066**, 67, 2005.

[14] M. Li, X. Tian, N. Zhu, D. J. Schreyer, and D. Chen, "Modeling Process-Induced Cell Damage in the Bio-Dispensing Process," *Tissue Eng. Part C*, 2009 (in press).

[15] X. B. Chen, G. Schoenau, and W. J. Zhan, "Modeling of time-pressure fluid dispensing processes," *IEEE Trans. Electron. Packag. Manuf.* **23**, 300, 2000.

[16] F. N. Cogswell, "Converging Flow of Polymer Melts in Extrusion Dies," *Polym. Eng. Sci.* **12**, 64, 1972.

[17] G. Bohme, *Applied mathematics and mechanics*. Amserdam: Elsevier Science Publishers B.V., 1987.

Reprint Author

Daniel X.B. CHEN, Ph.D., P.Eng.

Professor

Department of Mechanical Engineering

University of Saskatchewan

57 Campus Dr.

Saskatoon, SK S7N 5A9

Canada

Telephone: (306)966-1267

Fax: (306)966-5427

Email: xbc719@mail.usask.ca

Website: www.engr.usask.ca/~xbc719/

CHAPTER 6

MODELING OF CELL DAMAGE IN THE BIO-DISPENSING PROCESSES INVOLVING HIGH SHEAR STRESS

Submitted as:

- Li, M.G., Tian, X.Y., Schreyer, D.J., and Chen, X.B. Modeling of cell damage in the bio-dispensing processes involving high shear stress. Submitted to Biofabrication, May, 2010.

6.1 Introduction and Objectives

The previous chapter investigated the cell damage percent in tapered needle under low flow rate conditions (<0.02 mL/s). However, in the dispensing-based scaffold fabrication techniques, if tapered needle is used, the flow rate may reach 10 mL/s. Also, in other biofabrication process such as cell jetting and printing, the transient flow rate is also very high. Under high flow rate, cells are driven out of the needle at very high speed, which generates high shear stress on cells and may cause cell damage in a very short time period.

The time periods for cell damage under low shear stresses are greatly different from those under high shear stress. Thus, the cell damage law established in the previous chapters may not work well as applied to high speed bio-dispensing processes. The objective of this research is to study the cell damage under high shear stress and develop cell damage model for bio-dispensing processes involving high shear stress.

6.2 Method

A cell damage model in the bio-dispensing process with high shear stresses is first developed and the parameters in this cell damage model are identified from the bio-dispensing experiments. Then this cell damage model with the identified parameters is validated through bio-dispensing experiments with different process parameters.

6.3 Results

The parameters in the cell damage model are identified and the results show that the time period for cell damage under high stress is much shorter than that under low stress. This cell damage law is also applied to high speed bio-dispensing processes and both the simulation and experimental results show that cell damage percents in these processes are very high.

6.4 Contributions

The main contribution of this paper is the development of cell damage model under high shear stresses. This will facilitate the prediction of cell damage in bio-manufacturing processes involving high shear stresses, including cell ink-printing and cell jetting processes and optimization of these processes to retain cell viability.

Modeling of Cell Damage in the Biodispensing Process Involving High Shear Stresses

M.G. Li[1], X.Y. Tian[2], D. J. Schreyer[3], and X.B. Chen[1,2]*

[1]Department of Mechanical Engineering, University of Saskatchewan
[2]Division of Biomedical Engineering, University of Saskatchewan
[3]Department of Anatomy and Cell Biology, University of Saskatchewan
Saskatoon, SK, S7N 5A9, Canada

*Corresponding author Email : xbc719@mail.usask.ca

Abstract: In cell printing and jetting, due to the high speed of the flows in the needle, cells normally experience high shear stresses (~60,000 Pa), which may cause cell damage in a very short time. The cell damage prediction model developed under low shear stresses (~1200 Pa) in the previous research does not work well as applied to these bio-process involving high stresses. In this work, we propose a normal distribution cell damage law to relate cell damage to high shear stress, in which the mean and standard deviation of time for cell damage are considered to be functions of shear stress. The parameters in this cell damage law were identified directly from the high speed biodispensing experiments, thus avoiding the time-consuming parameter identification experiments needed in the previous research. For validation, this cell damage law with the identified parameters was applied to biodispensing experiments under different process conditions. The agreement between the experimental and simulation results shows the effectiveness of the method proposed.

Keywords: Biomanufacturing, cell damage, shear stress, modeling

1. Introduction

To enhance the efficiency and improve the performance of the cell-involved biomanufacuring process, high speed fluid delivery methods were employed in different bioproduct fabrication techniques, such as cell jetting [1-3] and cell printing [4-8]. In these processes, cell-encapsulated biomaterials are driven out of a fine needle

by either high air pressures or mechanical impact at high speeds. For example, in direct cell writing process, the velocity of the ejected cell-encapsulated biomaterials can be up to 50 m/s – 1000 m/s [9]. In these high speed flows, cells encapsulated in the biomaterials are subjected to high shear stresses and are more vulnerable to be damaged than those in the process with low stresses. In our biodispensing systems [10], when using tapered needle (Fig. 1), the flow velocity at the needle exit and the shear stress in the flow are up to 10 m/s and 50, 000 Pa, respectively. The cell damage rate under these conditions is up to 90% in our experiments, which is much higher than those under low speed conditions (~40%) [10].

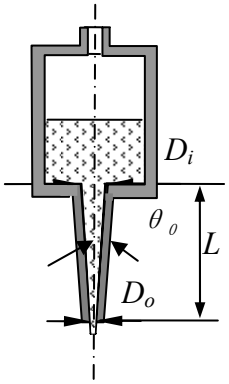

Fig. 1. Biodispensing process using a tapered needle.

To model the cell damage rate in these processes, three steps are normally needed. First is to establish a cell damage law to relate cell damage rate to stress and stress exposure time; the second is to analyze the process-induced stresses cells experience and the cell traveling times during the processes; and finally apply the established cell damage law to the stress analysis to represent the cell damage rate.

Power law function and its modifications are commonly used as cell damage laws [11-14] , but they are not applicable to large range of stress since they may exceed 100% as the stress become high. For improvement, a normal distribution function was proposed as the cell damage law and was successfully applied in low speed biodispensing process for cell damage prediction [10]. However, the parameters in this cell damage law were identified under low stress conditions (~1200 Pa) and are fixed for a range of stresses. Thus it may not represent cell damage under high stresses (50, 000 Pa) since cell damage occurs under high stresses much more quickly

than that under low stresses [15]. To better understand the mechanism of mechanical cell damage, a strain energy density (SED) criterion was employed to measure the cell damage [16]. This method theoretically improved the current cell damage laws and may also be applicable to cell damage modeling under high stresses. However, the time effect, which is critical to cell damage, was not considered in this method. In the research, the time for loading and unloading is at least in the order of a few seconds, which is much longer than the time for cell damage under high stresses (in the order of 10^{-3} to 10^{-6} second [15]). Accordingly, this method may not predict the cell damage occurs in a few milliseconds under high stresses in the printing or jetting processes.

To address this issue, a new cell damage law that can represent cell damage rate in high speeds and high stresses situations is desired. In this work, a normal distribution function with stress-varying mean and standard deviation is proposed to model cell damage at a large range of stresses. With the stress-varying parameters, this cell damage law can reflect cell vulnerability to each stress and thus it can precisely represent cell damage in high or complex stress conditions.

Representing the stresses and cell traveling time during the processes is another key step. The stresses acts on cells in the high speed flow in the nozzle are usually distributed in a complex manner and are functions of both the operational and nozzle geometrical parameters. Hence, merely using of the maximum shear stress at the nozzle wall to model the cell damage, as reported in [14, 17], are inappropriate. In addition, given that the flow velocity of the cell suspension in the nozzle is not uniform, the exposure times of the cells to the stresses also varies in the process. These suggest that quantitative representation of the stresses act on cells and the cell traveling times during the process is necessary and critical for the development of the process-induced cell damage models.

In addition, to develop the aforementioned cell damage law, the parameters in it need to be identified through experiments. In the previous research [10], to identify those parameters, massive measurements by means of specific instruments (e.g., rheometer) are needed, which is costly and time-consuming. Besides, due to the fact that a rheometer can only generate limited shear stresses, it cannot be used to

characterize cell damage under high shear stresses and identify the parameters in the cell damage law. Therefore, the capacity of being able to characterize cell damage under high shear stress and identify the parameters in the cell damage law directly from biodispensing processes is an advantage. In this work, such a method is presented and its effectiveness is illustrated by experiments.

2. Establishing cell damage law

For cell damage prediction in low speed flow, a bivariate normal distribution function was used and it takes the form of [17]:

$$CD_{pr,sh}(s,t) = \int_t \int_s f(s,t) ds dt \tag{1}$$

where $f(s,t)$ is the probability density function and given by

$$f(s,t) = \frac{1}{2\pi\sigma_s\sigma_t\sqrt{1-\rho^2}} \exp\left[-\frac{z}{2(1-\rho^2)}\right] \tag{2}$$

where $z \equiv \left(\frac{s-\mu_s}{\sigma_s}\right)^2 - 2\rho\left(\frac{s-\mu_s}{\sigma_s}\right)\left(\frac{t-\mu_t}{\sigma_t}\right) + \left(\frac{t-\mu_t}{\sigma_t}\right)^2$; μ_s and μ_t are the mean values of shear stress s and exposure time t, respectively; σ_s and σ_t are the standard deviations of the s and t, respectively; and ρ is the correlation coefficient between s and t. These parameters can be identified by experiments and the advantages of this function as a cell damage law over others such as power law function are stated in [10]. This cell damage law has been successfully applied for cell damage rate prediction in the biodispensign processes with low speed flow rates. However, it is not appropriate to use a single mean value and a single standard deviation to represent cell damage for large range stresses since the mean values of exposure time may vary significantly. For example, the mean value in the cell damage law under the stress of 0 ~ 1200 Pa is about 10 s and the deviation is 2.5 s [17]. However, cells can be damaged in 0.01 s under the stress of 2000 Pa and lower than 0.00001 s if the stress is up to 30,000 Pa [15]. This suggests that the cell damage law in the process with high speeds cannot be obtained through simple adaptation of the

bivariate normal distribution function. This issue is addresses by developing a new cell damage law as follows.

The development of the cell damage law for the process involving high stresses is based on the following considerations:

1. The probability of cell damage at a given stress conform to the following normal distribution:

$$I_{law}(t) \sim N(\mu_t, \sigma_t^2) \tag{3}$$

where t is the time period that cells experience the stress, μ_t and σ_t are the mean and standard deviation of the cell damage time to be identified by experiments, respectively.

2. The mean μ_t and standard deviation σ_t are function of stress. In the literature [15], the time course for the red blood cell damage was reported to decrease with stress and their relationship in logarithm is approximated by using a reciprocal function, as shown in Fig. 2.

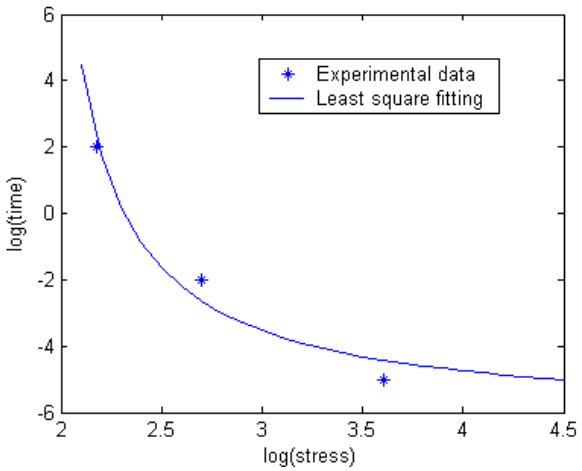

Fig. 2 Relation between time and stress for red blood cell damage(adapted from [15])

In this work, it is proposed that the stress and the corresponding mean of time be expressed by

$$\log(\mu_t) = \begin{cases} \dfrac{a}{\log(\tau) - c} + b & \text{if } \log(\tau) > c \\ +\infty & \text{if } \log(\tau) \le c \end{cases} \tag{4}$$

where *a*, *b*, and *c* are constants. It is known that cells have the ability to be adaptive to low stress by reorganizing their cytoskeleton. Thus, for a certain low stress, no matter how long the stress applied on cells, cells may not be damaged, indicating that the mean value of exposure time (μ_t) is infinite under this stress. Constant *c* is especially used to represent this mechanical property of cells. For instance, if the stress applied on cells satisfies $\log(\tau) = c$, then the time for cell damage is infinite according to Eq. (4) and the corresponding stress (10^c Pa) is called non-damage stress.

3. The standard deviation is considered to be proportional to the mean value. In our previous study, for a certain range of stress, the mean of time is about five folders of standard deviation [17]. In this work, we extend this finding to high stress situations by assuming that at certain stress the mean value is proportional to standard deviation by a constant:, i.e.,

$$\sigma_t = \frac{\mu_t}{d} \tag{5}$$

3. Modeling cell damage in high speed biodispensing processes

The cell damage rate in the high speed biodispensing process can be obtained by applying the cell damage law described above into the process, which is presented in this section. A spherical polar coordinate is used in the tapered needle, as shown in Fig. 3. *P* is pressure applied to the fluid biomaterials, P_e the pressure in the cell suspension at the exit of the needle, D_i and D_o are the diameters at the entrance and the exit of the tapered needle, respectively, θ_0 is the half cone angle, and *L* the length of the tapered needle. For a given length *L* and diameters D_i and D_o, the half cone angle can be expressed as

$$\theta_0 = \arctan\left(\frac{D_i - D_o}{2L}\right) \tag{6}$$

The shear rate of the flow in the tapered needle at position r along θ direction can be expressed as [18]

$$A(\theta, r) = \frac{2CQ}{r^3}\cos\theta\sin\theta\,. \tag{7}$$

where C is a constant and is defined as $C = 3/2\pi(1+2\cos\theta_0)(1-\cos\theta_0)^2$. Q is the volume flow rate in the tapered needle.

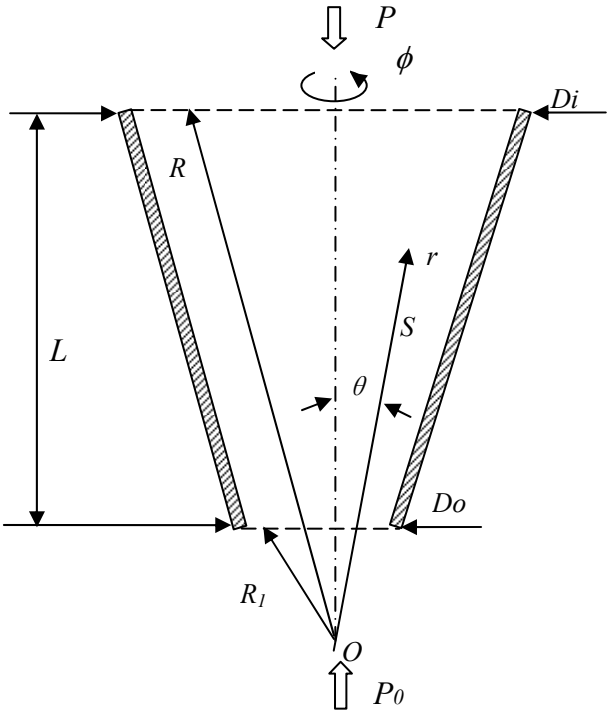

Fig. 3. Schematic of flow analysis in a tapered needle.

Thus, in the non-Newtonian cell suspension with consistency index K and behavior index n, the shear stress that cells experience at position (θ,r) in the tapered needle is

$$\tau(\theta, r) = KA^n\,. \tag{8}$$

For non-Newtonian fluid flow through a tapered needle, the velocity at the position (θ,r) is given by [18]

$$V(\theta,r) = -\frac{CQ(\cos^2\theta - \cos^2\theta_0)}{r^2} \quad , \tag{9}$$

Then, on a streamline *S*, the time period that cells take to travel from the entrance ($(L + R_1\cos\theta_0)/\cos\theta \approx R$) of the needle to the position *r* can be given by

$$t(\theta,r) = \int_r^R \frac{1}{-V(\theta,r)} dr\,. \tag{10}$$

Along the streamline *S*, the cell damage rate at position (θ,*r*) can be obtained by integrating the cell damage density function (Eq. (3)) from the time at the entrance (zero) to the time of arriving at this position:

$$I_s(\theta,r) = \int_0^{t(\theta,r)} I_{law}[t(\theta,r)]dt\,, \tag{11}$$

For the normal distribution density function of $I_{law}[t(\theta,r)]$ at position (θ,*r*), the mean μ_t can be written as follow from Eq. (4):

$$\mu_t = 10^{\frac{a}{\log[\tau(\theta,r)]-c}+b} \tag{12}$$

and the standard deviation σ_t is given in Eq. (5).

Thus, the cell damage rate at the exit of the needle on this streamline can be expressed as

$$I_s(\theta) = \int_{R1}^{R-R1} I_{law}[t(\theta,r)]t'dr\,. \tag{12}$$

Suppose cells are evenly distributed in the cell suspension at a cell density *den*. The total cell number in a unit length at the outside of the exit of the needle is then $\pi(\theta_0 R_1)^2 \cdot den$. The number of total dead cells in the same unit can be expressed as $\int_0^{\theta_0} 2\pi\theta R_1^2 \cdot den \cdot I_s(\theta)d\theta$. The cell damage rate in the tapered needle dispensing system is then

$$I = \frac{2\int_0^{\theta_0} I_s(\theta)}{\theta_0^2}. \tag{13}$$

This cell damage model takes the stress and time variation in the needle into account and can well represent the cell damage rate at any position in needle. It will well address the cell damage prediction in the high speed biodispensing processes.

4. Experiments and Results

4.1 *Chemical formulation*. Sodium alginate powder (Sigma, St. Louis, MO) was dissolved in deionized water overnight to form a 7% (w/v) solution.

4.2 *Cell suspension preparation***.** Schwann cells (derived from Schwann cell line ATCC) were grown in Dulbecco's Modified Eagle's medium (DMEM) (Sigma, St. Louis, MO) supplemented with 5% fetal bovine serum (FBS) and 1% antibiotic. The cells were then incubated at 37°C in a humidified atmosphere of 95% air and 5% CO_2. Immediately prior to use in our experiments, 10 mL of alginate solution was added respectively into 5 mL of cell culture medium to form 4.5% alginate cell suspensions. The final cell density was about 1×10^6 /mL. They were gently mixed with a pipette to ensure a uniform cell distribution. All experiments were conducted at room temperature (~23°C).

4.3 *Cell viability assay*. Niagara blue was used to stain cells and assess cell viability. The number of living/dead cells was counted manually under a light microscope (Leica, Microsystem, Bannockburn, IL) immediately following the dispensing process.

4.4 *Flow behaviour characterization of cell suspensions.* The flow behavior of cell suspension is expressed as a power law function

$$\tau = K\dot{\gamma}^n \tag{14}$$

where τ is shear stress and $\dot{\gamma}$ is shear rate. K is the consistency index with the unit of $Pa\cdot s^m$, n is the flow behavior index (dimensionless).

To obtain the parameter K and n, cell suspensions (0.5 mL) were carefully delivered to a cone-and-plate rheometer (HBDV-III, Brookfield, MA) and examined with a CP-52 spindle. The flow behavior parameters K and n were then identified from the obtained flow curves. The results are that K = 13.5 and n = 0.6.

4.5 *Parameter identification for cell damage law*. The parameters in the cell

damage law were identified through experiments by using the cone-and-plate rheometer and the biodispensing system, as reported in [17].

The first experiment is to identify the parameter c in the cell damage law using the cone-and-plate rheometer. The stress that cells can survive for an hour with no damage is considered as the non-damage stress. In these experiments, 0.5 mL of cell suspension was gently delivered to the cone-and-plate chamber and different shear stress of 50, 60, 70, 80, 90 and 100 Pa were applied on cells for an hour. Each experiment was repeated four times. The results show that cell damage under shear stress of 70 Pa or lower for an hour has no effect on cell viability ($p = 0.43$). Thus, 70 Pa was took as the non-damage stress, and $c = \log(70)$ or $c = 1.8$.

The second experiment is to identify the parameters of a, b, and d by using the biodispensing system with tapered needle. In each experiment, 15 mL of cell suspension was loaded into the syringe using a pipette, after which an air pressure of 200, 300, 400, 500, 600 KPa, respectively, was applied. A tapered needle with a diameter of 0.25 mm was used in each experiment. Control cell suspensions were kept in tubes. The differences in cell damage rate between the test samples and controls were attributed to the biodispensing process. Each condition was repeated four times. The flow rate and cell damage at each of these air pressures were recorded and shown in Table 1.

Table 1 Flow rate and cell damage under different air pressures (n=4)

Pressure (100kPa)	2	3	4	5	6
Flow rate (mL/s)	0.8	1.7	2.8	4.3	5.9
Cell damage (%)	30.0	52.2	67.1	85.6	89.4

Then the flow rate and cell damage were used to identify the cell damage law parameters using Eqs. (3)-(5) and Eqs. (7)-(13). In particular, the function of non-linear least square regression in MATLAB was used to estimate the parameters a, b and d. The function estimates the parameters by starting at an initial guess and then altering the guess until the algorithm converges, as used in other parameter estimation

applications [10]. By doing so, the parameters were found to be a = 3.19, b = 7.21 and d = 4.50. The experimental cell damage rates and the corresponding data fitting results are shown in Fig.4. Substituting these parameters into Eq. (4) obtains the relation between the stresses and mean of damage time, and into (3) yields the cell damage law at different stresses, as shown in Fig. 5.

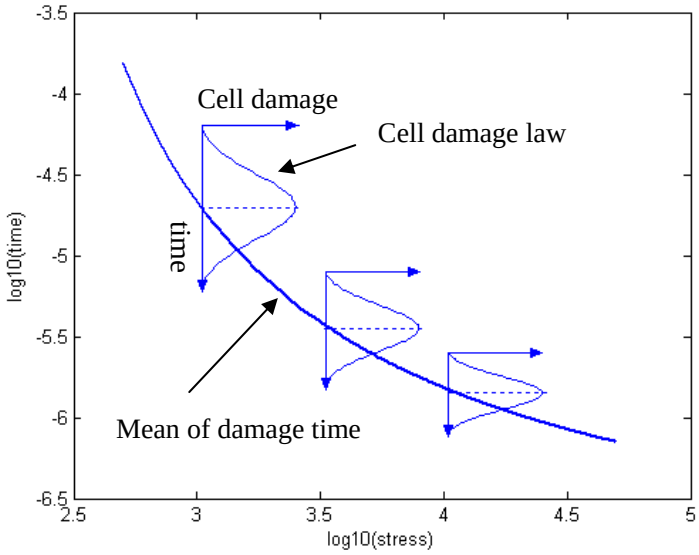

Fig.5 Identified cell damage law

It can be seen that the time course for cell damage decrease with stress. Also, at each stress the cell damage conforms to distribution functions with different means and standard deviations. This is a great advantage for cell damage prediction since the shear stress in the tapered needle are functions of both cone angle (θ) and radial direction (r) and it varies everywhere, depending on the physical location in the needle. For example, with needle diameter of 0.25 mm and flow rate of 5 mL/s, the shear stress distribution at the needle wall ($\theta = \theta_0$) ranges from 0 to 60,000 Pa (Fig.6) according to the simulation based on Eqs. (7) and (8). The shear stresses also vary along the cone angle direction. Thus it is essential to apply this cell damage law with the corresponding parameters to the biodispensing processes at different positions to obtain accurate cell damage rate.

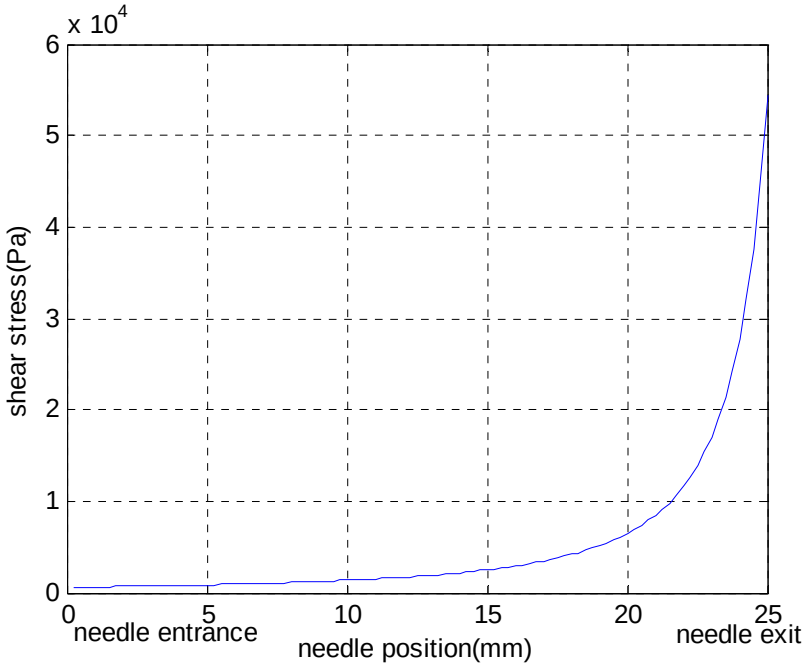

Fig. 6 Shear stress distribution at the needle wall.

4.6 *Verification of the cell damage model***.** The cell damage model was verified using the same biodispensing system but with different needle diameter and different flow rates from the parameter identification experiments. In the verification experiments, diameter of 0.35 mm tapered needle (L = 25 mm, Di = 3.0 mm) was used and flow rates of 1.2, 2.5, and 4.1 mL were produced by applying air pressure of 200, 300 and 400 KPa, respectively. The cell damage rates in these experiments under these flow rates were obtained and shown in Fig. 7 as asterisks. Based on the developed cell damage model of Eqs. (7)-(13), simulation was also performed by applying the cell damage law of Eqs. (3)-(5) with identified parameter and the results are shown as solid curve in Fig. 7 for comparison. The close agreement between the experimental and simulation results demonstrates the effectiveness of the cell damage law for high stress and the cell damage model for high speed biodispensing processes.

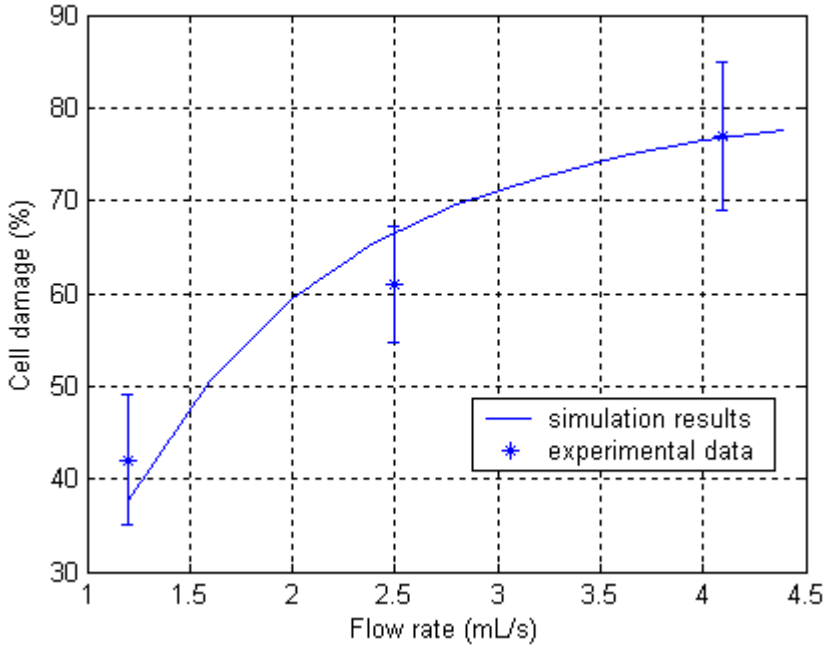

Fig. 7 Cell damage in 0.35mm diameter tapered needle (n=5)

5. Conclusions

As cells are subjected to very high shear stresses in the high speed biomanufacturing process, it is crucial to develop cell damage law under these stresses conditions to predict cell damage rate in these processes. In this work, a normal distribution function with stress-varying mean and standard deviation was proposed as the cell damage law. Since the parameters in this cell damage law can reflect cell vulnerability to different shear stresses and different time periods, it can precisely represent cell damage rate in stresses and time varying situations. In addition, this method allows for establishing the cell damage law under high shear stress, which is impossible if using a rheometer due to the fact that a limited shear stress can be generated by the rheometer. Based on this cell damage law, a cell damage model for high speed biodispensing processes was also developed.

The parameters in the cell damage law were identified directly from experiments and then they were applied to the high speed biodispensing process to predict the cell damage rates in these processes. Experiments were carried out to verify these models. The simulation results agree with the experimental ones, indicating the validation of

the developed models. The developed cell damage law can also be applied to other time varying high stress conditions to estimate cell damage in those processes, such as cell ink-printing, cell jetting and other stress varying biomanufacturing techniques.

Acknowledgements

The authors acknowledge financial support from the Canada Foundation for Innovation (CFI) and the Saskatchewan Health Research Foundation (SHRF).

Reference

[1] A. Kwok, S. Arumuganathar, S. Irvine, J. R. McEwan, and S. N. Jayasinghe, "A hybrid bio-jetting approach for directly engineering living cells," *Biomedical Materials*, vol. 3, pp. -, 2008.

[2] S. Arumuganathar, S. Irvine, J. R. McEwan, and S. N. Jayasinghe, "Aerodynamically assisted bio-jets: the development of a novel and direct non-electric field-driven methodology for engineering living organisms," *Biomedical Materials*, vol. 2, pp. 158-168, 2007.

[3] N. Mongkoldhumrongkul, J. M. Flanagan, and S. N. Jayasinghe, "Direct jetting approaches for handling stem cells," *Biomedical Materials*, vol. 4, pp. -, 2009.

[4] T. Xu, H. Kincaid, A. Atala, and J. J. Yoo, "High-throughput production of single-cell microparticles using an inkjet printing technology," *Journal of Manufacturing Science and Engineering-Transactions of the Asme*, vol. 130, pp. -, 2008.

[5] J. A. Barron, D. B. Krizman, and B. R. Ringeisen, "Laser printing of single cells: Statistical analysis, cell viability, and stress," *Annals of Biomedical Engineering*, vol. 33, pp. 121-130, 2005.

[6] B. Derby, "Bioprinting: inkjet printing proteins and hybrid cell-containing materials and structures," *Journal of Materials Chemistry*, vol. 18, pp. 5717-5721, 2008.

[7] T. Xu, C. A. Gregory, P. Molnar, X. Cui, S. Jalota, S. B. Bhaduri, and T. Boland, "Viability and electrophysiology of neural cell structures generated by the inkjet printing method," *Biomaterials*, vol. 27, pp. 3580-3588, 2006.

[8] T. Xu, J. Jin, C. Gregory, J. J. Hickman, and T. Boland, "Inkjet printing of viable mammalian cells," *Biomaterials*, vol. 26, pp. 93-99, 2005.

[9] W. Wang, Y. Huang, M. Grujicic, and D. B. Chrisey, "Study of impact-induced mechanical effects in cell direct writing using smooth particle hydrodynamic method," *Journal of Manufacturing Science and Engineering-Transactions of the Asme*, vol. 130, pp. -, 2008.

[10] M. G. Li, X. Y. Tian, N. Zhu, D. J. Schreyer, and X. B. Chen, "Modeling Process-Induced Cell Damage in the Biodispensing Process," *Tissue Engineering Part C-Methods*, vol. 16, pp. 533-542, 2010.

[11] Blackshe.Pl, F. D. Dorman, and Steinbac.Jh, "Some Mechanical Effects That Influence Hemolysis," *Transactions American Society for Artificial Internal Organs*, vol. 11, pp. 112-&, 1965.

[12] M. Giersiepen, L. J. Wurzinger, R. Opitz, and H. Reul, "Estimation of Shear Stress-Related Blood Damage in Heart-Valve Prostheses - Invitro Comparison of 25 Aortic Valves," *International Journal of Artificial Organs*, vol. 13, pp. 300-306, 1990.

[13] R. Paul, J. Apel, S. Klaus, F. Schugner, P. Schwindke, and H. Reul, "Shear stress related blood damage in laminar Couette flow," *Artificial Organs*, vol. 27, pp. 517-529, 2003.

[14] B. Vickroy, K. Lorenz, and W. Kelly, "Modeling shear damage to suspended CHO cells during cross-flow filtration," *Biotechnology Progress*, vol. 23, pp. 194-199, 2007.

[15] L. B. Leverett, E. C. Lynch, C. P. Alfrey, and J. D. Hellums, "Red Blood-Cell Damage by Shear-Stress," *Biophysical Journal*, vol. 12, pp. 257-&, 1972.

[16] K. C. Yan, K. Nair, and W. Sun, "Three dimensional multi-scale modelling and analysis of cell damage in cell-encapsulated alginate constructs," *Journal of Biomechanics*, vol. 43, pp. 1031-1038, 2010.

[17] K. Nair, M. Gandhi, S. Khalil, K. C. Yan, M. Marcolongo, K. Barbee, and W. Sun, "Characterization of cell viability during bioprinting processes," *Biotechnology Journal*, vol. 4, pp. 1168-1177, 2009.

[18] G.Bohme, *Non-Newtonian Fluid Mechanics*, vol. 31. Amsterdam: Elsevier Science Publishers B.V., 1987.

CHAPTER 7

CONCLUSIONS AND FUTURE WORK

7.1 Conclusions

Dispensing-based RP is a promising technique for tissue scaffold fabrication. The aim of this research work is to investigate and represent the process performance of this technique, with the objective of achieving a quantitative control over the features of scaffolds fabricated. The main conclusions of this research are summarized as follows.

1. The flow rate of paste-like biomaterials in the dispensing-based RP process can be affected by the slip occurring between the biomaterial and the needle wall, and this influence can be accurately modeled. Based on the mechanical properties of the biomaterials, the pore size and porosity of scaffolds can be predicted by means of the developed models.

2. Experimental results shows that the influence of hydrostatic pressure on cell (both Schwann cell and 3T3 fibroblasts) damage was determined to be small, whereas the influence of shear stress and time period acting on cells was found to be significant. This suggests that cell damage in the bio-dispensing process was largely attributed to shear stresses and exposure times in the dispensing needle, while having little connection to the hydrostatic pressure present in the reservoir.

3. To establish the cell damage law that describes the relationship between the cell damage and the force applied on the cell, the use of a bivariate normal distribution function is more appropriate than the use of the power law equation reported in the literature, as the limit exhibited by the power law equation is overcome when either the shear stress or the exposure time becomes very large.

4. The cell damage percents of both Schwann cells and 3T3 fibroblasts vary with the process parameters employed in the bio-dispensing processes. Particularly, the cell damage percents increases with the air pressure applied and decreases with the needle diameter. Needle length also affects cell damage, but in a complicated manner. In the examined case, it is shown that the cell damage percent generally increases with the needle length. It is also revealed that cell damage is not evenly distributed in the dispensed strand but concentrates around the strand surface due to the high shear stress and long exposure time at the needle wall. Significantly, the aforementioned relationship can be well represented by means of developed models.

5. The needle geometry has a significant effect on the flow rate and cell damage in the dispensing-based bio-manufacturing process and tapered needles are better than cylindrical ones in these two aspects. Specifically, the flow rate in a tapered needle is much higher than that in a cylindrical needle given the same process conditions. Thus, to produce the same flow rate, the air pressure needed for a tapered needle is much lower than that for a cylindrical needle. In cell involved bio-manufacturing process, for the given flow rate, the cell damage percents in a tapered needle is much lower than in a cylindrical needle. The above findings suggest that tapered needles should preferably be selected for use in the bio-dispensing process in order to preserve the cell viability. By means of the models developed, both the flow rate and cell damage in these two types of needles can be predicted.

6. The method developed to establish the cell damage law in high shear stress (~ 60 KPa) directly from the bio-manufacturing process, instead of the use of such instruments as rhometers, has proven to be effective. This method overcomes the limited shear stress (~ 1 KPa) that a rhoemeter can usually generate and has been successfully applied to investigate the cell damage in the bio-manufacturing processes involving high shear stresses. It is also found that high shear stress can damage cells in a very short time period compared to that under low stress, and that the logarithm of the mean of time and the logarithm of the stress can be represented by using a reciprocal function.

7.2 Future Work

Based upon the work presented in this dissertation, a number of projects can be taken up to extend the current research.

1. Development of a model for the mechanical propertes of the scaffolds fabricated. The scaffold mechanical properties depend on the mechanical properties of the scaffold material and the scaffold microstructure. Developing models to represent this dependency will be an interesting research project and the results from this project would allow one to design the scaffold microstructure for desired scaffold mechanical properties.

2. Development of cell damage models for other dispensing methods, including rotary screw and positive displacement. The dispensing method used in the current research is time-pressure and the stresses cells experience in the other two methods are different from this one, which may cause different cell damage. The proposed project can develop cell damage models for these dispensing methods by analyzing the stresses in these processes and applying the developed cell damage law to these processes.

3. Optimization of bio-dispensing processes to retain maximum cell viability. Cell damage percents in different bio-dispensing processes are functions of geometrical parameters of the needle and the operational parameter, air pressure, which have a complex nonlinear effect on cell damage. Optimization of the cell damage model can be performed to find the appropriate parameters in these processes to minimize cell damage percents.

It is worth explicitly stating the limitations of the methods used in the current study so that future work based upon this research moves forward successfully. First, the scaffold pore size and porosity models were developed for paste-like materials, which are mixtures of fine particles and high molecular weight polymers. They have very high yield stresses and the strands formed can support the weights of themselves. Thus the models may be not applicable to the materials with low yield stress, such as pure polymer solutions, since they cannot hold a 3D structure as

fabricated into scaffolds. Second, different cell types have different mechanical properties. Cell damage laws established are cell-dependant and the cell damage law established for one cell type may not be valid on another. For a specific cell type, similar cell damage experiments as those conducted in the current study should be performed, and, depending on the experimental results, different functions may be selected to establish the cell damage law. Third, in the high speed bio-dispensing process, the dispensed cell suspensions were collected using a water-filled glass cup and thus mechanical impact occurred when the cell suspension landed in the water, which may also cause cell membrane failure. In this research, the effect of cell impact with water was not considered.

APPENDIX A

MATLAB CODES FOR MODEL SIMULATION

1. The following codes employ the method described in chapter 3

```
clear all; clc;
R = 305*1.0e-6;%needle radius
L = 12*1.0e-3;% needle length
P = [1:0.1:4.5]*1.0e5
Tw = R*P/(2*L)%wall stress
nb = 0.628;%power law index of bonder
mb = 63;%consistency index of bonder
delta = 30*0.06/1.0e6;%wall slip thickness
A = (1-delta/R)^((1/nb) +1);
B = (1/nb +1)* mb^(1/nb);
beta = (R/B)*(1-A);
Us = beta*(Tw.^(1/nb));
Qs = pi*R*R*Us;%slip flow

%flow rate calculation of 45% HA mixture
m = 130.5;%power alw index of mixture
n = 0.705;%consistency index of mixture
T0 =720;%yield stress
%shear flow rate
s = 1/n;
C = (Tw-T0)/Tw;
Q1 = pi.*R.^3.*(Tw./m).^s.*(C.^(s+3)./(s+3) + 2.*(T0./Tw).*(C.^(s+2)./(s+2)) +
(T0./Tw).^2.*(C.^(s+1)./(s+1)));
Q = Qs+Q1;%total flow rate from simulation
%the flow rate in experiments were calcuatled from moving speed of
%dispensing head
experiment_speed = [3.3 5.5 8.6 11.5];%moving speed of dispensing head
error_speed = [0.10 0.08 0.045 0.10]%error
experiment_P = [1.5 2.5 3.5 4.5 ]*1.0e5;%air pressure
plot(P, Q*10e9); hold on;%plot similated flow rate without wall slip
plot(P, Q1*10e9,'-.');%plot similated flow rate with wall slip
errorbar(experiment_P, experiment_speed*pi*R*R*10e6, error_speed ,'d');%plot
experimental flow rate
xlabel('Pressure(pa)');
ylabel('flow rate(mg/s)');
legend('Model with slip','Model without slip','Experimental data');
grid on;
```

```
%flow rate calculation of mixture with different HA volume fraction
P = 3.5*1.0e5;%air pressure
Tw = R*P/(2*L)%wall stress
nb = 0.628;%power law index of bonder
mb = 63;%consistency index of bonder
delta = 30*0.06/1.0e6;%wall slip thickness
A = (1-delta/R)^((1/nb) +1);
B = (1/nb +1)* mb^(1/nb);
beta = (R/B)*(1-A);
Us = beta*(Tw.^(1/nb));
Qs2 = pi*R*R*Us;%slip flow

VF = [0.40 .45 .50 .55 .60];%volume fraction of HA
m = [102, 130.5, 152.3, 180, 210];%power law index of mixture
n = [0.70, 0.71, 0.73, 0.74, 0.76];%consistency index of mixture
s = 1./n;
T0 =[690, 720, 760, 780, 810];%yield stress of mixture
C = (Tw-T0)/Tw;
Q2 = pi.*R.^3.*(Tw./m).^s.*(C.^(s+3)./(s+3) + 2.*(T0./Tw).*(C.^(s+2)./(s+2)) +
(T0./Tw).^2.*(C.^(s+1)./(s+1)));
Q = Qs2+Q2;%total flow rate from simulation

figure(2);
VF1 = 0.4:0.01:0.6;
speed2 = [13.1 8.6 6.2 4.8 3.4];%moving speed of dispensing head
error_VF = [0.11 0.08 0.105 0.10, 0.06]%speed error
plot(VF1, 620.67*VF1.^4-1530.9*VF1.^3+1413*VF1.^2-584.41*VF1+93.449);hold on; %from
curve fitting of Q2
plot(VF1, 1624*VF1.^4-3473.2*VF1.^3+2811.7*VF1.^2-1029.2*VF1+145.62,'-.');%from curve
fitting of Qs2
errorbar( VF, speed2*pi*R*R*1e6, error_VF,'d');hold on;
grid on;
xlabel('HA volume fraction');
ylabel('flow rate (mg/s)');
legend('Model with slip', 'Model without slip','Measured data');

clear all; clc;
t_s = [13.5 15.3 18.5 20]%elasticity limit stress
hz1 = [213 310 401 426]./610;%regulated hight
error=[65, 50, 44, 40]./610%regulated error
porosity1 = [0.28 0.39 0.50 0.54].*100;%experimental results
error_porosity=[0.08, 0.07, 0.07, 0.05]*100/2;%error
t = 11:1:25;%elasticity limit stress for simulation
d = 0.6e-3;%diameter of needle
```

```
r = d/2;
den = 1460;%density of material
L = 1.5e-3%span of strands
g = 9.8%gravity
angle = 90;%crossing angle
theta = angle*pi/180

%pore size calculation
Acs = pi*r*r%cross section area of strand
G = 0.25*den*g*pi*d*d*L
A = G./(t*2);
t_c1 = 0.5*den*g*L*sin(theta);%critical stress
t_c2 = 0.5*den*g*L;                %critical stress
t_c = max(t_c1, t_c2);          % choose the greater one
AD = sqrt(2.*A./(pi.*sin(theta)));
EF = AD*1.414;
hf = r-0.5*sqrt(d*d-EF.*EF.*sin(theta).*sin(theta));
hz = d-2.*hf;
errorbar(t_s, hz1, error, '*');hold on;
legend('Model prediction','Experiment data');
plot(t,hz./d);% vertical pore size
xlabel('Elasticity limit stress(Pa)');
ylabel('dimensionless vertical pore size');
grid on;

%porosity calculation
t = 13:1:25;%%elasticity limit stress for simulation
A = G./(t*2);
t_c1 = 0.5*den*g*L*sin(theta);%critical stress
t_c2 = 0.5*den*g*L; %critical stress
t_c = max(t_c1, t_c2); % choose the greater one
AD = sqrt(2.*A./(pi.*sin(theta)));
EF = AD*1.414;
hf = r-0.5*sqrt(d*d-EF.*EF.*sin(theta).*sin(theta));
hz = d-2.*hf;
porosity = 1-200*Acs./(L*(199*hz+d));
figure(2);
errorbar(t_s, porosity1,error_porosity,'*');hold on;
legend('Model prediction', 'Experiment data');
plot(t, porosity.*100);
xlabel('elasticity limit stress (Pa)');
ylabel('Porosity, %');
grid on;
```

2. The following codes employ the method described in chapter 4

```
clc; clear;
%%%%% data of cell damage under pure shear
shear_stress = [80, 200, 400, 600, 800,1000, 1200]
time = [0, 10, 60, 120, 300]
Cell_damage = [0,0,0,0,0,0,0;
      0,0,0,0.03,0.225,0.412,0.729;
      0,0,0,0.125,0.60,0.802,0.92;
      0,0,0.0796,0.607,0.796,0.89,1;
      0,0.202,0.418,0.723,0.953,1,1];

%Normal distributioin fitting
xdata = [shear_stress time];
beta0 = [10, 10, 10,50] % for normal distribution fitting
[beta,resnorm]                                                                    =
lsqcurvefit(@CellDamageLaw_NormalDistribution,beta0,xdata,Cell_damage);

%Model Verificationneedle_dia = [150, 250, 330, 410, 510];
cell_damage_dia = [0.39, 0.23, 0.10, 0.04, 0.05];
error_dia=[0.05 0.06 0.06 0.045 0.040]

pressure_applied = [1 2 3 4 5]
cell_damage_pressure = [0.03, 0.05, 0.19, 0.24, 0.39];
error_pressure=[0.04 0.04 0.055 0.06 0.06]

%velocity distribution in the needle
k=28.7;
n=0.78;
% parameters of the dispensing system
L=20e-3; %needle lenght
D=0.150e-3; % needle diameter
R=D/2;% needle radius
b=R;%
syms r
A=n/(n+1);
beta = [3.0904 10.0814 250.558 634.7271]
%effect of pressure on cell damage
for i = 1:15
      P = 100000+(30000*(i-1));
      B=P*R/(2*k*L);
      C=1-power((r/R),1+1/n);
      V = A*power(B,1/n)*R*C;%velocity distribution in the needle along radius
```

```
    T = L/V;% cell exposure time
    stress = P*r/(2*L);%shear stress distribution in the needle along radius

f=inline(r*0.25*(1+erf((stress-beta(4))/(1.4142*beta(3))))*(1+erf((T-beta(2))/(1.4142*beta(1)
))))
    I1(i)= double(quadl(f,0,b)*2/R^2);
end
for i = 1:15
    P1(i) = 100000+(30000*(i-1));
end
figure(1);
errorbar(pressure_applied, cell_damage_pressure*100, error_pressure*100,'*'); grid on;
hold on;
plot(P1/1.0e5,I1*100);
xlabel('Pressure applied(bar)');
ylabel('Cell damage (%)');
legend('simulation results', 'experimental data');

%effect of needle diameter on cell damage
syms r;
P2=500000
for i = 1:50
    D = 1e-6*(140+(10*i));
    R = D/2;
    B=P2*R/(2*k*L);
    C=1-power((r/R),1+1/n);
    V = A*power(B, 1/n)*R*C;%velocity distribution in the needle along radius
    T = L/V;% cell exposure time
    stress = P2*r/(2*L);%shear stress distribution in the needle along radius
    b = R;

f1=inline(r*0.25*(1+erf((stress-beta(4))/(1.414*beta(3))))*(1+erf((T-beta(2))/(1.414*beta(1)))
))
    I2(i)= double(quadl(f1,0,b)*2/R^2);
end
for i = 1:50
    D1(i) = 1e-6*(140+(10*i));
end
figure(2);
errorbar(needle_dia,cell_damage_dia*100, error_dia*100,'*');grid on; hold on;
plot(D1*1e6,I2*100);
xlabel('needle inner diameter(microns)');
ylabel('Cell damage (%)');
legend('simulation results', 'experimental data');
```

```
%effect of needle length on cell damage
celldamage_length = [4 6 25 38 35];
needlelength = [40 60 80 100 120];
error_length=[0.037 0.048 0.043 0.047 0.049];

syms r;
P2=500000
D=0.84e-3; % needle diameter
for i = 1:120
    L = 1e-3*i;
    R = D/2;
    B=P2*R/(2*k*L);
    C=1-power((r/R),1+1/n);
    V = A*power(B, 1/n)*R*C;%velocity distribution in the needle along radius
    T = L/V;% cell exposure time
    stress = P2*r/(2*L);%shear stress distribution in the needle along radius
    b = R;

f3=inline(r*0.25*(1+erf((stress-beta(4))/(1.414*beta(3))))*(1+erf((T-beta(2))/(1.414*beta(1)))
))
    I3(i)= double(quadl(f3,0,b)*2/R^2);
end
for i = 1:120
    L8(i) = i;
end
figure(3);
errorbar(needlelength, celldamage_length, error_length*100,'*'); grid on; hold on;
plot(L8,I3*100);
grid on;
xlabel('needle length(mm)');
ylabel('Cell damage (%)');
legend('Model prediction','Experimental results');

%cell damage distribution in the dispensed strand in radial direction
syms r;
P2=500000
L=80e-3
D = 0.84e-3;
R = D/2;
for i = 1:421
    position = (i-1)*1e-6;
    B=P2*R/(2*k*L);
    C=1-power((position/R),1+1/n);
```

```
        V = A*power(B, 1/n)*R*C;%velocity distribution in the needle along radius
        T = L/V;% cell exposure time
        stress = P2*position/(2*L);%shear stress distribution in the needle along radius
        I9(i)=0.25*(1+erf((stress-beta(4))/(1.414*beta(3))))*(1+erf((T-beta(2))/(1.414*beta(1))))
end
for i = 1:421
        position(i) = (i-1)*1e-6;
end
figure(4);
plot(position/R,I9*100);hold on; grid on;
xlabel('needle radial position r/R');
ylabel('Cell damage (%)');

%cell viability estimation under same flow rate conditions.
D_flow_rate = [0.33 0.41 0.51 0.61 0.84]*1e-3;
P_flow_rate = [4.7690 1.9010 0.9020 0.4900 0.193]*1e5;
celldamage_flowrate = [18 20 6 3 2];
error_flowrate=[0.030 0.04 0.020 0.02 0.01];

syms r;
L=25.4e-3;
for i = 1:5
        D = D_flow_rate(i);
        P = P_flow_rate(i);
        R = D/2;
        B=P*R/(2*k*L);
        C=1-power((r/R),1+1/n);
        V = A*power(B, 1/n)*R*C;%velocity distribution in the needle along radius
        T = L/V;% cell exposure time
        stress = P*r/(2*L);%shear stress distribution in the needle along radius
        b = R;

f10=inline(r*0.25*(1+erf((stress-beta(4))/(1.414*beta(3))))*(1+erf((T-beta(2))/(1.414*beta(1)
))));
        I10(i)= double(quadl(f10,0,b)*2/R^2);
end

figure(5);
errorbar(1:5, celldamage_flowrate, error_flowrate*100,'*'); grid on; hold on;
plot(1:5, I10*100);hold on;grid on;
xlabel('combinition sets of needle diameter and air pressure');
ylabel('Cell damage (%)');
legend('Model prediction','Experimental results');
```

3. The following codes employ the method described in chapter 5

```
%flow rate codes
clc; clear all;
P = 300000;
%%%cylindrical needle
Lc = 20e-3;
D = 0.25e-3;
R = D/2;
%%%tapered needle
L = 20e-3;%25.4e-3;
D1 = 0.25e-3;%%diameter at the exit
R1 = D1/2;
D0 = 3.0e-3;%%diameter at the entry
R0 = D0/2;
theta = 0.0685;%atan(R0/L)%rad;
%%%flow behaviors
K = 10.80;
n = 0.53;
%%flow rate for cylindrical needle
for i=1:10
    P = 50000*i;
    tw = R*P/(2*Lc)
    Q1(i) = pi*(n/(3*n+1))*power(P/(2*K*Lc), 1/n)*power(R, (3*n+1)/n);
End

%%flow rate for tapered needle
for i=1:10
    P = 50000*i;
    A = P*3*n*tan(theta)/(2*K*(1-power(R1/R0, 3*n)));
    Q2(i) = power(A, 1/n)*pi*R1*R1*R1/4;
end
P = [1:10]*50;
figure(1);
plot(P, Q1*1e6);hold on;grid on;
plot([100 200 300, 400, 500], [0.0006 0.003 0.00481 0.00940 0.016], '*');
plot(P, Q2*1e6,'-.');hold on; grid on;
plot([100 200 300 400 500],[0.3 0.51 1.7 2.6 4], 'o');
xlabel('Pressure applied (kPa)');
ylabel('Flow rate (mL/s)');
legend('simulated flow rate using cylindrical needle','experimental results using cylindrical needle','simulated flow rate using tapered needle','experimental results using tapered needle');
```

```
%flow rate with needle diameter
Qc = [0.006 0.02 0.06];%experimental results
Qt = [1.8 3.1 5.9];%experimental results
P=300000;
%%%cylindrical needle
Lc = 20e-3;
D = [0.25 0.33 0.41 0.51]*1e-3;
R = D/2;
%%%tapered needle
L = 20e-3;%25.4e-3;
D1 = [0.25 0.33 0.41]*1e-3;%%diameter at the exit
R1 = D1/2;
D0 = 3.0e-3;%%diameter at the entry
R0 = D0/2;
theta = [0.0685 0.0665 0.0645]%atan(R0/L)%rad;

for i = 1:17
    %%flow rate for cylindrical needle
    D = (i+24)/100000;
    R = D/2;
    tw = R*P/(2*Lc);
    Q3(i) = pi*R*R*R*n*power(tw, 1/n)/(power(K, 1/n)*(3*n+1));
    %%flow rate for tapered needle
    R1=R;
    theta = atan((D0-D)/(L*2));
    A = P*3*n*tan(theta)/(2*K*(1-power(R1/R0, 3*n)));
    Q4(i) = power(A, 1/n)*pi*R1*R1*R1/4;
end
Dia = 25:41
figure(2);
plot(Dia/100,Q3*1e6);grid on; hold on;
plot(D1*1e3,Qc,'*');
plot(Dia/100,Q4*1e6,'-.');
plot(D1*1e3, Qt,'o');
xlabel('needle diameter(mm)');
ylabel('flow rate (mL/s)');
legend('simulated flow rate for cylindrical needle','experimental results for cylindrical needle','simulated flow rate for tapered needle','experimental results for tapered needle');

%cell damage codes
clear all; clc;
pressure_applied = [2 3 4 5]
cell_damage_pressure = [0.01, 0.05, 0.12, 0.18];
error_pressure=[0.02 0.035 0.04 0.043]
```

```
mu = [631.84, 9.88];%
sigma = [252.63, 3.15];%the first number is for stress and the second for time
rho = 0.29;%corelation coefficient
syms stress; syms time;
pdf =
exp((-1/(2*(1-rho^2)))*(((stress-mu(1))/sigma(1))^2-2*rho*(stress-mu(1))*(time-mu(2))/(sig
ma(1)*sigma(2))+((time-mu(2))/sigma(2))^2))/(2*pi*sigma(1)*sigma(2)*sqrt(1-rho^2));
%reform the pdf for numerical integration
pdf = char(pdf);
pdf=strrep(pdf, '*', '.*');
pdf=strrep(pdf, '/', './');
pdf=strrep(pdf, '^', '.^');

% parameters of the dispensing system
L=45e-3; %needle lenght
D=0.250e-3; % needle diameter
R=D/2;      % needle radius
b=R;%
syms r
A=n/(n+1);
%%%tapered needle
L_t = 20e-3;
Do = 0.25e-3;%%diameter at the exit
Ro = Do/2;
Di = 2.8e-3;%%diameter at the entry
Ri = Di/2;
theta = 0.08;%atan(Ri/L_t)%rad

beta = [3.0904 10.0814 250.558 634.7271]
%effect of pressure on cell damage
%k=10.7;
%n=0.75;
for i = 1:11
    P = 200000+(30000*(i-1));
    B=P*R/(2*k*L);
    C=1-power((r/R),1+1/n);
    V = A*power(B,1/n)*R*C;%velocity distribution in the needle along radius
    T = L/V;% cell exposure time
    stress = P*r/(2*L);%shear stress distribution in the needle along radius

f=inline(r*0.25*(1+erf((stress-beta(4))/(1.4142*beta(3))))*(1+erf((T-beta(2))/(1.4142*beta(1)
))))
    I1(i)= double(quad(f,0,b)*2/R^2);
```

```
    tw = R*P/(2*0.02)
    Q1(i) = pi*R*R*R*n*power(tw, 1/n)/(power(k, 1/n)*(3*n+1));
end
for i = 1:11
    k=10.8;n=0.53
    P = 200000+(30000*(i-1));
    tw = R*P/(2*0.02)
    Q2(i) = pi*R*R*R*n*power(tw, 1/n)/(power(k, 1/n)*(3*n+1));
end
Q1 = [0.0027 0.0056 0.010 0.015];
for i = 1:11
    P1(i) = 200000+(30000*(i-1));
end
figure(1);
errorbar(Q1, cell_damage_pressure*100, error_pressure*100,'o'); grid on; hold on;%experimental data
plot(Q2*1e6,I1*100);
errorbar(Q1, [0.8 0.5 2.5 2.5 ], [0.6 0.8 2.2 2.1],'*');%experimental data
plot(Q1,[0.56 0.43 1.32 3.5])%simulation results from below
xlabel('Flow rate(mL/s)');
ylabel('Cell damage (%)');
%legend('simulation results', 'experimental data');

%Cell damage with needle diameter
clear all;clc;
P = 500000;
%%%cylindrical needle
Lc = 20e-3;
D = [0.25 0.33 0.41 0.51]*1e-3;
R = D/2;
%%%tapered needle
L_t = 20e-3;%25.4e-3;
D1 = [0.25 0.33 0.41]*1e-3;%%diameter at the exit
R1 = D1/2;
D0 = 3.0e-3;%%diameter at the entry
R0 = D0/2;
theta = [0.0685 0.0665 0.0645]%atan(R0/L)%rad;
%%%flow behaviors
K = 25.80%6.73;
n = 0.76%0.58%0.76;

Q = [0.006 0.02 0.06]%flow rate under 5 bar(mL)with needle d=0.25, 0.33, 0.41 respectively
%pressure needed for tapered needle to produce the same flow rate above at
```

```
%the same diameters. This is no use in the following cell damage
%calculation
for i = 1:6
    Q = i*10e-8;
    A = power(Q*(3*n+1)/(pi*n), n);
    R = power(A*K*2*Lc/P, 1/(3*n+1));
    D = 2*R%diameter of cylindrical needle to produce such flow rate under 5 bar
    BB = 1-(D/D0)^3;
    theta = atan((D0-D)/(L_t*2));
    Pt(i) = 2*K*power(4*Q/(pi*R^3),n)*BB/(3*n*tan(theta));
end

%%flow rate for cylindrical needle p=5bar,diameter = 0.25-0.41mm
mu = [631.84, 9.88];%
sigma = [252.63, 3.15];%the first number is for stress and the second for time
rho = 0.29;%corelation coefficient

syms r1; %radius direction in spherical polar coordinates
syms r2;
syms r3; %angle direction in spherical polar coordinates
for i = 1:17
    D = (i+24)/100000;
    R = D/2;
    tw = R*P/(2*Lc);
    %flow rate using cylindrical needle at the diameter from 0.25-0.41mm
    Q1(i) = pi*R*R*R*n*power(tw, 1/n)/(power(K, 1/n)*(3*n+1));

    D1 = D;
    R1 = D1/2;
    theta = atan((D0-D)/(L_t*2));
    L1 = R1/sin(theta);
    Q = Q1(i);%flow rate obtained in cylindrical needle is substituted into tapered needle

    K = 10.80%k and n are different than in cylindrical needle because shear stress are
different
    n = 0.44%
    %% cell damage using bivariate normal distribution cell damage law
    const = 3/(2*pi*(1+2*cos(theta))*(1-cos(theta))^2);%constant
    shear_rate = 0.5*const*Q*sin(r3)/(r1^3);
    stress = K*power(shear_rate, n);
    v = const*Q*(cos(r3)^2-cos(theta)^2)/(r2^2);%velocity at r2 location
    time = ((L_t+L1)^3-r2^3)/(3*const*Q*(cos(r3)^2-cos(theta)^2));%time for cells arrive at
r2 location
%follow is the possibility density fun of cell damage law
```

```
%deriverative of stress
    d_stress = -3*n*K*power(0.5*const*Q*sin(r3), n)/power(r1, 3*n+1);
    d_time = -(r2)^2/(const*Q*(cos(r3)^2-cos(theta)^2));
    pdf =
exp((-1/(2*(1-rho^2)))*(((stress-mu(1))/sigma(1))^2-2*rho*(stress-mu(1))*(d_time-mu(2))/(si
gma(1)*sigma(2))+((d_time-mu(2))/sigma(2))^2))/(2*pi*sigma(1)*sigma(2)*sqrt(1-rho^2));

    pdf = pdf*d_stress*d_time*r3;%r3 is angle, from cell damage function
%reform the pdf for numerical integration
    pdf = char(pdf);
    pdf=strrep(pdf, '*', '.*');
    pdf=strrep(pdf, '/', './');
    pdf=strrep(pdf, '^', '.^');
    celldamge_tapered(i) = triplequad(pdf, L1,L_t+L1, L1,L_t+L1,0, 0.99*theta, 1e-6,
@quad8)*2/theta^2;
end
%celldamge_tapered=[0.05032   0.0445670.0329370.0337660.0297030.0219050.017281
    0.0171390.0133170.0104930.0085651    0.0071908    0.0053744    0.0048463
    0.0037406    0.0027863    0.0032823]
%plot(celldamge_tapered);

%cell damage in cylindrical needle
K = 25.80%6.73;
n = 0.76%0.58%0.76;
syms r;
A=n/(n+1);
for i = 1:17
    D = (i+24)/100000;
    R = D/2;
    B=P*R/(2*K*Lc);
    C=1-power((r/R),1+1/n);
    V = A*power(B, 1/n)*R*C;%velocity distribution in the needle along radius
    T = Lc/V;% cell exposure time
    stress = P*r/(2*Lc);%shear stress distribution in the needle along radius

f1=inline(r*0.25*(1+erf((stress-mu(1))/(1.414*sigma(1))))*(1+erf((T-mu(2))/(1.414*sigma(2))
)));
    I222(i)= quad8(f1,0,R)*2/R^2;
end

for i=1:17
    D(i) = (i+24)/100;
end
%comparison of cell damage in cylindrical and tapered needle
```

```
figure(7);
errorbar([0.250 0.330 0.410],[18 8 4], [5 3 2],'o');grid on; hold on;%experimental results in cylindrical needle
plot(D,I222*100,'-.');%simulation
errorbar([0.250 0.330 0.410],[2.0 1.9 1], [2 2.5 1],'*');%experimental results in tapered needle
plot(D,celldamge_tapered*100,'-');%simulation
xlabel('needle inner diameter(mm)');
ylabel('Cell damage (%)');

%cell damage with alginate concentration
clear all; clc;
cell_damage = [0.01, 0.03, 0.11, 0.18];
error=[0.01 0.015 0.025 0.013]

%%%%    velocity distribution in the needle
% rheological behavior of Alginate acid Tau = K*power(y, n)
k1= [3 8 15.85 25.7]
n1=[0.85 0.83 0.79 0.75]
k= [2.37 3.01 6.85 10.82]
n=[0.67 0.65 0.60 0.54]
%k=17.7;
%n=0.78;
%k=10.8
%n=0.53
P = 500000;

%%%tapered needle
L_t = 20e-3;
Do = 0.25e-3;%%diameter at the exit
Ro = Do/2;
Di = 3e-3;%%diameter at the entry
Ri = Di/2;
theta = 0.08;%atan(Ri/L_t)%rad
L1 = Ro/sin(theta);

% parameters of the cylindrical needle
L=20e-3; %needle lenght
D=0.25e-3; % needle diameter
R=D/2;        % needle radius
b=R;%
syms r
A=n/(n+1);
```

```
beta = [2.8 9.0814 250.558 634.7271]
mu = [634.84, 10];%
sigma = [250, 3.09];%the first number is for stress and the second for time
rho = 0.29;%corelation coefficient
%effect of pressure on cell damage
P=500000;
for i = 1:4
    B=P*R/(2*k1(i)*L);
    C=1-power((r/R),1+1/n1(i));
    V = A*power(B,1/n1(i))*R*C;%velocity distribution in the needle along radius
    T = L/V;% cell exposure time
    stress = P*r/(2*L);%shear stress distribution in the needle along radius

f=inline(r*0.25*(1+erf((stress-beta(4))/(1.4142*beta(3))))*(1+erf((T-beta(2))/(1.4142*beta(1)
))))
    I1(i)= double(quadl(f,0,b)*2/R^2);

    tw = R*P/(2*0.02)
    Q1(i) = pi*R*R*R*n(i)*power(tw, 1/n(i))/(power(k(i), 1/n(i))*(3*n(i)+1));


syms r1; %radius direction in spherical polar coordinates
syms r2;%radius direction in spherical polar coordinates
syms r3; %angle direction in spherical polar coordinates
%a = 0.1*theta;
%for i = 1:5
Q = Q1(i); %flow rate
% P = i*1e5;
%       A1 = P*3*n*tan(theta)/(2*K*(1-power(Ro/Ri, 3*n)));
%      Q = power(A1, 1/n)*pi*Ro^3/4; %flow rate

const = 3/(2*pi*(1+2*cos(theta))*(1-cos(theta))^2);%constant
shear_rate = 0.5*const*Q*sin(r3)/(r1^3);
stress = k(i)*power(shear_rate, n(i));
v = const*Q*(cos(r3)^2-cos(theta)^2)/(r2^2);%velocity at r2 location
%time = (L_t-r2)^3/(3*const*Q*(cos(r3)^2-cos(theta)^2));%time for cells arrive at r2 location
time = ((L_t+L1)^3-r2^3)/(3*const*Q*(cos(r3)^2-cos(theta)^2));%time for cells arrive at r2
                                                                %location
%%system
%follow is the possibility density fun of cell damage law
pdf                                                                                 =
exp((-1/(2*(1-rho^2)))*(((stress-mu(1))/sigma(1))^2-2*rho*(stress-mu(1))*(time-mu(2))/(sig
ma(1)*sigma(2))+((time-mu(2))/sigma(2))^2))/(2*pi*sigma(1)*sigma(2)*sqrt(1-rho^2));
%deriverative of stress
```

```
d_stress = -3*n(i)*k(i)*power(0.5*const*Q*sin(r3), n(i))/power(r1, 3*n(i)+1);
d_time = -(r2)^2/(const*Q*(cos(r3)^2-cos(theta)^2));
pdf = pdf*d_stress*d_time*r3;
%reform the pdf for numerical integration
pdf = char(pdf);
pdf=strrep(pdf, '*', '.*');
pdf=strrep(pdf, '/', './');
pdf=strrep(pdf, '^', '.^');
%damage(i) = 2*triplequad(pdf, L1,L_t+L1, L1,L_t+L1,0, 0.9*theta, 1e-6, @quad8)/theta^2;
end

figure(1);
errorbar([2 3 4 5], cell_damage*100, error*100,'o'); grid on; hold on;
plot([2 3 4 5 ],I1*100);
errorbar([2 3 4 5], [1.5 0.8 2.5 2.6], [1.5 1 2 2],'*');
plot([2 3 4 5],[1.36 1.77 3.1 4.7 ])
xlabel('Alginate concentration(%)');
ylabel('Cell damage (%)');
%legend('simulation results', 'experimental data');
```

4. The following codes employ the method described in chapter 6

```
clear all; clc;
%tapered needle parameters
L_t = 25.4e-3;
Do = 0.35e-3;%diameter at the exit
Ro = Do/2;
Di = 3e-3;%diameter at the entry
Ri = Di/2;
theta=atan((Ri-Ro)/L_t)%rad
L1 = Ro/sin(theta);%distance from the convergence point of the needle to the needle tip
%flow behaviors
K = 13.8;
n = 0.62;
Q1 = [12:4:44]*1e-7; %flow rate
Q_exp=[1.2 2.5 4.1]*1e-6;
Damage_exp = [0.42 0.61 0.77];
error_D350 = [0.07 0.062 0.08];

beta = [3.2 7.2];
syms r1; %radius direction in spherical polar coordinates
syms r2; %angle direction in spherical polar coordinates

for i = 1:length(Q1)
Q = Q1(i); %flow rate
```

```
const = 3/(2*pi*(1+2*cos(theta))*(1-cos(theta))^2);%constant
shear_rate = 0.5*const*Q*sin(r2)/(r1^3);
stress = K*power(shear_rate, n);
v = const*Q*(cos(r2)^2-cos(theta)^2)/(r1^2);%velocity at r1 location
time = ((L_t+L1)^3-r1^3)/(3*const*Q*(cos(r2)^2-cos(theta)^2));%time for cells arrive at
                                                              %r1 location
log_mu = beta(1)/(log(stress)/log(10)-1.8)-beta(2);
mu = 10^(log_mu);
sigma = mu/5;
%possibility density fun of cell damage law
pdf = (1/(sqrt(2*pi)*sigma))*exp(-(time-mu)^2/(2*sigma^2));
%deriverative of time
d_time = -(r1)^2/(const*Q*(cos(r2)^2-cos(theta)^2));
d_time = -d_time;%because of the reverse direction to the coordinate system
pdf = pdf*d_time*r2;%r2 is from the final cell damage integration equation
start_theta = asin((100/K)^(1/n)*(L1+L_t)^3/0.5*const*Q);%this is the theta that stress is
                                                         %70 pa at (L1+L_t)

%reform the pdf for numerical integration
pdf = char(pdf);
pdf=strrep(pdf, '*', '.*');
pdf=strrep(pdf, '/', './');
pdf=strrep(pdf, '^', '.^');
damage(i) = 2*dblquad(pdf, L1,L_t+L1, 0.02, 0.99*theta, 1e-6, @quad8)/theta^2;
end

figure(1)
errorbar(Q_exp*1e6,Damage_exp*100, error_D350*100,'*');grid on; hold on;
plot(Q1*1e6, damage*100);
xlabel('Flow rate (mL/s)');
ylabel('Cell damage (%)');
legend('simulation results', 'experimental data');

figure(2)
stress_simu = 500:100:50000;
log_stress_simu = log10(stress_simu);
log_mu_simu = beta(1)./(log_stress_simu-1.8)-beta(2);

plot(log_stress_simu, log_mu_simu,'linewidth',2);hold on;
xlabel('log10(stress)');
ylabel('log10(time)');

yy1 = normpdf([1:100], 50, 20);
plot(yy1*20+3.0,-5.2+[1:100]*1e-2);
```

```
line([3.02,3.42],[-4.2 -4.2]);
line([3.02 3.02], [-4.2 -5.2]);

yy2 = normpdf([1:100], 50, 20);
plot(yy2*20+3.5,-5.8+[1:100]*0.7e-2);
line([3.52,3.90],[-5.1 -5.1]);
line([3.52 3.52], [-5.1 -5.8]);

yy3 = normpdf([1:100], 50, 20);
plot(yy3*20+4.0,-6.1+[1:100]*0.5e-2);
line([4.02 4.4],[-5.6 -5.6]);
line([4.02 4.02], [-5.6 -6.1]);
```